# SYNTHESIS, CHARACTERIZATION, CYTOTOXIC ACTIVITY AND BIOLOGICAL INTERACTIONS OF TUNGSTENOCENE (IV) DERIVATIVES

By
Moralba Domínguez García

A thesis submitted in partial fulfillment of the requirements for the degree of
MASTER OF SCIENCE
in
CHEMISTRY
UNIVERSITY OF PUERTO RICO
MAYAGÜEZ CAMPUS
2012

Approved by:

| | |
|---|---|
| _____ | _____ |
| Mayra E. Cádiz, Ph.D.<br>Member, Graduate Committee | Date |
| _____ | _____ |
| Nilka Rivera, Ph.D.<br>Member, Graduate Committee | Date |
| _____ | _____ |
| Enrique Meléndez, Ph.D.<br>President, Graduate Committee | Date |
| _____ | _____ |
| Moises Orengo, Ph.D<br>Representative of Graduate Studies | Date |
| _____ | _____ |
| Rene Vieta, Ph.D.<br>Interim Director of the Department | Date |

## Abstract

The design of medicinal compounds for cancer therapy is still a challenge. Organometallics offer a wide variety of promising anticancer drug candidates but this field is largely unexplored. This study has been focused on the development of modified tungstenocene complexes as new metal-based drugs, since little is known about them as anticancer agents. Four new complexes were synthesized in aqueous solution; $[Cp_2W(maltolato)]Cl$, $[Cp_2W(ethylmaltolato)]Cl$, $[Cp_2W(kojato)]Cl$ and $Cp_2W(malonate)$, their structures were elucidated and characterized by UV/Vis, IR, $^1$H-NMR spectroscopy, cyclic voltammetry and elemental analysis indicating that complexes contain bidentate ligands bound to W(IV), forming 5- and 6-membered chelating rings. Cytotoxic activity studies of the synthesized complexes were performed on HT-29 colon and MCF-7 breast cancer cells by MTT assay, where the new complexes showed higher cell inhibition ($IC_{50} \sim 10^{-4}$ M) in comparison with tungstenocene dichloride ($IC_{50} = 0.01$ M) for HT-29, whereas for MCF-7 all complexes showed inhibition concentrations of same order of magnitude ($IC_{50} \sim 10^{-4}$ M). The high solubility in water of the complexes should allow an easy transport into the cancer cell. Therefore, interaction studies were achieved with both human serum albumin and apo-transferrin proteins, to understand complexes delivery into the body and up to the cell. These studies were performed in Tris buffer solution at pH 7.4, using cyclic voltammetry and fluorescence techniques. The results suggest that there is an interaction, which is higher for new complexes than parent compound, based mainly in hydrophobic and electrostatic interactions. In conclusion, this study is the starting point for the development of new and promising tungstenocene (IV) derivatives as complexes with anticancer properties.

## Resumen

El diseño de compuestos medicinales contra el cáncer es un gran reto. Los compuestos organometalicos ofrecen una amplia variedad de candidatos a medicamentos anticáncer, pero todavía falta mucho por explorar en este campo. Este estudio ha sido enfocado en el desarrollo de complejos modificados de tungstenoceno como nuevos candidatos a fármacos basados en compuestos metálicos, debido a lo poco conocido de estos como agentes anticancerígenos. Cuatro nuevos complejos fueron sintetizados en medio acuoso; $[Cp_2W(maltolato)]Cl$, $[Cp_2W(etilmaltolato)]Cl$, $[Cp_2W(kojato)]Cl$ y $Cp_2W(malonato)$, sus estructuras fueron elucidadas y caracterizadas por espectroscopia UV/Vis, IR, $^1$H-NMR, voltametría cíclica y análisis elemental, indicando que los complejos contienen ligandos bidentados enlazados a W(IV), formando anillos quelatos de 5 y 6 miembros. Se realizaron estudios sobre la actividad citotóxica de los nuevos complejos usando el ensayo MTT en células cancerígenas del colon HT-29, y de seno MCF-7, donde los nuevos complejos mostraron una inhibición celular más alta ($IC_{50} \sim 10^{-4}$ M) en comparación con el dicloruro de tungstenoceno ($IC_{50} = 0.01$ M) en las HT-29, mientras que las células de MCF-7, todos los complejos exhibieron concentraciones del mismo orden de magnitud ($IC_{50} \sim 10^{-4}$ M). La alta solubilidad de los complejos en agua debe permitir un fácil transporte hacia el interior de las células cancerígenas. Por tanto, estudios de interacción fueron llevados a cabo con dos proteínas; albumina humana y apo-transferrina, con el fin de entender la transporte llevado a cabo hasta la célula. Estos estudios fueron realizados en buffer Tris a pH 7.4 usando las técnicas de voltametría cíclica y fluorescencia. Los resultados sugieren que existe una mayor interacción con los nuevos complejos en comparación con el dicloruro de tungstenoceno y esta interacción se basa principalmente en fuerzas hidrofóbicas y electrostáticas.

En conclusión, este estudio es el punto de partida para el desarrollo de nuevos y prometedores derivados de tungstenoceno para actuar como complejos con propiedades anticancerígenas.

*To my dear parents*

*Daniel and Elena*

**Acknowledgements**

First of all, I would like to thank God. He blessed me with the opportunity to study the master degree in Puerto Rico, a country with spectacular places and wonderful people.

I thank the University of Puerto Rico - Mayaguez Campus, the Department of Chemistry, in particular to Professor Enrique Meléndez for the opportunity to work in his laboratory, and give me the necessary tools to be better scientific and human being. Thanks to the graduate committee, Dr. Mayra E. Cadiz, and Dr. Nilka Rivera for their suggestions.

A very special thank to my parents Daniel and Elena, my sisters Carolina and Catalina, my best friends Ingrid and Jose Arturo, whose accompanied me during this journey and they were a great motivation and encouragement in the difficult moments.

I would also like to thank to Jose L. Vera by his friendship and technical support in the laboratory, and my lab partners, Wanda, Xiomara, Jesus, Jorge, Angel, and Shakira, my friends Ruth, Gabriela, Ariel, and Colombian friends by their company and unforgettable moments.

## Table of Contents

List of figures .....X
List of tables .....XII
List of schemes .....XIII
**1. Introduction.....1**
1.1 Objectives .....4
1.2 Literature review.....5
1.2.1 Metal complexes as anticancer agents .....5
1.2.2 Metallocenes with anticancer properties.....7
1.2.3 Ligands applications and its anticancer properties in metal complexes .....10
1.2.4 Interactions between metallocene with both human serum albumin and apo-transferrin proteins.....13
2. **Synthesis and characterization of tungstenocene derivatives.....17**
2.1 Synthesis of tungstenocene derivatives .....17
2.1.1 Materials for the synthesis of tungstenocene derivatives .....17
2.1.2 Synthesis of tungstenocene derivatives complexes .....17
2.2 Characterization of tungstenocene derivatives .....19
2.2.1 Solubility properties.....19
2.2.2 $^{1}$H-NMR Spectroscopy .....19
2.2.3 FT-IR Spectroscopy.....20
2.2.4 Elemental analysis .....20
2.2.5 UV-Vis Spectroscopy .....20
2.2.6 Cyclic voltammetry.....20
2.3 Results and Discussion .....21
2.3.1 Synthesis of tungstenocene derivatives .....21
2.3.2 Solubility properties.....23
2.3.3 $^{1}$H-NMR Spectroscopy .....23
2.3.4 FT-IR Spectroscopy.....27
2.3.5 Elemental analysis .....33
2.3.6 UV-Vis Spectroscopy .....33

2.3.7 Cyclic voltammetry....35
**3. Cytotoxic activity on colon and breast cancer cells ....40**
3.1 Materials and methods....40
3.1.1 Materials ....40
3.1.2 Cancer cell lines....40
3.1.3 MTT Cancer viability assay ....41
3.2 Results and Discussion ....42
**4. Biological interaction of tungstenocene dichloride and its derivatives with human serum albumin (HSA) and human apo-transferrin (apo-hTf) ....46**
4.1 Materials and methodology....46
4.1.1 Tris buffer solution ....46
4.1.2 Proteins solutions....46
4.1.3 Complex solutions ....46
4.1.4 Interaction studies by fluorescence spectroscopy....47
4.1.5 Interaction studies by cyclic voltammetry....47
4.2 Results ans Discussion....48
4.2.1 Interaction by fluorescence spectroscopy....48
4.2.2 Interaction by cyclic voltammetry....64
**5. Conclusions and future works ....73**
**Appendix**....76
A.1. $^{1}$H-NMR Spectrums ....76
A.1.1 $^{1}$H-NMR spectrum of tungstenocene dichloride in DMSO-$d_6$ ....76
A.1.2 $^{1}$H-NMR spectrum of maltol in DMSO-$d_6$ ....76
A.1.3 $^{1}$H-NMR spectrum of ethylmaltol in DMSO-$d_6$ ....77
A.1.4 $^{1}$H-NMR spectrum of kojic acid in DMSO-$d_6$....77
A.1.5 $^{1}$H-NMR spectrum of malonate in DMSO-$d_6$....78
**Bibliography** ....79

## List of figures


Figure 1.1 Structure of cisplatin and metallocene dihalide....2

Figure 1.2 Structure of cisplatin analogs, carboplatin and lobaplatin....5

Figure 1.3 Structure of budotitane, KP418, spirogermanium....7

Fifure 1.4 Structure of titanocenyl amide and titanocenyl-dehydroepiandrosterone....10

Figure 1.5 Structure of ligands....10

Figure 1.6 Structure of maltol containing complexes....11

Figure 1.7 Structure of diam(m)ineplatinum(II) complexes with 2,2-bis(hydroxymethyl)malonate....12

Figure 1.8 Structure of molybdenocene derivatives with maltol and malonate as ligands....13

Figure 1.9 Human serum albumin protein....14

Figure 1.10 a) Apo-hTf (non-glycosilated) b) Transferrin structure and amino acids that bind and hold iron in a N-terminus transferring lobe....11

Figure 2.1 $^{1}$H-NMR spectrum of [$Cp_2W$(maltolato)]Cl in DMSO-$d_6$....25

Figure 2.2 $^{1}$H-NMR spectrum of [$Cp_2W$(ethylmaltolato)]Cl in DMSO-$d_6$....25

Figure 2.3 $^{1}$H-NMR spectrum of [$Cp_2W$(kojato)]Cl in DMSO-$d_6$....26

Figure 2.4 $^{1}$H-NMR spectrum of $Cp_2W$(malonato) in $D_2O$....26

Figure 2.5 IR spectra from $Cp_2WCl_2$, maltol, and [$Cp_2W$(maltolato)]Cl....29

Figure 2.6 IR spectra from $Cp_2WCl_2$, ethylmaltol, and [$Cp_2W$(ethylmaltolato)]Cl....30

Figure 2.7 IR spectra from $Cp_2WCl_2$, kojic acid, and [$Cp_2W$(kojato)]Cl....31

Figure 2.8 IR spectra from $Cp_2WCl_2$, malonate, and $Cp_2W$(malonato)....32

Figure 2.9 UV-Vis spectra of tungstenocene and its derivatives....35

Figure 2.10 UV-Vis spectra of free ligands....35

Figure 2.11 Cyclic voltammograms of tungstenocene and the new complexes in acetonitrile (0.1M $Bu_4NPF_6$)....37

Figure 2.12 Cyclic voltammograms of tungstenocene and its derivatives in Tris buffer (0.1 M). 38

Figure 2.13 Cyclic voltammograms of tungstenocene and its derivatives in KCl (0.1 M). ....38

Figure 2.14 Cyclic voltammograms of ligands in Tris buffer (0.1 M). ....39

Figure 3.1 Dose response curve of $Cp_2WCl_2$ against colon cancer cell HT-29....43

Figure 3.2 Dose response curve of tungstenocene derivatives against colon cancer cell HT-29 ..43
Figure 3.3 Dose response curve of tungstenocene and its derivatives against breast cancer cell MCF-7 .....45
Figure 4.1 Fluorescence quenching spectra of HSA with different complexes. a. $Cp_2WCl_2$, b. $Cp_2W$(malonate), c. [$Cp_2W$(ethylmaltolato)]Cl, d. [$Cp_2W$(kojato)]Cl, e. [$Cp_2W$(maltolato)]Cl.....50
Figure 4.2 Fluorescence quenching spectra of apo-hTf with different complexes. a. $Cp_2WCl_2$, b. $Cp_2W$(malonate), c. [$Cp_2W$(ethylmaltolato)]Cl, d. [$Cp_2W$(kojato)]Cl, e. [$Cp_2W$(maltolato)]Cl.....52
Figure 4.3 Stern-Volmer plots of HSA at 15°C and 37°C with different complexes. a. $Cp_2WCl_2$, b. [$Cp_2W$(ethylmaltolato)]Cl, c. [$Cp_2W$(kojato)]Cl , d.[$Cp_2W$(maltolato)]Cl, e. $Cp_2W$(malonate).....54
Figure 4.4 Stern-Volmer plots of apo-hTf at 25°C and 37°C with different complexes. a. $Cp_2WCl_2$, b. [$Cp_2W$(ethylmaltolato)]Cl, c. [$Cp_2W$(kojato)]Cl, d.[$Cp_2W$(maltolato)]Cl, e. $Cp_2W$(malonate).....58
Figure 4.5 Van`t Hoff plots of interaction between HSA with the complexes .....61
Figure 4.6 Van`t Hoff plots of interaction between HSA with the complexes .....63
Figure 4.7 $Cp_2WCl_2$ Titration voltammograms. A) buffer, b) HAS, and c) apo-hTf .....65
Figure 4.8 [$Cp_2W$(maltolato)]Cl Titration voltammograms. A) buffer, b) HSA, and c) apo-hTf .....66
Figure 4.9 [$Cp_2W$(ethylmaltolato)]Cl Titration voltammograms. A) buffer, b) HSA, and c) apo-hTf .....67
Figure 4.10 [$Cp_2W$(kojato)]Cl Titration voltammograms. A) buffer, b) HSA, and c) apo-hTf ...68
Figure 4.11 $Cp_2W$(malonate) Titration voltammograms. A) buffer, b) HSA, and c) apo-hTf .....69

## List of tables

Table 2.1 Solubility of tungstenocene derivatives complexes .....23
Table 2.2 Assignment of IR frequencies for $Cp_2WCl_2$, maltol, and [$Cp_2W$(maltolato)]Cl .....29
Table 2.3 Assignment of IR frequencies for $Cp_2WCl_2$, ethylmaltol, and [$Cp_2W$(ethylmaltolato)]Cl .....30
Table 2.4 Assigment of IR frequencies for $Cp_2WCl_2$, kojic acid, and [$Cp_2W$(kojato)]Cl .....31
Table 2.5 Assigment of IR frequencies for $Cp_2WCl_2$, malonato, and $Cp_2W$(malonate) .....32
Table 2.6 Elemental analysis results of tungstenocene derivatives .....33
Table 2.7 Electronic spectral data from tungstenocene and its derivatives .....34
Table 3.1 Cytotoxic activity of tungstenocene and its derivatives against colon cancer cell HT-29 .....44
Table 3.2 Cytotoxic activity of tungstenocene and its derivatives against breast cancer cell MCF7.....45
Table 4.1 Quenching constant of the interaction between HSA and complexes .....55
Table 4.2 Quenching constant of the interaction between apo-hTf and complexes .....59
Table 4.3 Thermodynamic parameters of the interaction between HSA with the complexes.....61
Table 4.4 Thermodynamic parameters of the interaction between apo-hTf with the complexes .63
Table 4.5 Interaction percentage between HSA and complexes by cyclic voltammetry.....71
Table 4.6 Interaction percentage between apo-hTf and complexes by cyclic voltammetry.....71

## List of schemes

Scheme 2.1 Synthesis of tungstenocene derivatives complexes .....18
Scheme 2.2 Zwitterionic forms of 3-hydroxy-4-pyrone, R=H or OH, R´= $CH_3$ or $C_2H_5$ .....22
Scheme 3.1 MTT reduction .....42

## 1. Introduction

Cancer has caused 7.6 million deaths worldwide (13% of all deaths) in 2008; 12 million deaths worldwide are projected to continue rising in 2030. In the United States, cancer is the second most common cause of death after heart disease. The most common cancer in men is prostate and in women is breast cancer. About one in three persons will develop cancer during their lifetimes and probably two out of nine patients, who previously had cancer and overcame the disease, develop a second primary cancer. Therefore, it is of vital importance to pursue studies in cancer and its possible treatments [1, 2, 3, 4].

Cancer is a group of diseases characterized by uncontrolled growth and spread of abnormal cells. It often invades surrounding tissues and the abnormal cells can be transported by the lymphatic system toward other organs (metastasis). Many types of cancers exist and their symptoms depend on the location, the malignant nature and advance of metastasis process [1].

Cancer is treated with surgery, radiation, chemotherapy, hormone therapy, biological therapy, and targeted therapy, although the type of treatment depends on the location and phase of the disease. The most used treatment is chemotherapy which destroys cancer cells, thus slowing and stopping the cancer from spreading. There are many anticancer drugs proceeding from several sources, including dyestuffs, chemical warfare agents, plants, microbes, fungi and metal coordination compounds. They are known to affect cellular processes in a dramatic way, presenting toxicity to cancer cells, but the challenge is the death of the cancer cells without causing damage to healthy cells [5].

In the last 30 years, platinum based drugs have dominated the treatment of several cancer. They principally bind to DNA avoiding its transcription, replication and cell division. However, they produce serious side effects and the lack of specificity combined with toxicity lead to resistance. Thus, cells decrease the metal accumulation mechanisms and increase the deactivation and repair mechanisms, therefore the scientific community is searching other complexes as potential anticancer agents [6, 7, 8].

After the discovery of cis-platin (figure 1.1), several non-platinum metal complexes have shown to have potential use in chemotherapy. For instance, metallocene dihalides and diacid complexes with general formula $Cp_2MX_2$, (figure 1.1, where Cp = $\eta^5$-$C_5H_5$; M = Ti, V, Nb, Mo, Re; X = halide or diacid ligand) showed antitumor activity against a wide variety of tumor cells. Their stability, coordination and mechanism of action are different of platinum drugs. Among all the metallocenes tested, only titanocene dichloride has entered clinical trials phase I and II, exhibiting also antiviral, anti-inflammatory and insecticidal activity [9, 10]


Cisplatin Metallocene dihalide

**Figure 1.1** Structure of cisplatin and metallocene dihalide.

The design of medicinal compounds for cancer therapy is still a challenge, but organometallic chemistry offers a wide variety of promising anticancer drug candidates which remains

unexplored. It is the case with tungstenocene (IV) dichloride, little is known as an anticancer agent and the preliminary studies against Ehrlich's ascites tumor (EAT) on CF-1 mice has shown sporadic activity [11]. However, molybdenocene (IV) dichloride and derivatives have been extensively investigated, showing cytotoxic activity and stability at physiological conditions [12]. Based on the anticancer properties of molydenocene dichloride, and the fact that its chemical behavior is similar to tungstenocene dichloride, it is crucial to carry out a study concerning the development of new tungstenocene (IV) derivatives complexes to evidence their cytotoxic activity against different cancer types and hence to create new alternatives of chemotherapeutics to improve the quality of life of cancer patients in our society.

For the above reasons, this study is focused in the synthesis of tungstenocene derivatives, their characterization, and evaluation of cytotoxic activity on two human cancer cell lines, HT-29 colon cancer and MCF-7 breast cancer *in vitro*. Moreover, studies about their biological interaction with both human serum albumin and apo-transferrin proteins by cyclic voltammetry and fluorescence spectroscopy techniques were pursued to understand complex’s delivery and transport in the body and up to the cell. Consequently, these studies show interesting results, which are the starting point for the development of new and promising tungstenocene derivatives as complexes with anticancer properties.

### 1.1 Objectives

The main objective of this research is investigate the cytotoxic properties of tungstenocene derivatives against breast and colon cancer cell lines as starting point to explore new and promising tungsten complexes as potential anticancer drugs.

The specific objectives proposed are:

1. To synthesize tungstenocene (IV) derivatives complexes that contain bidentade ligand (O, O')-donor.
2. To characterize the new tungstenocene derivatives complexes by different spectroscopy techniques such as NMR, UV/Vis, IR spectroscopy, and cyclic voltammetry and elemental analysis.
3. To evaluate the cytotoxic activity *in vitro* of tungstenocene dichloride and the new complexes on human colon cancer cells (HT-29) and human breast cancer cell (MCF-7).
4. To examine the biological interaction between the tungstenocene dichloride and the new complexes with both human serum albumin and apo-transferrin proteins using fluorescence spectroscopy and cyclic voltammetry techniques.

## 1.2 Literature review

### 1.2.1 Metal complexes as anticancer agents

In the last 30 years platinum based drugs have dominated the treatment of several cancers. The most frequently used drug is cis-platin (figure 1.1), in which the mechanism of action consists in lesions in DNA strand and adjacent bases. Both damages induce inhibition of the enzymes implicated in RNA transcription, DNA replication and chain elongation of DNA polymerization, and triggers the cell death [13, 14, 15]. Although cis-platin is not active against all types of cancer, it has been useful in the treatment of testicular carcinomas and ovarian, head and neck bladder, and lung cancers. Various analogs of cis-platin such as *cis*-diammine (cyclobutane-1,1-dicarboxylato)-platinum(II) or carboplatin, 1,2-di(aminomethyl)cyclobutaneplatinum(II) lactate or lobaplatin (figure 1.2) and their derivatives have been studied in tumors that show cis-platin resistance [6, 9, 16].

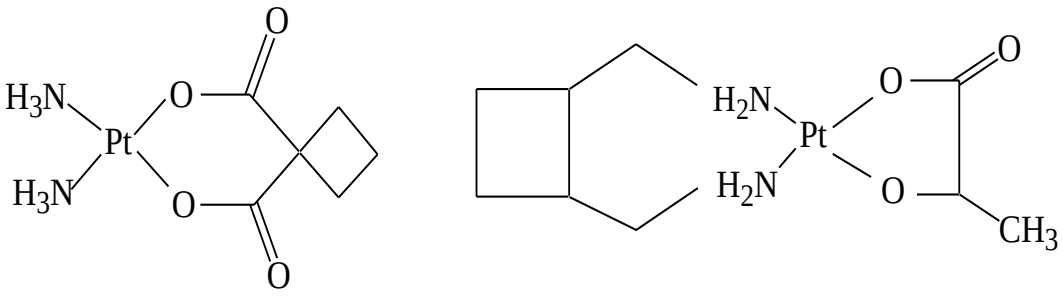


**Figure 1.2** Structure of Cisplatin analogs, carboplatin and lobaplatin

Other metal complexes different of platinum complexes have been reported with antitumor activity and some have entered clinical trials such as budotitane (*cis*-[$(CH_3CH_2O)_2(bzac)_2TiIV$] where bzac is 1-phenylbutane-1,3-diketonate, figure 1.3). It was the first non platinum transition-metal anticancer agent to be tested in clinical trials and it has been used against a wide variety of ascites (serious fluid abnormal accumulations), and solid tumors. A series of *cis*-[$X_2(bzac)_2MIV$] complexes (M = Ti, Zr, Hf, Mo, Sn, Ge) have been investigated in cancer cells to elucidate the role of the metal center into the anticancer activity. The cytotoxic activity varied in the following order Ti ~ Zr > Hf > Mo > Sn > Ge, which is roughly inverse to the rates of X dissociation from the metal ion. Spirogermanium (figure 1.3) is a germanium compound of azaspirane that contains nitrogen linked to a dimethylaminopropyl substituent. In clinical trial it showed activity against the lymphoproliferative leukemia disorders, nodular poorly differentiated lymphoma and diffuse lymphomas. Gallium nitrate in its clinical studies showed significant antitumor activity against non-Hodgkin's lymphoma and bladder cancer, indicating that gallium based drugs have potential as antineoplastic agents. Ruthenium (III) complexes (KP418 (figure 1.3), KP1019, and NAMI-A) exhibit lower cytotoxicity than cis-platin, but are better tolerated *in vivo* because they promote inhibition of angiogenesis and metalloproteinases and therefore metastasis *in vivo*. Titanocene dichloride ($Cp_2TiCl_2$) is a metallocene that has entered in clinical trials. It shows activity against colon, lung and breast cancers and there is no evidence of nephrotoxicity or myelotoxicity [9, 10, 17, 18, 19, 20].

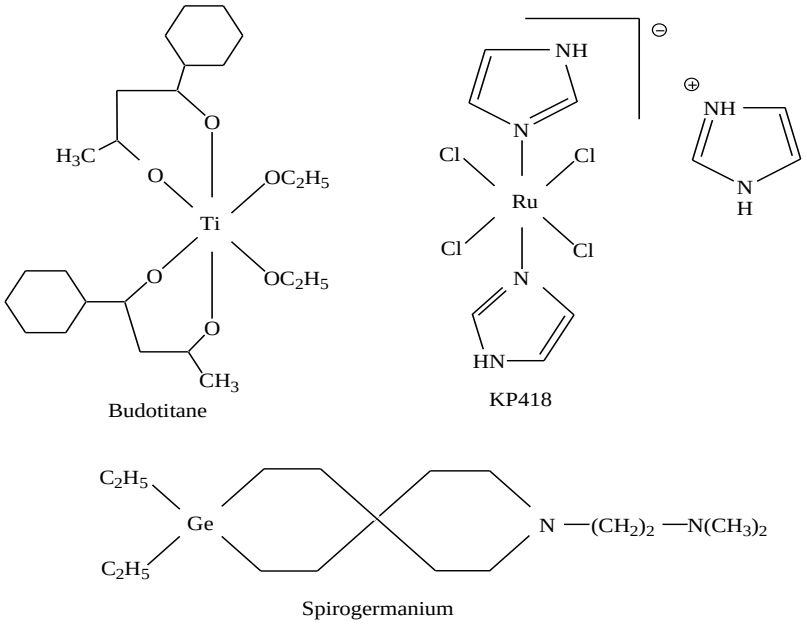


**Figure 1.3** Structure of budotitane, KP418, spirogermanium

### 1.2.2 Metallocenes with anticancer properties

Organometallic compounds have great structural variety and recently were found to be promising anticancer drug candidates. They are kinetically stable, relatively lipophilic and offer a wide variety of opportunities in the design of novel medicinal compounds. Metallocenes are complexes with general formula $Cp_2MX_2$ ($Cp = \eta^5\text{-}C_5H_5$, X = halide or diacid ligand, figure 1.1). Some of them have showed anticancer activity depending of metal ion. Formation of metallocene-DNA complexes is implicated in the mechanism of action, since both titanocene dichloride and vanadocene dichloride inhibit DNA and RNA synthesis and metal is accumulated in nucleic acid-rich regions of tumor cells. Studies about hydrolysis chemistry, stability at different pH values and the interaction with nucleic acid have confirmed that each of antitumor metallocene complexes have an independent mechanism of action [9].

The antitumor activity of metallocene complexes with M = Ti, V, Nb, and Mo have shown good activity, while Ta and W exhibit moderate effectiveness, and Zr and Hf are inactive. Cationic complexes of the type $[Cp_2M\ X_2]^+$, where M = Nb, Mo, and Re are active as well as ferrocenium ions. The central metal has an influence on the anticancer activity of the metallocenes, with a diagonal relationship in the periodic table. Thus, Ti-Nb and V-Mo are active metallocenes that generate an interaction with DNA subunits. Also Murray and Harding (1994) reported the formation of complexes between nucleotides and active metallocenes (Ti, Mo) but not with biological inactive metallocenes (Zr, Hf) [17, 11, 21].

Most studies have been focused on titanocene dichloride in different cancer cell lines. It showed activity to cis-platin resistance cells and lower toxic effects than cis-platin. Therefore, it has motivated the scientific community to pursue research in this field. *In vitro* experiments of titanocene dichloride showed antitumor activity in doxorubicin and cis-platin resistant ovarian carcinoma cells. Also, it is active against human adenocarcinomas of the stomach and colon, which are insensitive to common cytostatic agents. In xenografted of lung, breast, gastrointestinal tract and ovarian human carcinomas, titanocene dichloride showed to be as effective as paclitaxel and vinorelbine, presenting higher activity than cis-platin, 5-fluorouracil and cyclophosphamide. Titanocene dichloride has reached clinical phase I and II trials, but its disadvantage is low stability at physiological pH due to extensive hydrolysis [9, 10].

Other species of titanocene derivatives have shown activity, among them are the halides and pseudo halides of titanocene $Cp_2TiX_2$, where X = F, Br, I, NCS, $N_3$. They were evaluated in Ehrlich ascites tumor in mice and showed high antiproliferative activity similar to titanocene dichloride. Diacid complexes where X = carboxylates (trifluoroacetate, trichloroacetate and

hydrogenmaleinate), phenolates (*p*-nitrophenalate and pentafluorophenolate), dithiolenes and thiophenolate (pentafluorothiophenolate) have shown antiproliferative action against Ehlrich ascites tumor. Monosubstituted complexes of formula $Cp_2TiClX$, where X = 1,3,5-trichlorophenolate, 1-aminothiophenolate, 1-methylthiophenolate and selenophenolate have exhibited antitumor activity. Ionic titanocene complexes of general formula $[Cp_2TiXL]^+Y^-$ or $[Cp_2TiL_2]^{2+}[Y^-]_2$, where X is an anionic ligand and L is a neutral ligand, have been evaluated showing antiproliferative action [10].

Our research group recently has reported studies about the modification of titanocene dichloride by either replacing chloride with hydrophilic or biologically important ligands with cytotoxic activity. Titanocenyl amide complexes (figure 1.4) have good antiproliferative properties against breast cancer MCF-7, and colon cancer HT-29 cell lines. Titanocenyls complexes functionalized with steroidal esters exhibited more cytotoxicity than titanocene dichloride. Particularly titanocenyl–dehydroepiandrosterone complex (figure 1.4) has higher cytotoxicity than titanocene dichloride by two 2 orders of magnitude and shows more sensitivity and selectivity for the MCF-7 cell line. Also, titanocene-amino acid complexes $[Cp_2Ti(aa)_2]Cl_2$ (aa = L-cysteine, L-methionine, and D-penicillamine) and $[Ti_4(maltolato)_8(l\text{-}O)_4]$ were investigated, of which only $[Ti_4(maltolato)_8(l\text{-}O)_4]$ exhibited a toxicity slightly higher than titanocene dichloride at 24 h, however at 72 h., titanocene dichloride and $[Ti_4(maltolato)_8(l\text{-}O)_4]$ have higher cytotoxic activity [22, 23, 24, 25].

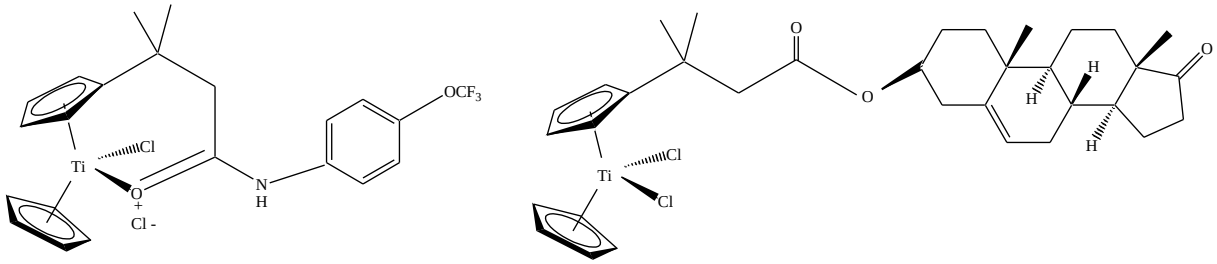


Titanocenyl amide

titanocenyl-dehydroepiandrosterone

**Figure 1.4** Structure of titanocenyl amide and titanocenyl-dehydroepiandrosterone.

### 1.2.3 Ligands applications and its anticancer properties in metal complexes

Maltol, ethylmaltol, kojic acid and malonate (figure 1.5) are bidentade ligands, (O, O')-donors, used in this research for the synthesis of new tungstenocene derivatives complexes. The three first belong to 3-hydroxy-4pyrones family, which form neutral and thermodynamically stable complexes with charged metal ions producing five-membered chelate ring through the keto group and the deprotonated OH [26].

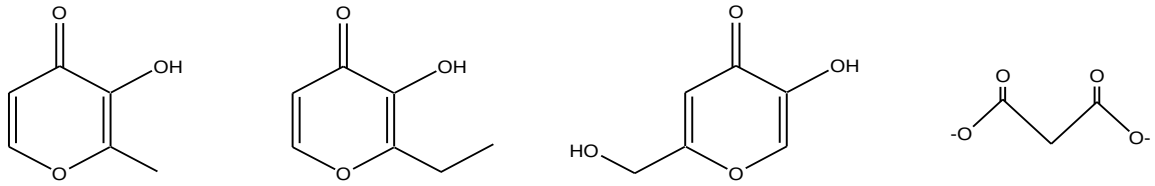


Maltol Ethylmaltol Kojic Acid Malonate

**Figure 1.5** Structure of ligands

Maltol and its close analogue ethylmaltol are produced on a large scale and used as flavor enhancer in food industry to impart malty taste and aroma. Different metal complexes have been synthesized using them as ligand for medicinal application as d-metal transporter to cell or

diabetes treatment. Bis(maltolato)oxovanadium(IV) and bis(ethylmaltolato)oxovanadium(IV) have undergone clinical trials for diabetes treatment, and aluminium tris(maltolato) has been studied for aluminium transport to the brain [26]. Additionally, coordination compounds that contain maltol as ligand have been tested for its anticancer activity like (1,2-diaminoethane) (maltolato) platinum(II) (figure 1.6) and (1R,2R-1,2-diaminocyclohexane) (maltolato) platinum(II), which have showed activity against HeLa and K562 human tissue cell with $IC_{50}$ values of 32 µM in HeLa and 26 µM in K562 cells [27]. Gallium maltolato has shown antiproliferative activity in four lines of hepatocellular carcinoma (HCC) cell with $IC_{50}$ values between 25-35 µM and at 30 µM induced apoptosis after 6 days [28]. Ruthenium(II)-p-cymene complexes with 2-substituted 3-hydroxypyran-4(1H)-one ligands showed cytotoxicity against colon carcinoma (SW480), ovarian carcinoma (CH1) and non-small cell lung carcinoma (A549) human cancer cells, yielding $IC_{50}$ values in the $10^{-5}$ M range [29]. Ruthenium derivative complexes that contain a bridge formed by two maltolato ligands (figure 1.6), also have showed activity anticancer against seven types of cancer cells showing concentrations since 0.075 to >100 µM range [30].

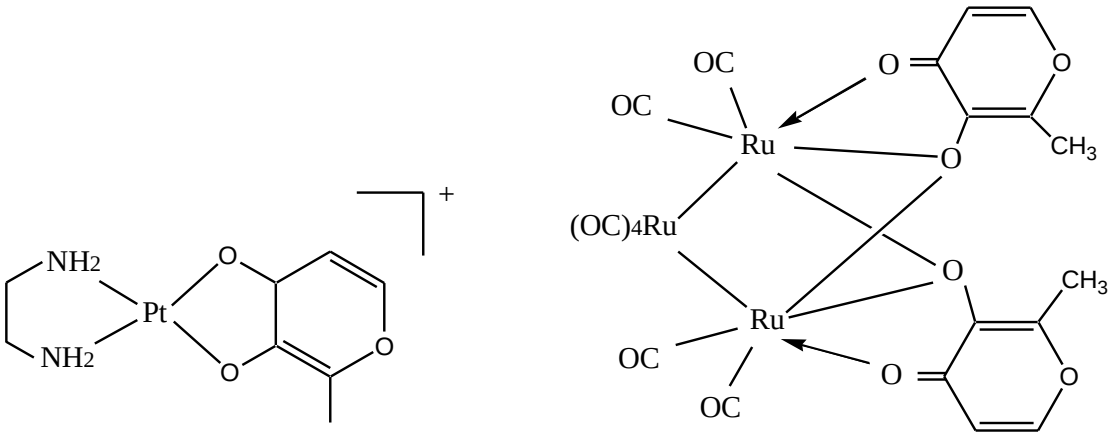


(1,2-diamoethane)(maltolato)platinum(II) $Ru_3(CO)_8(2Maltol\text{-}2H)$

**Figure 1.6** Structure of maltol containing complexes

Kojic acid (5-hydroxy-2-hydroxymethyl-4(1H)-pyrone) is a fungal metabolite produced during the fermentation of malting rice under aerobic conditions by *Aspergillus oryzae*. This is used as an additive to preserve or change in cosmetics to lighten skin color and inhibit the enzyme that promotes melanization [31]. Manganese and zinc complexes have shown to become radioprotectors in mice, exhibiting radioprotective effects against lethal dose of ɣ-irradiation in mice [32]. Also vanadium derivatives such as bis ((5-hydroxy-4-oxo-4 H-pyran-2-yl) methyl 2-hydroxy- benzoatato) oxovanadium (IV) (BSOV) have shown hypoglycemic properties, which can be used as strategy to become anti-diabetic agent [33].

Malonate is the dianionic form of propaneidioic acid and it is a flexible and versatile bidentate ligand for metal ions. Studies about cytotoxicity activity were carried out on six diam(m)ineplatinum(II) complexes with 2,2-bis(hydroxymethyl)malonate (figure 1.7) against human lung (A549), colon (HT-29), and gastric (SGC-7901) cancer cell showing a $IC_{50}$ values in the range of 2.18 to 59.8 µM, 1.72 to >100 µM and 4.42 to 30.3 µM range respectively [34].

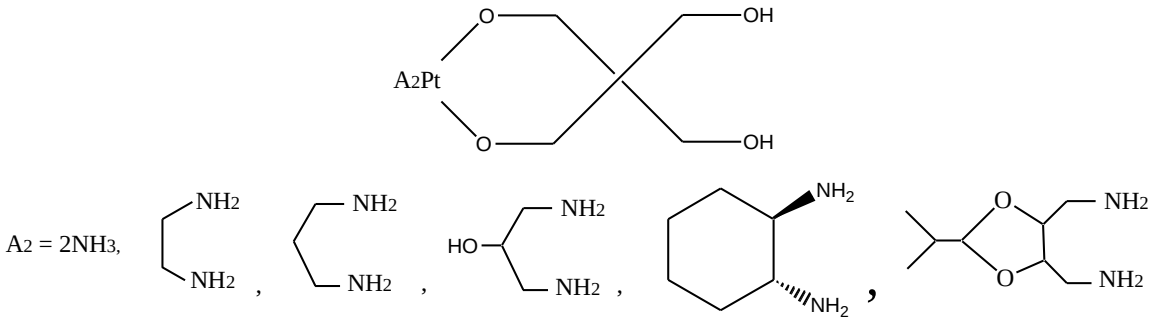


**Figure 1.7** Structure of diam(m)ineplatinum(II) complexes with 2,2-bis(hydroxymethyl)malonate

Additionally, our research group recently reported a study on the proliferative and antiproliferative activity of molybdenocene derivatives using malonate and maltol as ligands (figure 1.8), on HT-29 colon and MCF-7 breast cancer cell lines obtaining $IC_{50}$ values of 1.3 and 1.9 mM respectively for HT-29, whereas for MCF-7 exhibited proliferative activities [35].

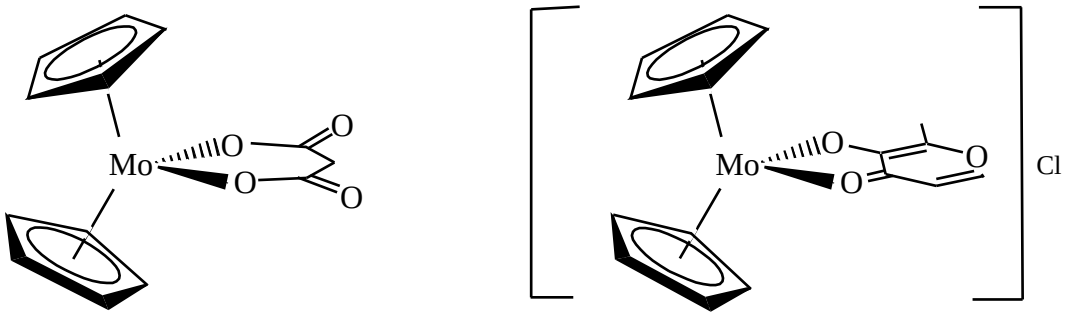


$Cp_2W$(malonate) [$Cp_2W$(maltolato)]Cl

**Figure 1.8** Structure of molybdenocene derivatives with maltol and malonate as ligands.

### 1.2.4 Interactions between metallocene with both human serum albumin and apo-transferrin proteins

Human serum albumin (HSA) is the most abundant protein in the blood plasma (figure 1.9), with a weigh of 66.5 kDa. This globular protein is synthesized in the liver and its principal function is to stabilize the osmotic pressure for the proper distribution of fluids in the body and act as a carrier of solutes to organs since it has large affinity to steroids, fatty acids, amino acids, metal ions ($Cu^{+2}$, $Zn^{+2}$), and drugs. HSA consist of a single peptide chain, which forms three homologous α-helical domains, named I, II, and III, with each domain divided in two subdomains A and B. The subdomains IIA and IIIA are hydrophobic cavities recognized as drug-binding sites named drug site I and II, respectively [36, 37, 38].

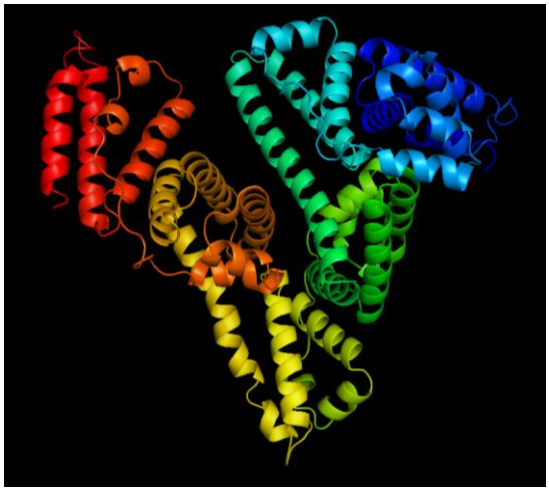

**Figure 1.9** Human serum albumin protein, PDB ID: 1E7I

Several interaction studies between metallocenes and HSA have been achieved electrochemically. Ravera in 2009, observed the interaction with titanocene dichloride through the variation of reduction peak (Ti (IV)/Ti (III)) before and after the addition of HSA solution and determined that titanocene dichloride has a higher affinity to HSA than DNA [39]. Feliciano in 2009, showed that $Cp_2MoCl_2$ has a greater interaction with HSA than with to DNA. Nevertheless, this interaction is weak in nature and decreases in molybdenocene derivatives, where oxygen-containing ligands substitutes the $Cl^-$ ligands ($[Cp_2Mo(maltolato)]Cl$ and $Cp_2Mo(malonate)$) [35].

Different studies about HSA interaction with drugs or complexes also have been evaluated by fluorescence spectroscopy under physiological pH conditions. For example, the interaction of $Cu(OAc)_2L_2 \cdot 2H_2O$ and $Ni(OAc)_2L_2 \cdot 2H_2O$ L=N,N-dibenzylethane-1,2-diamine with HSA were evaluated, and the enthalpy change $\Delta H°$ and the entropy change $\Delta S°$ were calculated, suggesting that the hydrophobic interaction is the predominant intermolecular force [40].

Human transferrin is an 80 kDa serum protein (figure 1.10) that transport iron(III) in the blood. This protein has a combination of α-helices and β-sheets to form two different lobes: N- and C-terminus. These two domains are held together by a short peptide and create a deep hydrophobic site; each lobe provides approximately an octahedral coordination site consisting of two tyrosine, histidine, aspartic acid, and bidentate carbonate (synergistic anion) as ligands where the ferric ion is loaded. The (-3) charge, contributed by two tyrosines and one aspartic acid, balances the (+3) charge of ferric iron. When the protein is not bound to the metal, it is known as apo-transferrin (apo-hTf) [41].

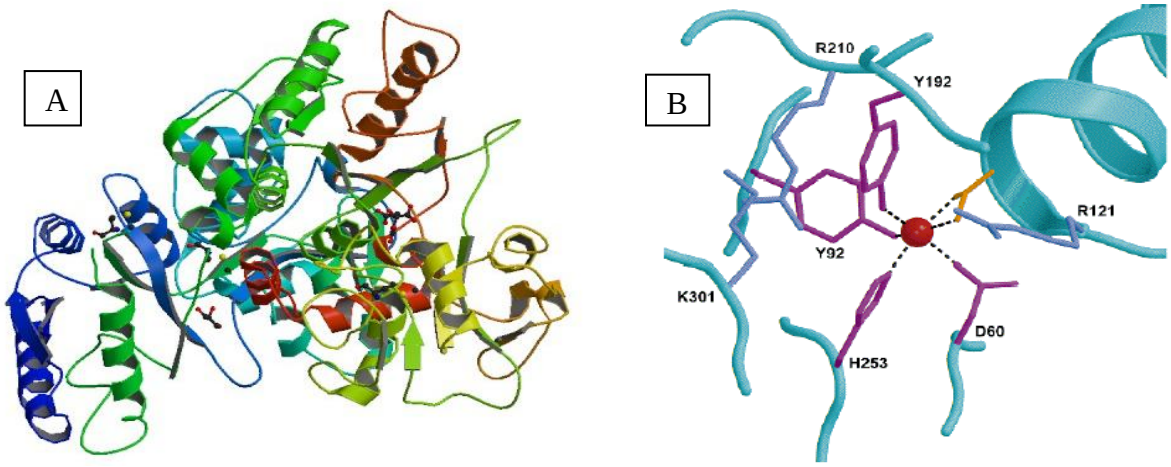


**Figure 1.10.** a) Apo-hTf (non-glycosilated), PDB:2HAU. b) Transferrin structure and amino acids that bind and hold iron in a N-terminus transferrin lobe [42].

Fe (III) binds first to apo-hTF at pH 7.4 and induces a conformational change in the protein, from the open lobe to the closed form. The holo-hTF (metal loaded into the binding site) binds to the specific transferrin receptors on the cell surface and is internalized into endosomes, where at pH 5.5 approximately, Fe (III) is released from the transferrin and remains bound to the receptor

at acidic pH. Then, it is recycled back to the surface of the cell, and ATP is a possible direct Fe (III) acceptor from transferrin and a major Fe (III) carrier inside cells [43].

Apo-hTf binds other metals ions such as $Ga^{+3}$, $Ru^{+3}$, $Yb^{+3}$, $Bi^{+3}$, $Ti^{+4}$. They can bind at the iron specific binding sites and hTf can act as a natural carrier for anticancer metal and chemotherapeutic drugs into cancer cells. There are high levels of transferrin receptors on the surface of cancer cells, attributed to increased requirement of iron for its metabolism, growth, and development. Therefore, apo-hTf can be used as strategy either for blocking iron uptake or for release of a cytotoxic metal complex inside cells if the adduct is labile under the acidic conditions in the endosomes [41].

Tinoco in 2008 demonstrated that, both albumin and apo-hTf routes of transport for Ti (IV) are possible, proposing that the titanocene dichloride binds to HSA by the hydrophobic sites interacting with the Cp rings or to transferrin by the direct coordination of the oxygen atoms of protein residues to the metal and it forms a stable complex to transport Ti(IV) into cells via transferrin endocytosis [38].

## 2. Synthesis and characterization of tungstenocene derivatives

### 2.1 Synthesis of tungstenocene derivatives

#### 2.1.1 Materials for synthesis of tungstenocene derivatives

The bis(cyclopentadienyl)tungstenocene dichloride 97% ($C_{10}H_{10}Cl_2W$) and the ligands, malonic acid disodium monohydrate salt, 98% ($C_3H_2O_4{\cdot}2Na$), 3-hydroxy-2-methyl-4-pyrone 99% (maltol, $C_6H_6O_3$), Kojic acid ($C_6H_6O_4$), 2-ethyl-3-hydroxy-4H-pyran-4-one, 99% (ethylmaltol, $C_7H_8O_3$), were obtained from Sigma-Aldrich. Water was previously deionized, and degassed with $N_{2(g)}$. The pH was adjusted with KOH 1.0 M solution. The tungstenocene derivatives were purified by column chromatography, using Lipophilic Sephadex (20-100 μm) as stationary phase and methanol as mobile phase, both materials were purchased from Sigma-Aldrich.

#### 2.1.2 Synthesis of tungstenocene derivatives complexes

150 mg (0.390 mmol) of $Cp_2WCl_2$ were charged in a three neck round bottom flask of 100 mL, with 25 mL of deionized degassed water. The solution was heated until thecomplex dissolved completely forming a violet solution. 0.390 mmol of the corresponding ligand (maltol, ethylmaltol, kojic acid and malonate) was added and the pH was adjusted with KOH 0.1 M (scheme 2.1). For ethylmaltol and maltol, the pH was adjusted to 5.5 and 6.0 respectively whereas for kojic acid and malonate the pH was adjusted to 7.6 and 9.0 respectively. The reaction was stirred overnight at room temperature under a nitrogen atmosphere and an amber solution was formed with a minor amount of black precipitate and the final pH decreased around 3 units for each case. The liquid phase was decanted, the solvent was removed under vacuum and

the resulting solid was purified by column chromatography, using lipophilic sephadex as solid phase and methanol as solvent.

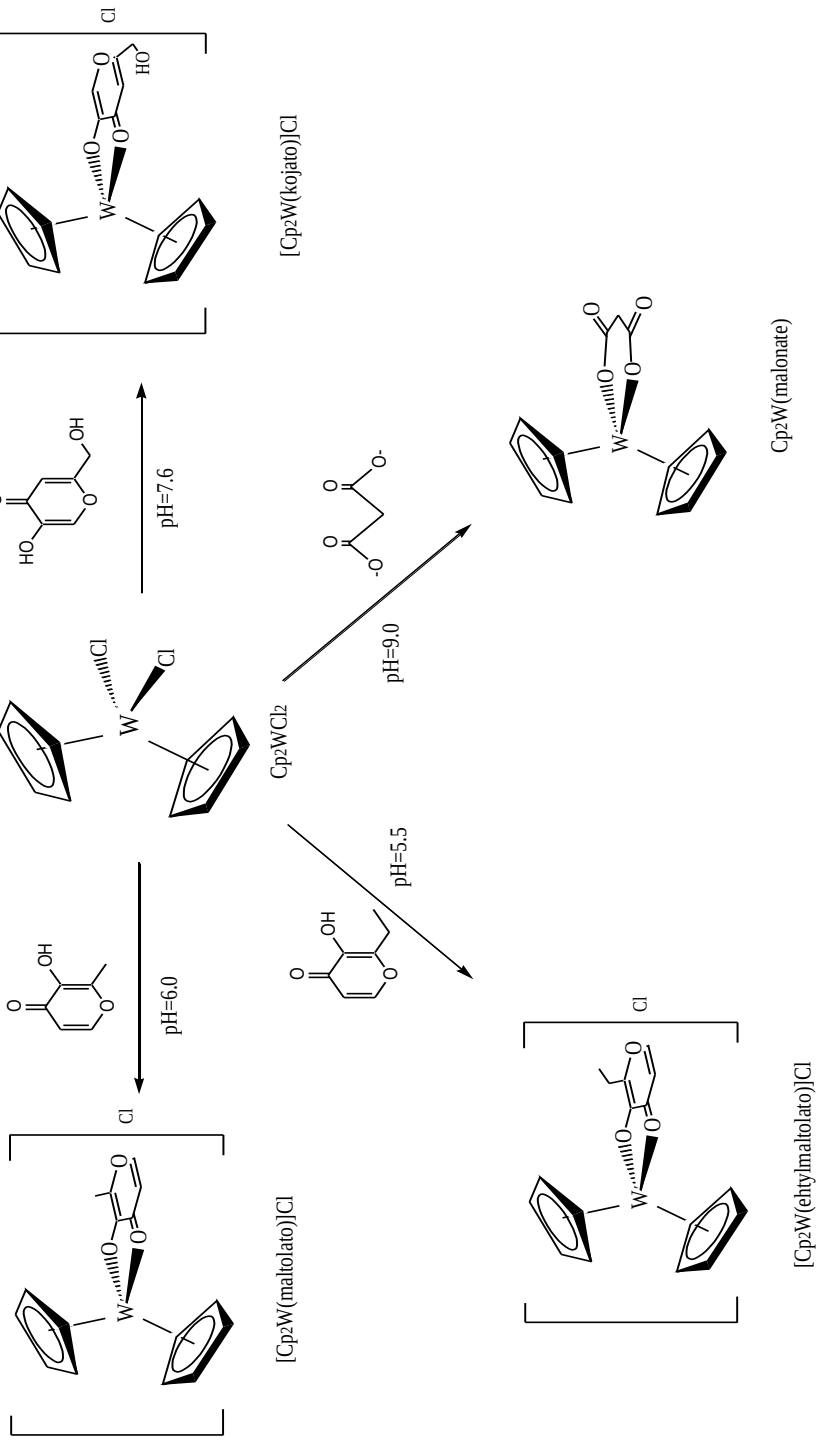


**Scheme 2.1** Synthesis of tungstenocene derivatives complexes

## 2.2 Characterization of tungstenocene derivatives

The new tungstenocene derivatives were characterized by Nuclear Magnetic Resonance (NMR), Fourier Transform Infrared (FT-IR), UV-Vis spectroscopy, elemental analysis, cyclic voltammetry.

### 2.2.1 Solubility properties

A solubility test for the new complexes was performed with the purpose of determining the polarity of complexes and the best solvent to achieve their structural characterization. A small amount of each complex was dissolved in ethanol, methanol, water, tetrahydrofurane, dimethylsulfoxide, dichloromethane, acetone, acetonitrile, chloroform, toluene and their solubility was evaluated qualitatively.

### 2.2.2 $^{1}$H-NMR Spectroscopy

The purity of tungstenocene dichloride, ligands, and the structures of the new tungstenocene derivatives were determined by NMR spectroscopy. The samples were dissolved in DMSO-$d_6$ 99.9% from Aldrich, with malonate and $Cp_2W$(malonate) exception, which were dissolved in $D_2O$ 99.9% from Aldrich due to malonate is insoluble in DMSO. A 500 MHz (11.74 Tesla magnetic field) Bruker Advance NMR Spectrometer with temperature control and Linux software was used to record $^{1}$H-NMR spectra.

### 2.2.3 FT IR Spectroscopy

The functional groups from tungstenocene dichloride, ligands and synthesized complexes were identified by FTIR spectroscopy. The IR spectra were recorded on a FT-IR Spectrometer PARAGON 1000 PC (Perkin Elmer) with samples as compressed KBR disc. Data collection was performed using the Spectrum RX (v3.02) software.

### 2.2.4 Elemental Analysis

The C and H content was determined through of an elemental analysis with the objective to corroborate the chemical formula of the tungstenocene derivatives. These analyses were carried out by Atlantic Microlab, in Georgia.

### 2.2.5 UV-Vis Spectroscopy

UV-Vis spectra were recorded in a double beam Jasco V-560 spectrophotometer at room temperature. Solutions of tungstenocene dichloride, tungstenocene derivatives and ligands at $5.0x10^{-4}$ M were prepared in a buffer solution of 0.1 M Tris-HCl/10 mM NaCl at pH 7.4.

### 2.2.6 Cyclic voltammetry

Electrochemical characterizations for tungstenocene dichloride, tungstenocene derivatives and ligands were carried out using an Epsilon Voltammetric analyzer with BASi Cell Stand C3, using Epsilon EC-2000XP software. The samples were dissolved in acetonitrile to observe reversible redox behavior and buffer Tris solution to observe the irreversible oxidation process in aqueous systems.

Tungstenocene dichloride, tungstenocene derivatives and ligands solutions (0.001 M) were prepared in an acetonitrile (0.1 M $Bu_4NPF_6$) to act as supporting electrolyte. Glassy carbon (BAS model MF-2012) was used a as working electrode, Ag/AgCl 3.0 M NaCl as a reference electrode and a Pt wire as auxiliary electrode. For the electrochemical characterization in aqueous solution, complexes and ligands solutions ($5.0x10^{-4}$ M) were prepared in Tris buffer (0.1 M Tris-HCl, 10 mM NaCl, and pH 7.4) and KCl (0.1 M) as supporting electrolyte and using the same working and reference electrode mentioned above.

The glassy carbon electrode cleaning procedure consisted of polishing with 0.05 μm alumina slurry, sonicating for 2 minutes in deionized water and drying with nitrogen. This process was achieved before each electrochemical measurement. The sweep was performed from 1500 to -0.1 mV for complexes dissolved in acetonitrile and 1000 to 0 mV for complexes dissolved in buffer solution with a scan rate of 100 mV/s and sensitivity of 100 μA.

## 2.3 Results and Discussion

### 2.3.1 Synthesis of tungstenocene derivatives

The tungstenocene dichloride is an organometallic complex consisting of two cyclopentadienyl (Cp) rings and two chloride ligands. The aromatic cyclopentadienyl rings have a delocalized negative charge that allow them to act both as σ or π-donors and π-acceptors to form a coordinated covalent bond with W(IV) and the chloride ligands act as lewis bases (weak σ and π-donors to metal), resulting in a pseudo-tetrahedral complex of 18 electrons (2 electrons from W (IV, $d^2$), 6 electrons from every ring, and 2 electrons from each $Cl^-$) [44].

The new tungstenocene complexes were prepared through the replacement of the chlorides by bidentade ligands; maltol, ethylmaltol, kojic acid and malonate. During the synthesis, initially the tungstenocene dichloride was dissolved in water, and the pH was increased to assure the ligand deprotonation, allowing the coordination between W(IV) and the bidentade ligands. A color change was observed from dark violet to amber, or to light pink for $Cp_2W$(malonate). The chloride replacement by the ligands provide more aqueous stability for the new complexes as compared with tungstenocene dichloride, due to the fact that W(IV) is a hard acid and the $Cl^-$ ligands are being replaced by hard bases (oxygen containing ligands).

On the other hand, maltol, ethylmaltol and kojic acid are bulky, monobasic ligands from 3-hydroxy-4-pyrone family, which are widely used as O,O-donor ligands because they have high affinity toward metal ions forming highly stable complexes at physiological pH. Their potential as ligand is due to the zwitterionic pseudo-aromatic character (scheme 2.2) on the heterocycle ring [26,31]. This feature allows them to act as a good π-donors toward W(IV), forming stable tungstenocene derivatives complexes with yields of 90, 85, and 75 % for maltol, ethylmaltol and kojic acid respectively. While malonic acid is a dibasic, small and not aromatic ligand, consequently it acts as σ and π-donor (hard base). It can explain the low percentages yield (35%) and its decomposition in aqueous media after purified (± 6h).

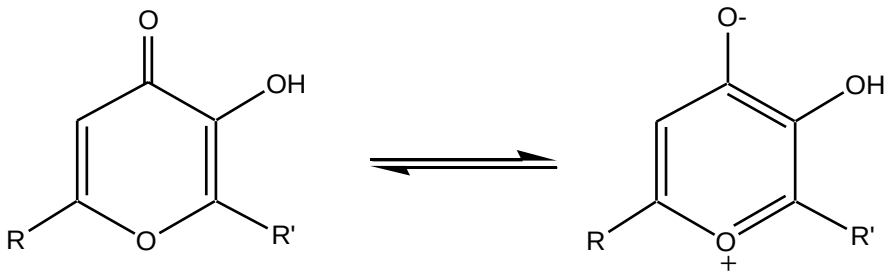


**Scheme 2.2** Zwitterionic forms of 3-hydroxy-4-pyrone, R=H or OH, R´= $CH_3$ or $C_2H_5$

### 2.3.2 Solubility properties

The ligands used are water soluble and they were chosen with the objective of to produce soluble complexes at physiological conditions. As a result, the tungstenocene derivatives complexes are soluble in protic and aprotics polar solvents through hydrogen bond or dipolar moment respectively, and they are insoluble in non polar solvents (table 2.1). Their solubility is due to polarity provided by the ligands.

| Solvent | Soluble | Partially soluble | Insoluble |
|---|---|---|---|
| Water | X | | |
| Methanol | X | | |
| Ethanol | X | | |
| Dimethyl sulfoxide | X | | |
| Chloroform | | X | |
| Dichloromethane | | X | |
| Acetone | | | X |
| Acetonitrile | | | X |
| THF | | | X |
| Toluene | | | X |

**Table 2.1** Solubility of tungstenocene derivativescomplexes**.**

### 2.3.3 $^{1}$H-NMR Spectroscopy

The $^{1}$H NMR spectra of tungstenocene dichloride and the new complexes were taken in DMSO-$d_6$, and $D_2O$. All spectra showed down field shifts in comparison with both free ligands and tungstenocene dichloride complex (A.1.1), which shows a singlet at 5.64 from Cp protons. It is due to electron density around the CH groups is reduced by the bond formed between oxygen atom from ligand and W(IV).

Figure 2.1 shows the $^{1}$H-NMR spectrum of the [$Cp_2W$(maltolato)]Cl complex in DMSO-$d_6$. The spectrum shows a signal at 5.91 ppm from Cp protons, a singlet at 2.36 ppm from $CH_3$, and two doublets at 8.36 and 7.05 from protons A and B of maltolato, respectively. In comparison with the free maltol spectrum (A.1.2), down field shifts are observed for A (8.02 ppm) and B (6.34 ppm) protons, and the OH signal at 8.82 ppm disappears corroborating the formation of a complex.

Figure 2.2 shows the $^{1}$H-NMR spectrum of the [$Cp_2W$(ethylmaltolato)]Cl complex in DMSO-$d_6$. The spectrum shows a signal at 5.91 ppm from Cp protons, a triplet at 1.14 ppm from $CH_3$, a quartet at 2.71 ppm from $CH_2$, and two doublets at 8.39 and 7.06 ppm from protons A and B of ethylmaltolato. In comparison with the free ethylmaltol spectra (A.1.3), down field shifts are observed for A (8.06 ppm) and B (6.34 ppm) protons, and the OH signal at 8.85 ppm disappears suggesting the formation of a complex.

Figure 2.3 shows the $^{1}$H-NMR spectrum of the [$Cp_2W$(kojato)]Cl complex in DMSO-$d_6$. The spectrum shows a signal at 5.92 ppm from Cp protons, a singlet at 4.5 ppm from $CH_2$, and two doublets at 8.36 and 6.99 ppm from protons A and B of kojato ligand. In comparison with the free kojic acid spectrum (A.1.4), down field shifts are observed for A (8.03 ppm) and B (6.34 ppm) protons, and the OH signal at 9.07 ppm disappears confirming the formation of a complex.

Figure 2.4 shows the $^{1}$H-NMR spectrum of the $Cp_2W$(malonate) complex in $D_2O$. The spectrum shows only two signals, one of these at 5.84 ppm from Cp protons, and a singlet at 3.27 ppm from $CH_2$ of malonic ligand. In comparison with the free malonate spectra (A.1.5), a down field shift is observed for $CH_2$ of free malonic ligand (3.05 ppm).

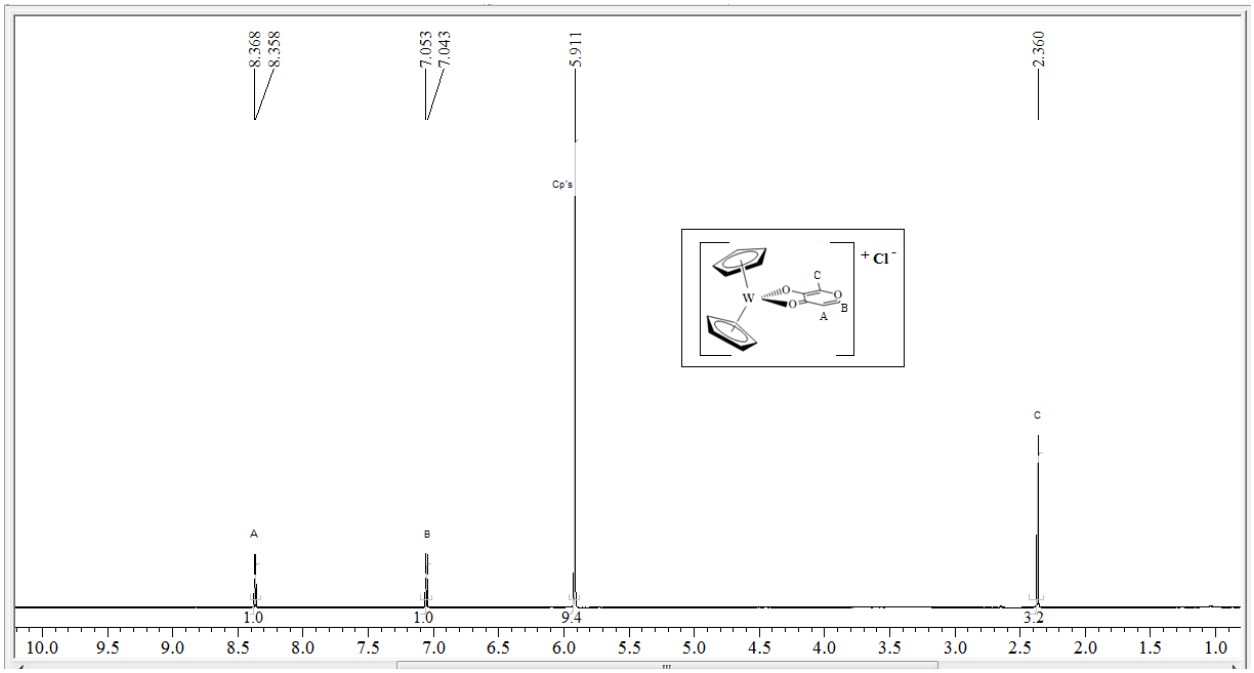


**Figure 2.1** $^{1}$H-NMR spectrum of [$Cp_2W$(maltolato)]Cl in DMSO-$d_6$

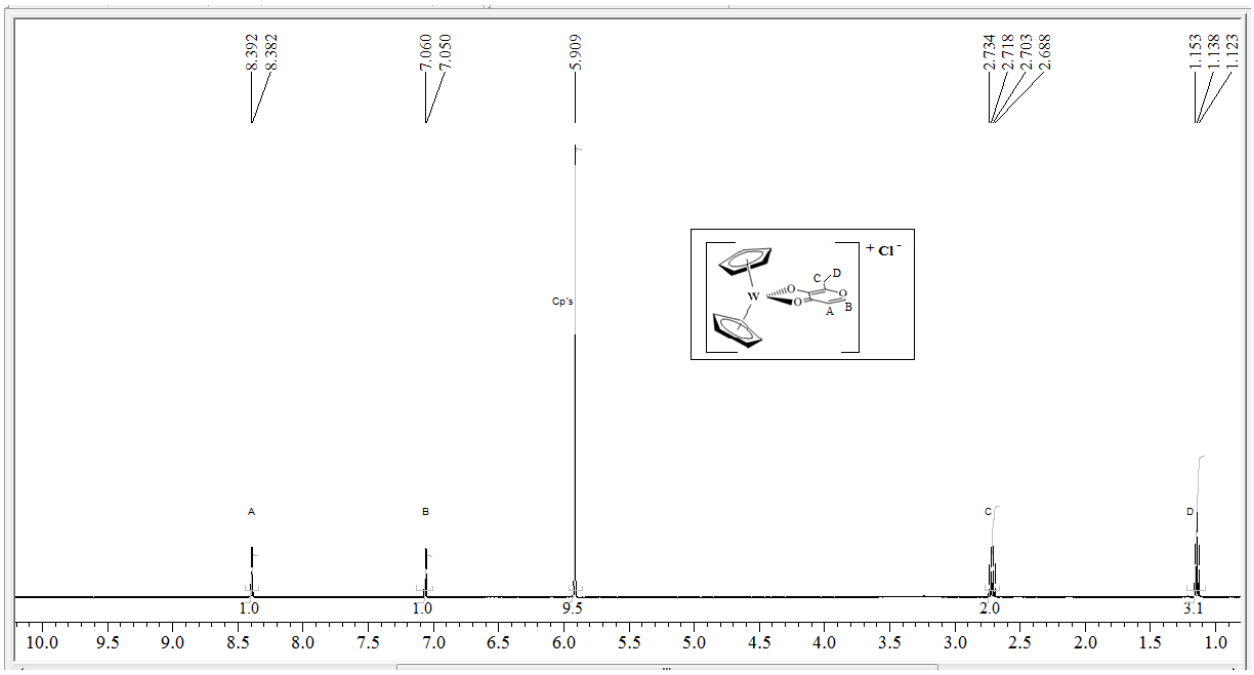


**Figure 2.2** $^{1}$H-NMR spectrum of [$Cp_2W$(ethylmaltolato)]Cl in DMSO-$d_6$

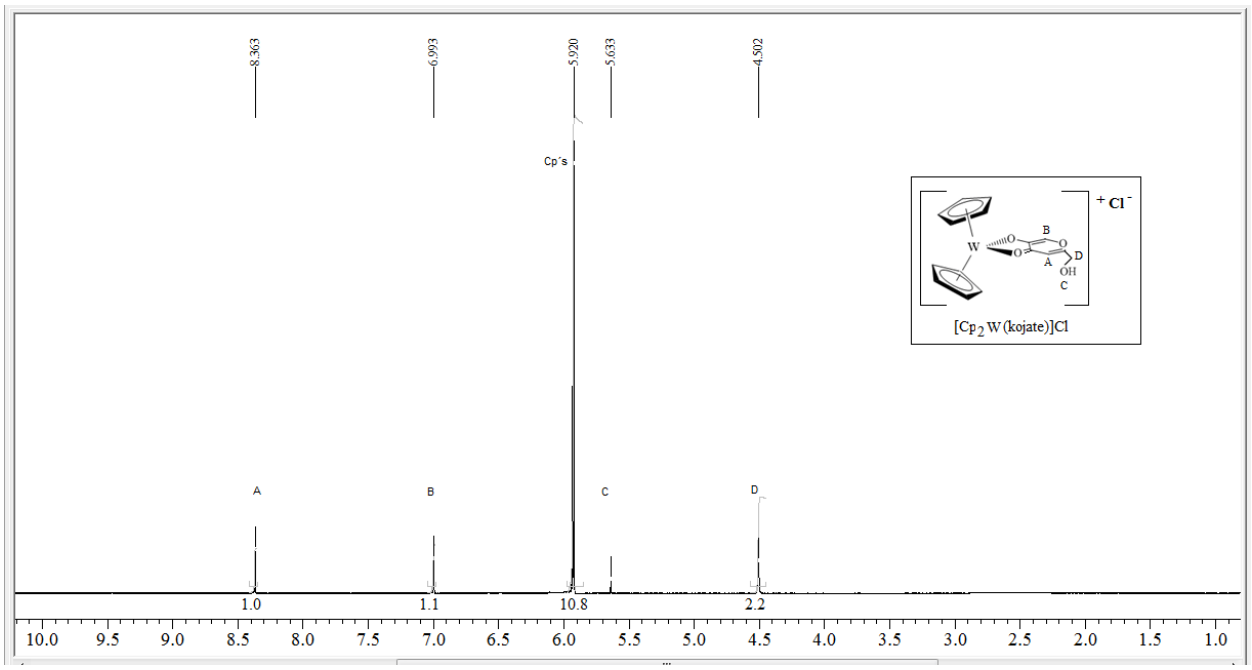


**Figure 2.3** $^{1}$H-NMR spectrum of [$Cp_2W$(kojato)]Cl in DMSO-$d_6$

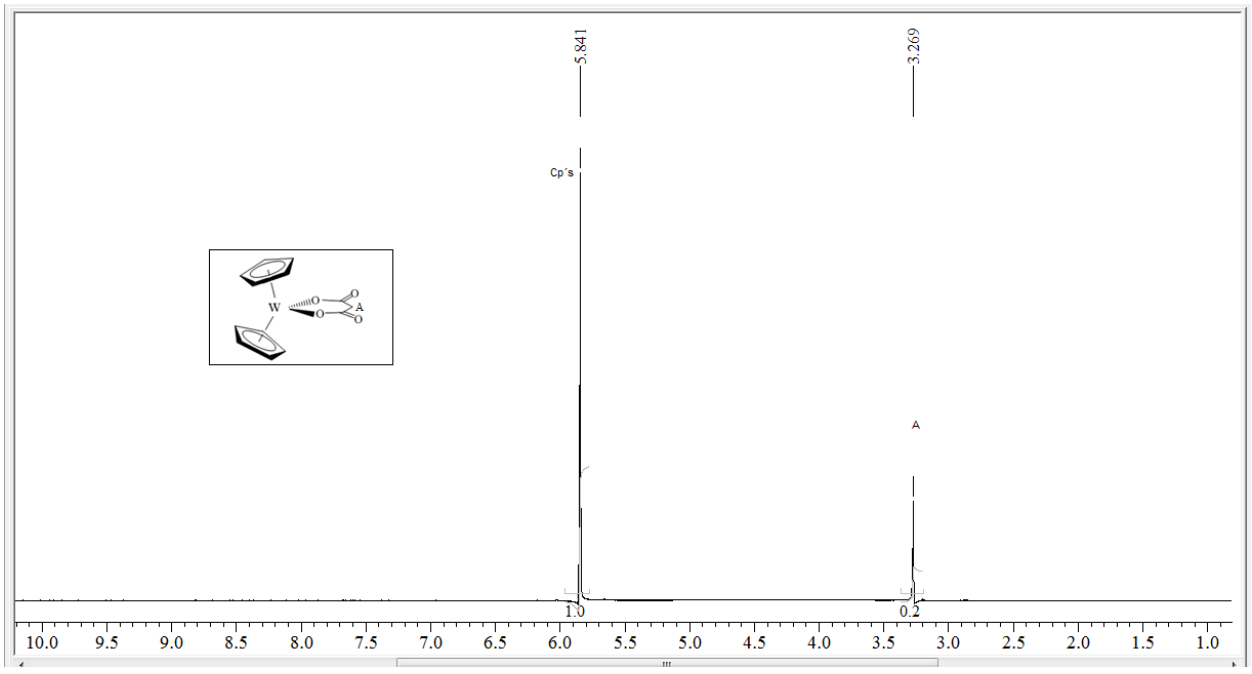


**Figure 2.4** $^{1}$H-NMR spectrum of $Cp_2W$(malonate) in $D_2O$

### 2.3.4 FT IR Spectroscopy

The infrared analysis was achieved for ligands, tungstenocene dichloride, and new complexes with the objective to compare the different functional groups and to examine how they change when the new complexes are formed. In general, the tungstenocene derivatives show characteristic bands from both Cp rings and their bidentade ligand respectively. The C-H stretching band from Cp (3114 $cm^{-1}$) appears at lower energy in the derivatives due to Cp rings and the ligands in the new complex getting $\pi$ back bond donation from W(IV), while the chlorides in tungstenocene are only $\pi$ donor. Therefore W(IV) donates more electronic density to Cp rings in new complexes than tungstenocene dichloride, as consequence the W-Cp bond in new complexes is stronger and the CH stretch vibrations are weaker generating that bands appear at shorter wavenumber, suggesting the complexes formation.

Likewise, the characteristic C=O bands from the free maltol, ethylmaltol and kojic acid ligands appear at 1652-1662 $cm^{-1}$, but in the new complexes appear at lower wavenumber (1605-1600 $cm^{-1}$) due to the coordination of carbonyl oxygen with W(IV). Furthermore, the combination bands of [$\nu$(C=O) + $\nu$(C=C)] at 1620-1634 $cm^{-1}$ and 1568-1582 $cm^{-1}$ in free ligands are also shifted to lower wavenumber (1548-1550 $cm^{-1}$ and 1470-1478 $cm^{-1}$). The characteristic C-O bands from the ligands appear at 1200 $cm^{-1}$ approximately, and in the new complexes this band appear at a higher energy due to coordination presented with W(IV), therefore the C-O bond strength increase, and its stretch vibrations are stronger, appearing at higher wavenumber.

These observations suggest that the ligands are coordinated as bidentades (O, O')-donor forming a five member ring with W(IV). Additionally, the new complexes show a shoulder at 3400 $cm^{-1}$

approximately, it is attributed to OH stretching from the presence of lattice water in the new complexes.

Table 2.2 summarizes the IR data for each $Cp_2WCl_2$, maltol, and [$Cp_2$W(maltolato)]Cl, and the figure 2.5 shows the their IR spectra respective to compare the different functional groups. Moreover, the band at 3274 $cm^{-1}$ in free maltol is attributed at ν(OH), which disappears when the oxygen coordinates to W(IV) after its depronation, corroborating the formation of complex.

Table 2.3 summarizes the IR data for each $Cp_2WCl_2$, ethylmaltol, and [$Cp_2$W(ethylmaltolato)]Cl, and the figure 2.6 shows the overlapping of their spectra. The band at 3200 $cm^{-1}$ in free ethylmaltol is attributed at ν(OH), which disappears when the oxygen coordinates to W(IV) after its depronation, confirming the formation of complex.

The table 2.4 summarizes the IR data for $Cp_2WCl_2$, kojic acid, and [$Cp_2$W(kojato)]Cl, and the figure 2.7 shows the three IR spectra overlapped to compare their different functional groups. The kojic acid exhibit a band at 3336 $cm^{-1}$ attributed at ν(OH) from both hydroxyl groups, while the [$Cp_2$W(kojato)]Cl shows two band at 3400 and 3216 $cm^{-1}$, which are attributed at ν(OH) from water lattice and OH group of kojato in the complex.

Table 2.5 summarizes the IR data for $Cp_2WCl_2$, malonate, and $Cp_2$W(malonate), and the figure 2.8 shows the three IR spectra overlaid. The $Cp_2$W(malonate) shows two bands at 1644 and 1348 $cm^{-1}$, which are attributed to C=O and C-O stretching respectively. These bands are at energy higher in comparison with free ligand due to malonate chelation that increase double bond characters on the carbonyl group, therefore these vibrations appear at higher wavenumber.

| Functional group | $Cp_2WCl_2$ ($cm^{-1}$) | Maltol ($cm^{-1}$) | [$Cp_2W$(maltolato)]Cl ($cm^{-1}$) |
|---|---|---|---|
| OH stretch | | 3274 | 3434 |
| CH stretch, Cp | 3114 | | 3086 |
| CH stretch | | 3058 | 3044 |
| C=O stretch | | 1656, 1632 | 1605,1548 |
| C=C stretch | 1426 | 1574 | 1430, 1478 |
| C-O stretch | | 1253, 1200 | 1270,1208 |
| CH deformation, Cp | 1010 | | 925 |
| CH deformation | 838 | 850 | 846 |
| CH bending | | 688 | |
| W-Ligand stretch | 590 | | 564 |

**Table 2.2** Assignment for IR frequencies for $Cp_2WCl_2$, maltol, and [$Cp_2W$(maltolato)]Cl.

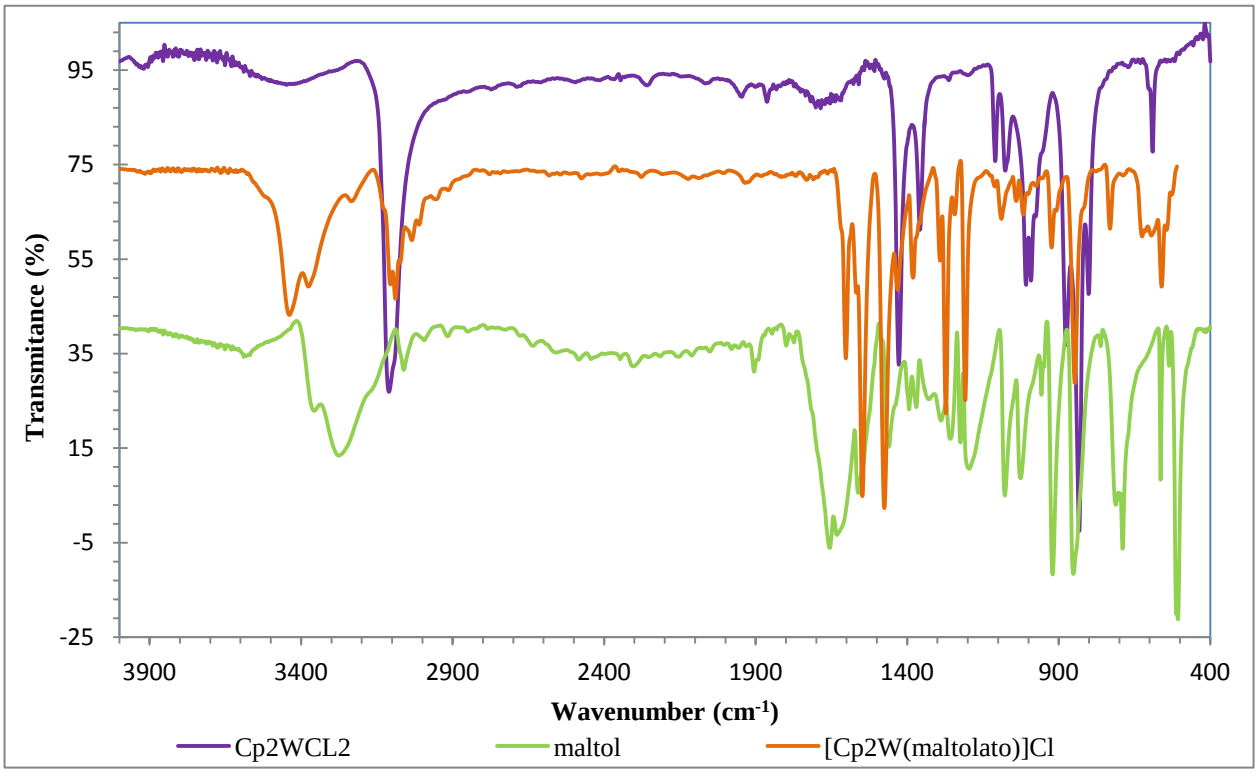


**Figure 2.5** IR spectra from $Cp_2WCl_2$, maltol, and [$Cp_2W$(maltolato)]Cl.

| Functional group | $Cp_2WCl_2$ ($cm^{-1}$) | Ethylmaltol ($cm^{-1}$) | [$Cp_2W$(ethylmaltolato)]Cl ($cm^{-1}$) |
|---|---|---|---|
| OH stretch | | 3200 | 3450 |
| CH stretch, Cp | 3114 | | 3046 |
| CH stretch | | 2988 | 2974 |
| C=O stretch | | 1652, 1620 | 1602, 1550 |
| C=C stretch, Cp | 1426 | 1568 | 1426, 1470 |
| C-O stretch | | 1192 | 1256, 1190 |
| CH deformation, Cp | 1010 | | 1000 |
| CH deformation | 838 | 976,938 | 946, 836 |
| CH bending | | 670 | |
| W-Ligand stretch | 590 | | 558 |

**Table 2.3** Assignment for IR frequencies for $Cp_2WCl_2$, ethylmaltol, and [$Cp_2W$(ethylmaltolato)]Cl.

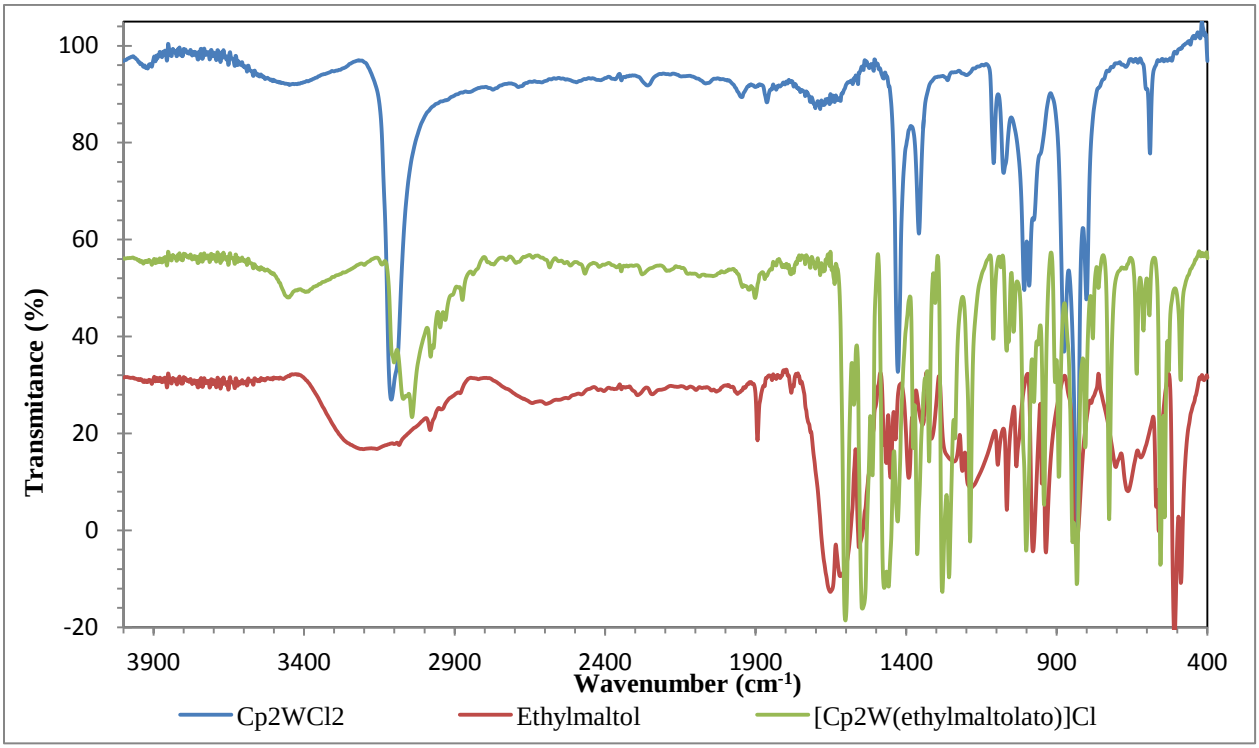


**Figure 2.6** IR spectra from $Cp_2WCl_2$, ethylmaltol, and [$Cp_2W$(ethylmaltolato)]Cl.

| Functional group | $Cp_2WCl_2$ ($cm^{-1}$) | Kojic acid ($cm^{-1}$) | $[Cp_2W(kojato)]Cl$($cm^{-1}$) |
|---|---|---|---|
| OH stretch | | 3336 | 3400, 3216 |
| CH stretch, Cp | 3114 | | 3105 |
| CH stretch | | 3090 | 3065 |
| C=O stretch | | 1662, 1634 | 1600, 1550 |
| C=C stretch, Cp | 1426 | 1582 | 1430, 1472 |
| C-O stretch | | 1273, 1238 | 1274, 1188 |
| CH deformation, Cp | 1010 | | 925 |
| CH deformation | 838 | 860 | 849 |
| CH bending | | 644 | |
| W-Ligand stretch | 590 | | 583 |

**Table 2.4** Assignment for IR frequencies for $Cp_2WCl_2$, kojic acid, and [Cp2W(kojato)]Cl.

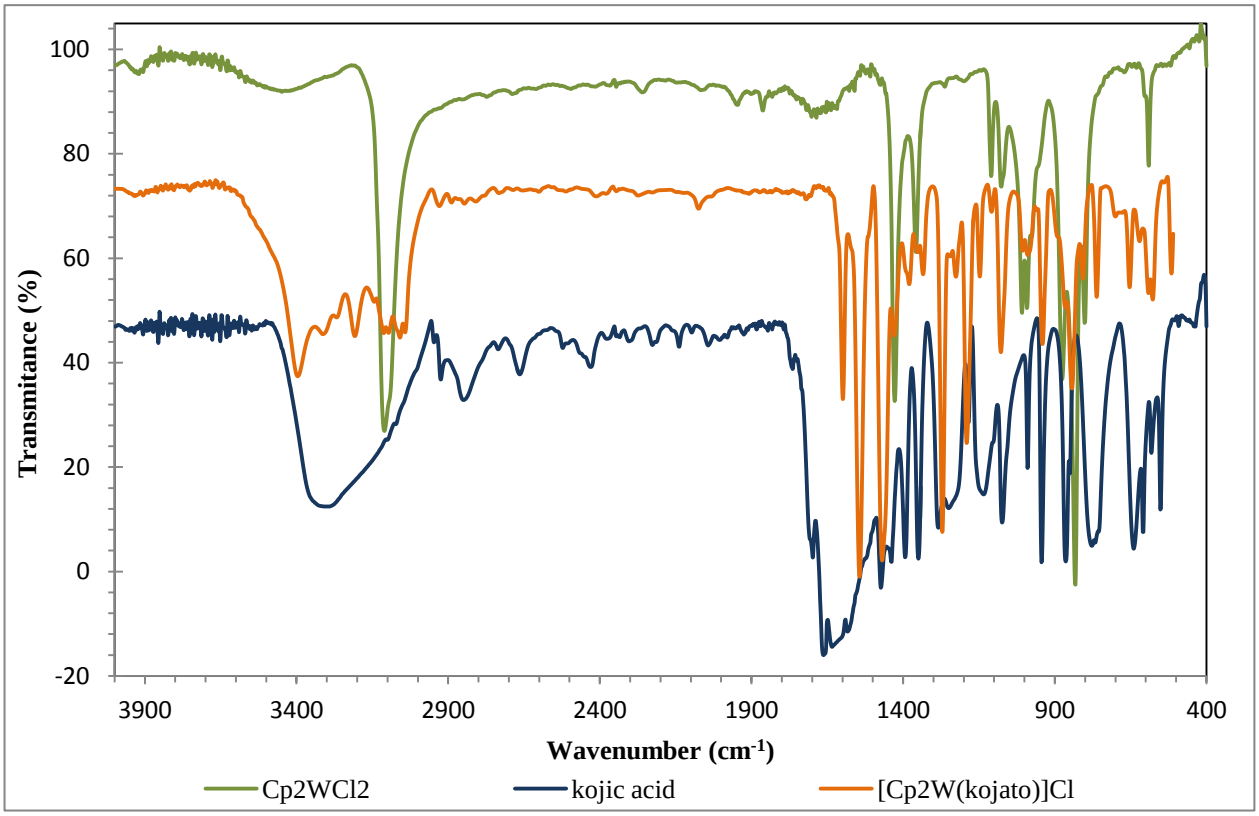


**Figure 2.7** IR spectra from $Cp_2WCl_2$, kojic acid, and [Cp2W(kojato)]Cl.

| Functional group | $Cp_2WCl_2$($cm^{-1}$) | Malonate($cm^{-1}$) | $Cp_2W$(malonate) ($cm^{-1}$) |
|---|---|---|---|
| OH stretch | | 3306 | 3420 |
| CH stretch, Cp | 3114 | | 3104 |
| C=O stretch | | 1600 | 1644 |
| C=C stretch, Cp | 1426 | | 1430 |
| C-O stretch | | 1348 | 1386 |
| CH deformation, Cp | 1010 | | 970 |
| CH deformation | 838 | 938 | 844 |
| CH bending | | 600 | |
| W-Ligand stretch | 590 | | 564 |

**Table 2.5** Assignment for IR frequencies for $Cp_2WCl_2$, malonate, and $Cp_2W$(malonate).

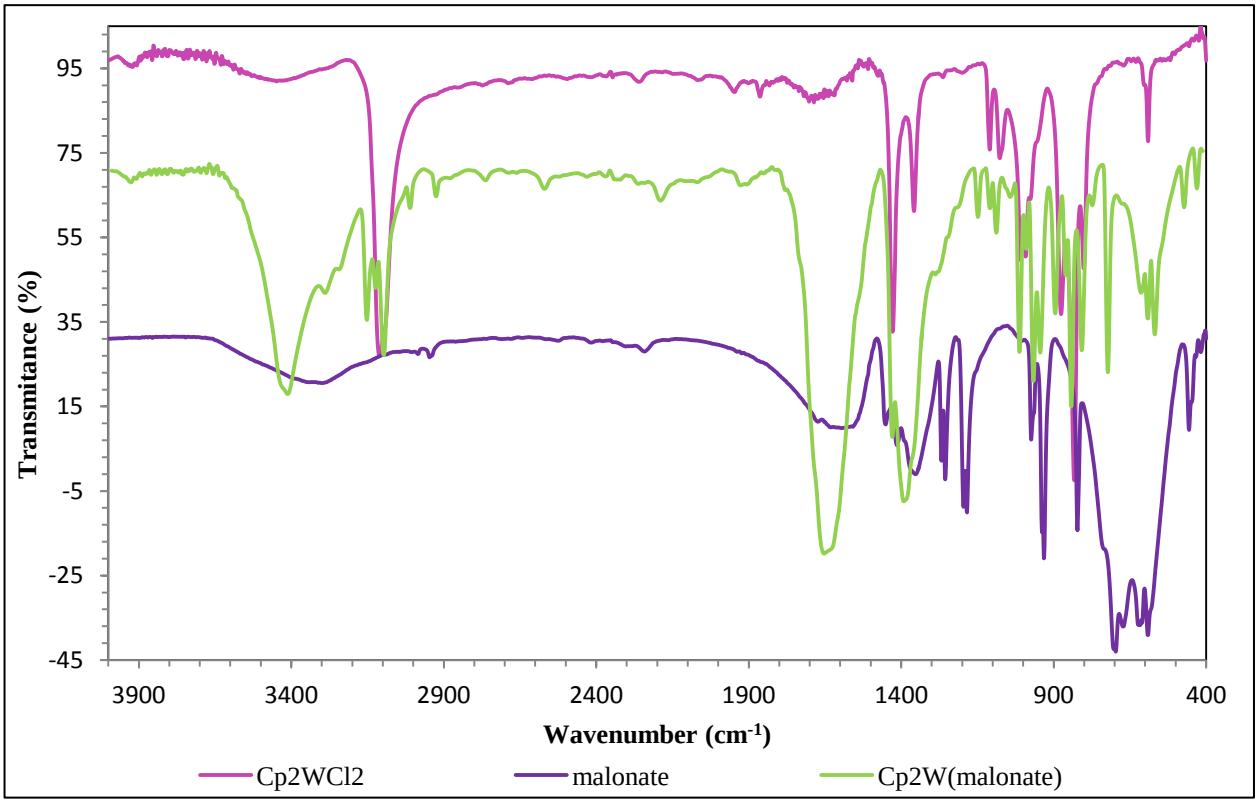


**Figure 2.8** IR spectra from $Cp_2WCl_2$, malonate, and [$Cp_2W$(malonate)]Cl.

### 2.3.5 Elemental analysis

Table 2.6 shows the experimental results of elemental analysis for the new complexes, which indicate they contain two Cp rings and their ligands respectively. The complexes are hygroscopic, hence the results show that they contain water must likely as solvate in their structures. In the case of complexes that contain maltol, ethylmaltol and kojic ligand, the results suggest that the complexes have a positive charge, which is equilibrated with the negative charge of chloride atom.

| **Complex** | **$C_{teor}$ (%)** | **$C_{exp}$ (%)** | **$H_{teor}$ (%)** | **$H_{exp}$ (%)** |
|---|---|---|---|---|
| $[Cp_2W(maltolato)]Cl\cdot(H_2O)$ | 39.02 | 38.89 | 3.32 | 3.33 |
| $[Cp_2W(ethylmaltolato)]Cl\cdot(H_2O)$ | 40.30 | 39.74 | 3.78 | 3.71 |
| $[Cp_2W(kojato)]Cl\cdot(H_2O)_{0.4}$ | 38.60 | 38.65 | 3.20 | 3.00 |
| $Cp_2W(malonate)(OH)_{1.8}$ | 34.85 | 34.87 | 3.11 | 3.07 |

**Table 2.6** Elemental analysis results of tungstenocene derivatives.

### 2.3.6 UV-Vis Spectroscopy

UV-Vis spectroscopy was used to compare the electronic transitions between tungstenocene dichloride and sinthesized complexes, which are shown in the table 2.7 and the figure 2.9, which corroborate the formation the new complexes. Tungstenocene dichloride exhibits an absorption band at 340nm, which is attributed to d-d transitions from W(IV), while the new complexes show a shift to red, appearing as a shoulder around 351 nm for $Cp_2W(malonate)$ and 420 nm for the others complexes. It is due to decreasing in $\Delta E$ between *e* and $t_2$ orbital promoted by the

formation of a new coordination bond. All complexes exhibit an absorption band about 210-233 nm, which is attributed at π-π* transitions from the Cp rings.

Figure 2.10 shows the absorption bands of ligands. Free malonate does not exhibit any absorption in UV-Vis region. However free maltol, ethylmaltol and kojic acid exhibit two absorption bands around 220 and 270 nm, which are attributed at n-π* and π-π* intraligand transitions. These bands are red shifted when the complexes are formed, suggesting the complexes formation.

| **Complex** | **$\lambda_{max}$ (nm)** | **ε (L/mol cm)** | **Peak assigment** |
|---|---|---|---|
| $Cp_2WCl_2$ | 210 | 8084 | π-π* transitions, intraligand Cp |
| | 340 | 205 | d-d transitions from W(IV) |
| $Cp_2W$(malonate) | 211 | 13832 | π-π* transitions, intraligand Cp |
| | 351 | 268 | d-d transitions from W(IV) |
| [$Cp_2W$(ethylmaltolato)]Cl | 227 | 20958 | n-π* and π-π* transition intraligand |
| | 333 | 6287 | n-π* and π-π* transition intraligand |
| | 420 | 317 | d-d transitions from W(IV) |
| [$Cp_2W$(maltolato)]Cl | 224 | 24910 | n-π* and π-π* transition intraligand |
| | 330 | 6287 | n-π* and π-π* transition intraligand |
| | 420 | 329 | d-d transitions from W(IV) |
| [$Cp_2W$(kojato)]Cl | 233 | 18743 | n-π* and π-π* transition intraligand |
| | 265 | 7545 | n-π* and π-π* transition intraligand |
| | 325 | 4012 | n-π* and π-π* transition intraligand |
| | 420 | 317 | d-d transitions from W(IV) |

**Table 2.7** Electronic spectral data from tungstenocene and its derivatives

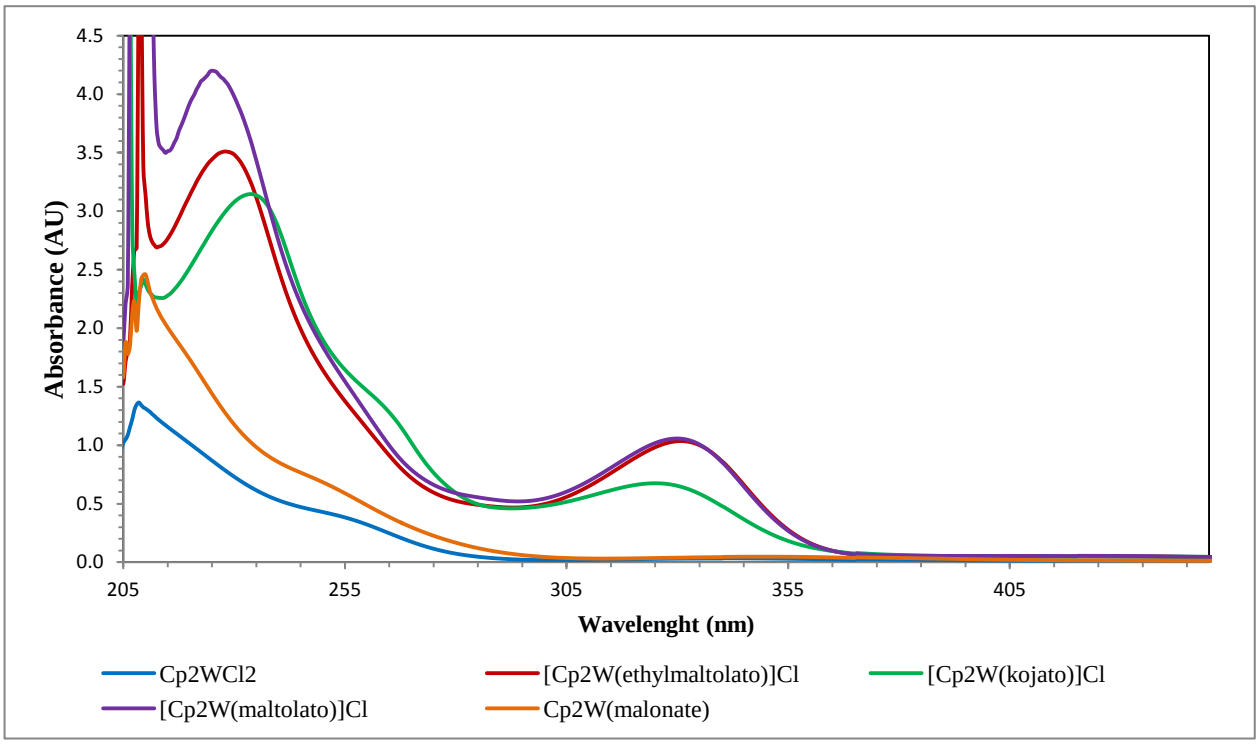


**Figure 2.9** UV-Vis spectra of tungstenocene and its derivatives

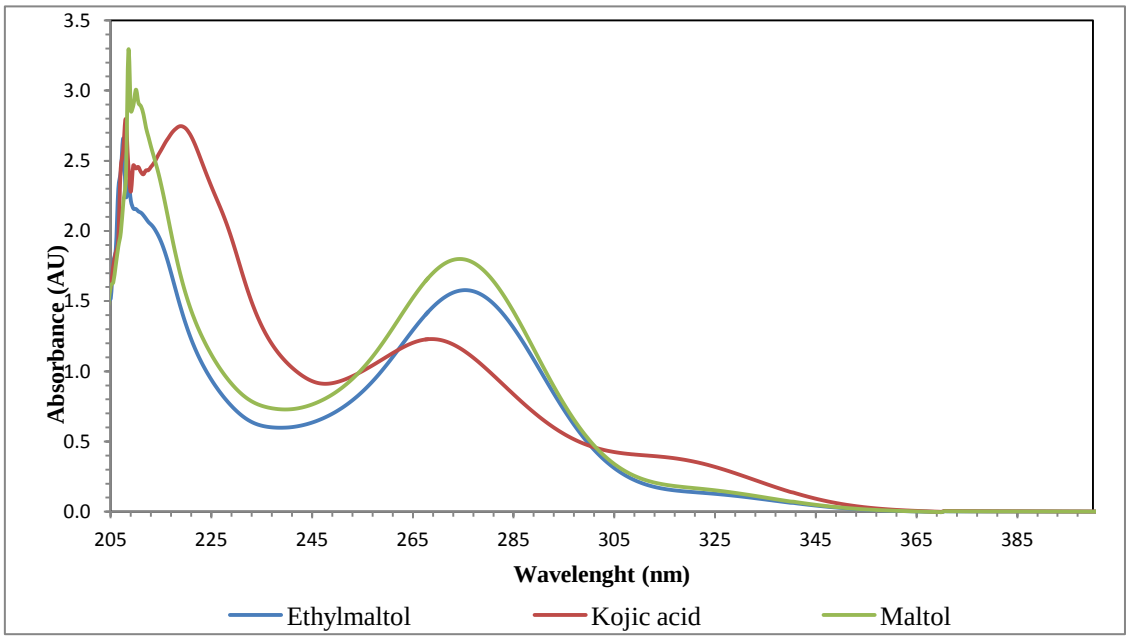


**Figure 2.10** UV-Vis spectra of free ligands

### 2.3.7 Cyclic voltammetry

Cyclic voltammetry studies about the complexes were achieved with the objective to observe the electrochemical behavior of new complexes. The figure 2.11 shows the redox behavior of tungstenocene dichloride and their derivatives in acetonitrile (0.1 M $Bu_4NPF_6$), it presents a reversible oxidation peak ($E_{pa}$ = 0.47 V), which involves one electron transfer attributed at $W^{V/IV}$ species, and a second reversible wave of small current at 1.0 V from formation of $[Cp_2W^{IV}(NCMe)Cl]^+$ / $[Cp_2W^{V}(NCMe)Cl]^{2+}$ species [45]. Whereas the tungstenocene derivatives complexes showed oxidation peaks at potentials higher than $Cp_2WCl_2$, suggesting a higher stability for the new species. The $Cp_2W$(malonate) voltammogram shows a reversible wave at 0.55 V, which is assigned to electron transfer of $W^{V/IV}$ species. The other tungstenocene derivatives showed two reversible oxidation peaks, which correspond to $W^{V/IV}$ redox couple in the range 0.67 – 0.73 V and redox couple of the 3-hydroxy-4-pyrones ligands in the complexes in the range 0.89 – 0.92 V.

The electrochemical study of the new complexes in aqueous system was carried out with the objective to observe their behavior in physiological conditions. The figure 2.12 shows irreversible oxidation of tungstenocene dichloride and the new complexes, which showed oxidation peaks at potentials higher than $Cp_2WCl_2$, suggesting a higher stability in aqueous solution under physiological conditions. The voltammograms exhibit two oxidation peaks; the first peak at potential more negative is attributed to the formation of W(V) or stable metal-oxo species making more difficult the reverse reduction process, and the second peak at potentials more positive is attributed to the irreversible oxidation of tris-(3-hydroxy-4-pyrones) species, since the voltammograms of the complexes in KCl (figure 2.13) showed the formation of W(V)

species assigned in potentials analogous to those of the first peak (figure 2.12), and the free ligands in Tris buffer solution showed irreversible oxidation peaks (figure 2.14) that appear at similar potentials to second peak in figure 2.11. In the case of $Cp_2W$(malonate) the oxidation peak due to malonate ligand is not present oxidation in buffer solution, however the figure 2.12 shows a second peak, which could correspond to irreversible oxidation of $W^V$-Tris species.

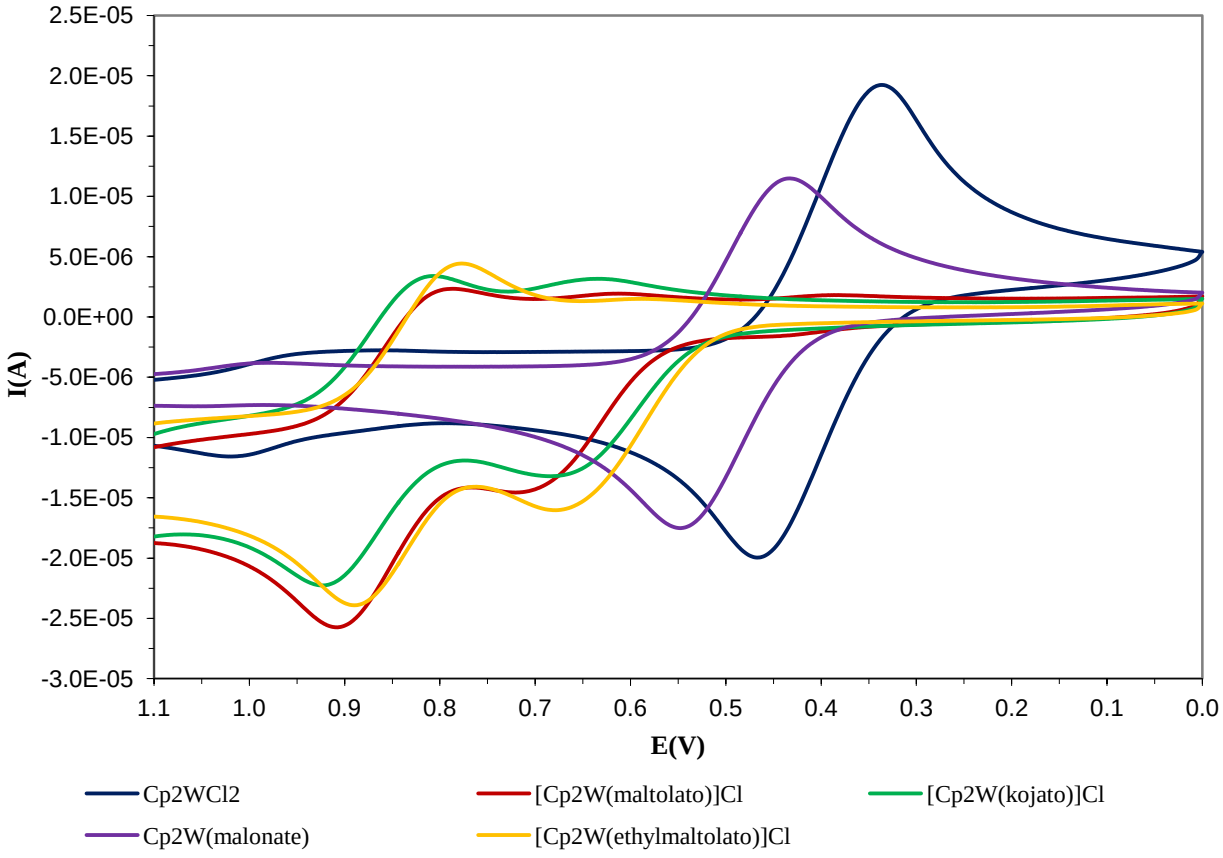


**Figure 2.11** Cyclic voltammograms of tungstenocene and the new complexes in acetonitrile (0.1M $Bu_4NPF_6$)

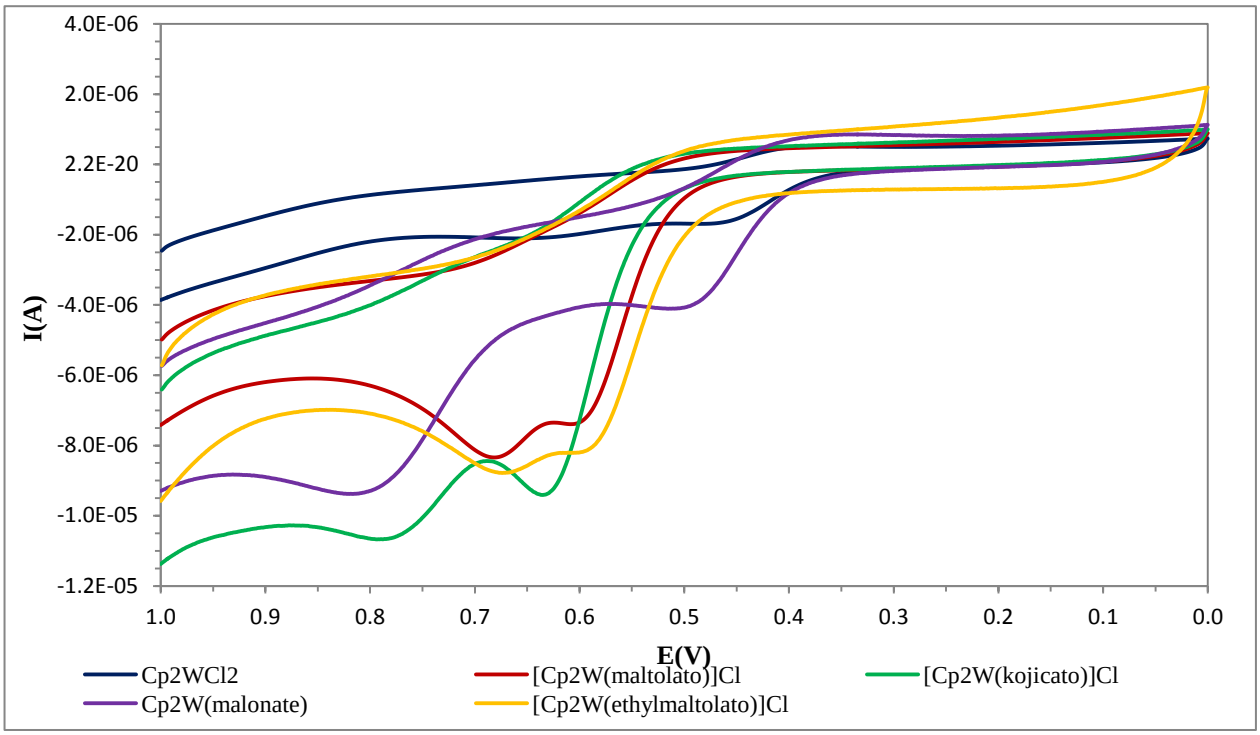


**Figure 2.12** Cyclic voltammograms of tungstenocene and its derivatives in Tris buffer (0.1 M).

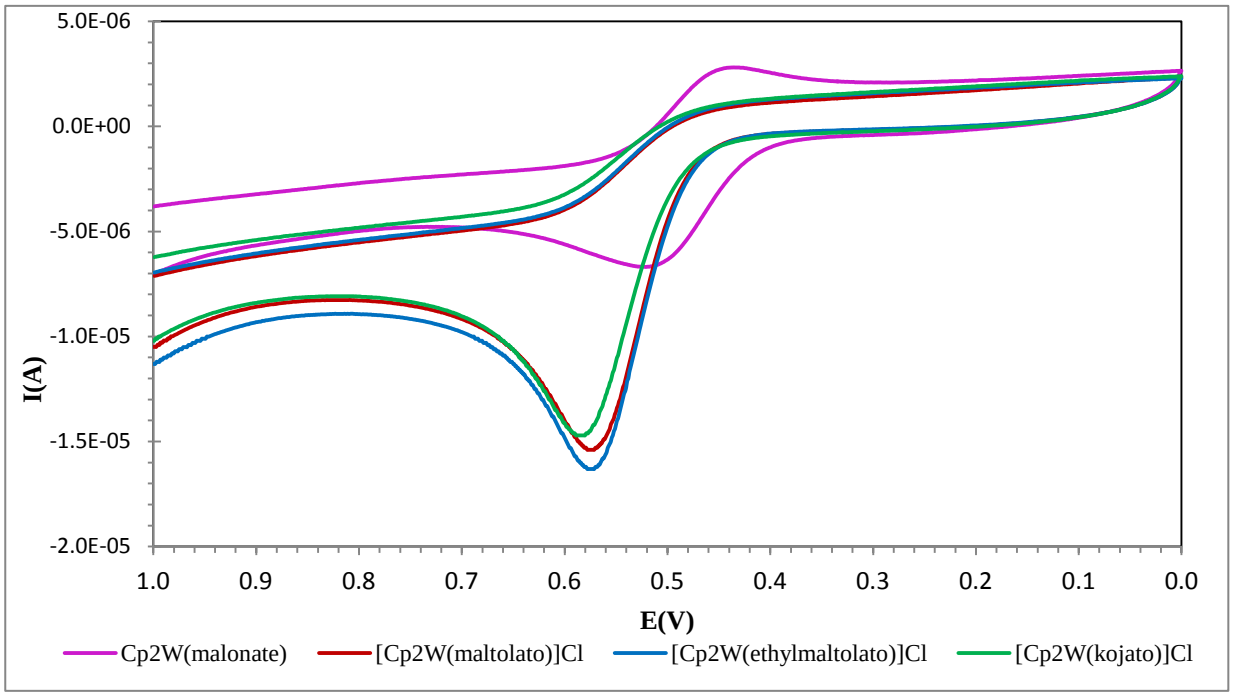


**Figure 2.13** Cyclic voltammograms of tungstenocene and its derivatives in KCl (0.1 M).

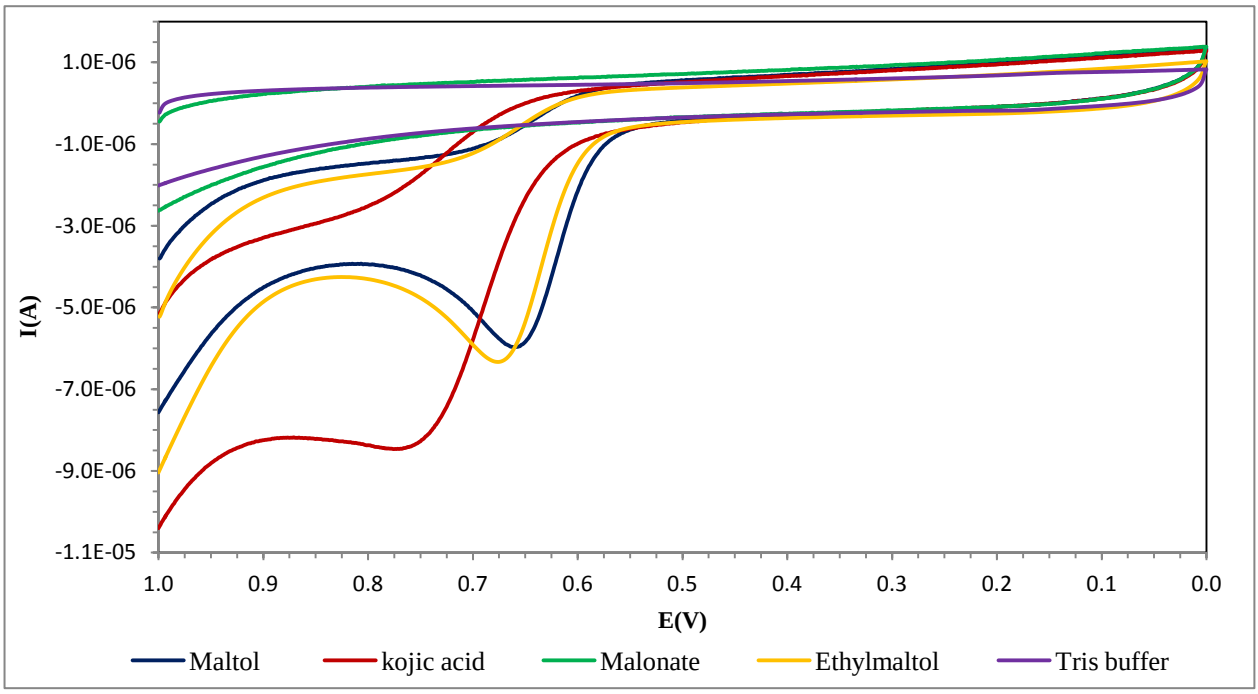


**Figure 2.14** Cyclic voltammograms of ligands in Tris buffer (0.1 M)

## 3. Cytotoxic activity on colon and breast cancer cells

Cytotoxic studies of tungstenocene dichloride and its derivatives on colon and breast cancer cell lines were achieved using a viability assay to observe the anticancer activity *in vitro*, calculating the concentration that inhibits 50% of cell growth ($IC_{50}$).

### 3.1 Materials and methods

#### 3.1.1 Materials

In the viability assay the following materials were used; 3-(4,5-dimethylthiazol-2-yl)-2,5-diphenyltetrazoliumbromide (MTT), Triton X-100, sodium chloride, potassium chloride, sodium phosphate and potassium phosphate, all purchased from Sigma-Aldrich and 2-propanol was purchased from Fisher. The cancer cells were grown and maintained in 75 $cm^2$ flask with canted neck, which were purchased from Corning and the dosifications were performed on Greiner 96 well plates from Cellstar.

#### 3.1.2 Cancer cell lines

The study was performed on colon cancer cells, which were donated by Dr. Jaime Matta from Pharmacology Department of Ponce School of Medicine, and the MCF-7 cancer cells were donated by Professor Madeline Torres from Chemical Engineer Department of University of Puerto Rico – Mayaguez.

HT-29 cancer cells were grown using McCoys´s 5A modified media with L-glutamine from ATCC, and MCF-7 cancer cell were grown using Hyclone DMEM / High glucose, supplemented with L-glutamine (4.00 mM), glucose (4.5 g/L) and sodium pyruvate purchased from Thermo

Scientific. The media were complemented with fetal bovine serum (10 %) purchased from Sigma-Aldrich. The antibiotic, antimycotic solution (1 %), was purchased from Cellgro and filtered with a bottle-top cellulose-acetate 0.2 μm filter before using. Both cancer cell lines were incubated in 75 $cm^2$ flask, under an atmosphere of air (95%) / CO2 (5%) USP grade at 37°C for its growing and maintaining.

### 3.1.3 MTT Cancer viability assay

The viability was evaluated seeding 10,000 cells (HT-29 or MCF-7) per well in a 96 well plate. After 24h of incubation, 25 μL of media per well were added to first two columns (control) and 25 μL of complex solutions per well dissolved in media were added to rest of the plate. Each column had a different concentration of complex starting since 0.01 to 0.00014 M, and then it was incubated by 72h. After incubation, 50 μL per well of a solution of MTT (2.4 mg/mL) dissolved previously in the medium was added and incubated by 2 hours, to produce purple formazan dye insoluble inside the mitochondria from living cell. When the time was completed, the cell medium was removed and rinsed with a cold phosphate buffer solution (PBS). Then, 180 μL per well of triton solution (10 %) in 2-propanol was added and incubated until the formazan purple crystals dissolved. The absorbance of the purple solutions resulting was measured at 490 nm achieving a background subtraction at 630 nm in a microplate reader ELx808 Biotek instruments. The $IC_{50}$ of complexes was calculated by fitting the data to sigmoidal dose response plot (variable slope) using Prism 3.0 software.

### 3.2 Results and Discussion

The concentration of tungstenocene dichloride and its derivatives to inhibit 50% of the cancer cells growth ($IC_{50}$) were obtained from MTT assay. This colorimetric method measures the absorbance produced by the reduction of MTT to formazan (scheme 3.1) in the living cell mitochondria. Therefore, the plot of complex/control absorbance versus the log complex concentration generates a sigmoidal curve of dose-response, which defines the percent of viability and the log complex concentration that induces changes in the cell viability.

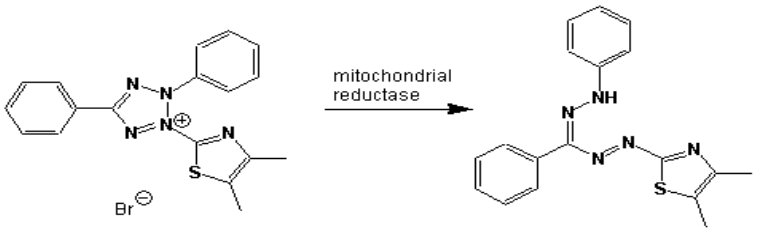


**Scheme 3.1** MTT reduction

The figure 3.1 shows the dose response curve of tungstenocene dichloride against colon cancer cell HT-29 and the figure 3.2 shows the dose response of tungstenocene derivatives. The cytotoxic values against cancer cell HT-29 are shown in the table 3.1, where the new complexes have higher cell inhibition ($IC_{50} \sim 10^{-4}$ M) in comparison with tungstenocene dichloride that presents an $IC_{50}$ of 10 (±1) mM. Therefore, the chloride replacement by the bidentade ligands in tungstenocene improves significantly the cytotoxic activity decreasing between one to two orders of magnitude approximately the concentration range. Moreover, examining the cytotoxic values of tungstenocene derivatives, it is possible to observe ligands with 3-hydroxy-4-pyrone group (maltolato, ethylmaltolato and kojato) have higher cytotoxic activity than $Cp_2W$(malonate), showing the lower value for [$Cp_2W$(kojato)]Cl with an $IC_{50}$ of 0.20 (±0.01) mM.

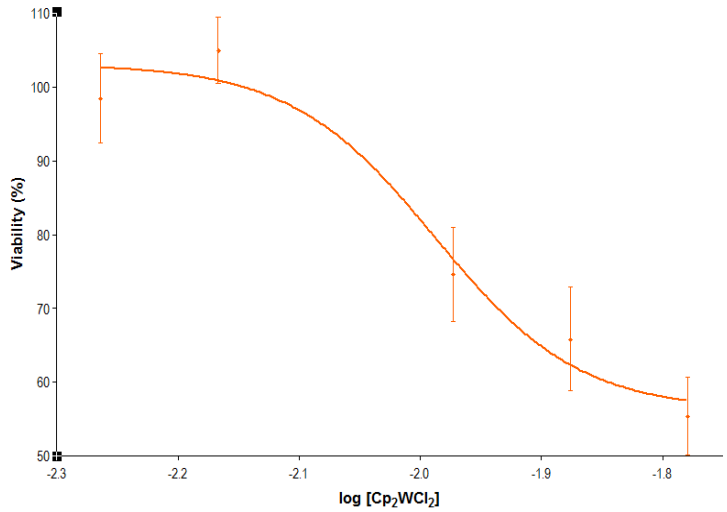


**Figure 3.1** Dose response curve of $Cp_2WCl_2$ against colon cancer cell HT29

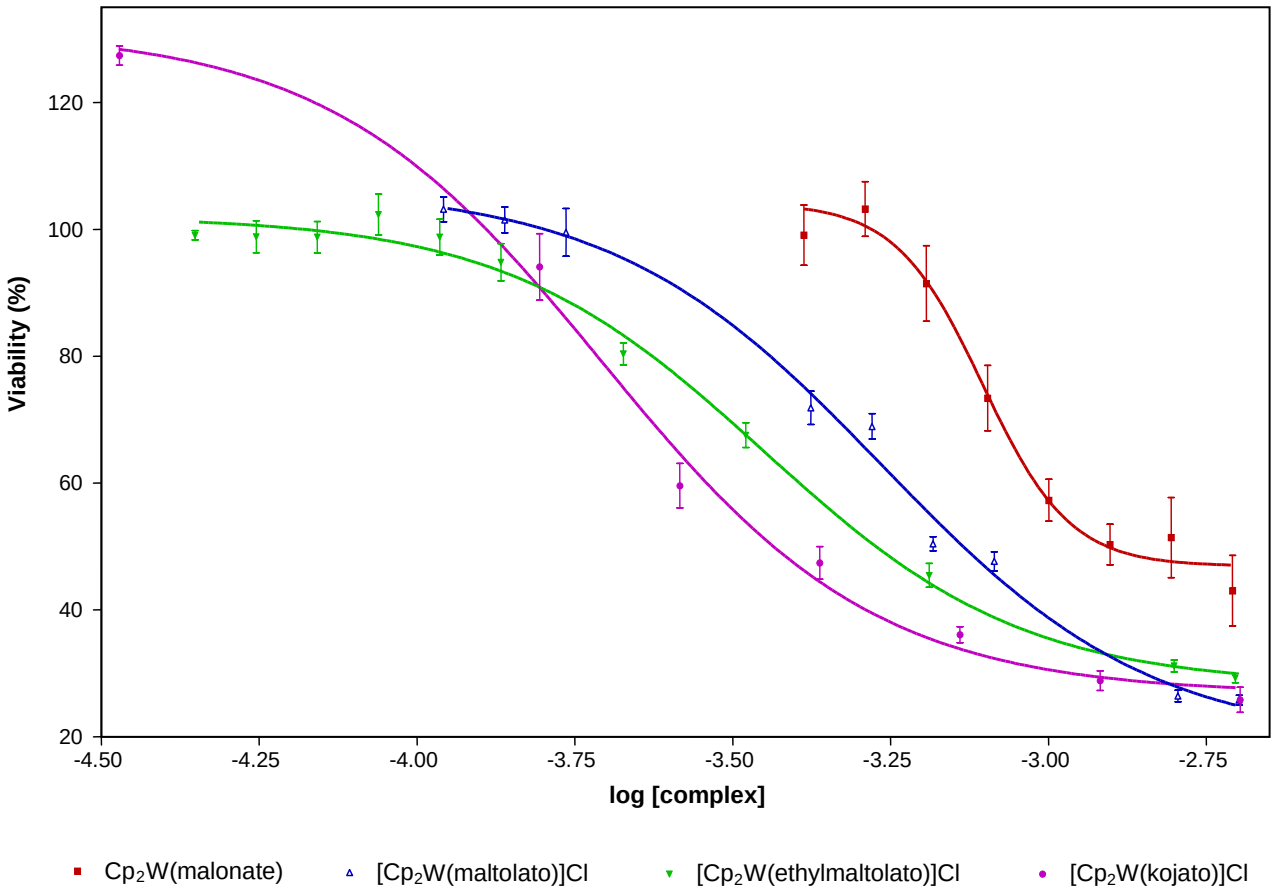


**Figure 3.2** Dose response curve of tungstenocene derivatives against colon cancer cell HT29

| Complex | $IC_{50}$ (mM) | SD (± mM) |
|---|---|---|
| $Cp_2WCl_2$ | 10 | 1 |
| $Cp_2W$(malonate) | 0.79 | 0.05 |
| [$Cp_2W$(maltolato)]Cl | 0.54 | 0.02 |
| [$Cp_2W$(ethylmaltolato)]Cl | 0.35 | 0.02 |
| [$Cp_2W$(kojato)]Cl | 0.20 | 0.01 |

**Table 3.1** Cytotoxic activity of tungstenocene and its derivatives against colon cancer cell HT-29

The figure 3.3 shows the dose response curve of tungstenocene dichloride and its derivatives against breast cancer cell MCF-7. The cytotoxic values are shown in the table 3.2, where the cell inhibition of the new complexes is same order of magnitude as tungstenocene dichloride ($IC_{50}$ ~ $10^{-4}$ M). However, the tungstenocene derivatives show $IC_{50}$ values slightly lower, showing the lower value for [$Cp_2W$(ethylmaltolato)]Cl with a concentration of 1.9 (±0.4) x$10^{-4}$ M. Therefore, the chloride replacement by the bidentade ligands in tungstenocene does not improve significantly the cytotoxic activity for MCF-7 breast cancer cell line.

Feliciano (2009) reported the cytotoxic activity of [$Cp_2Mo$(maltolato)]Cl and $Cp_2Mo$(malonate) complexes on HT-29 colon and MCF-7 breast cancer cell lines, obtaining $IC_{50}$ values of 1.31 (±0.02) mM and 1.9 (±0.3) mM respectively for HT-29, whereas for MCF-7 exhibited proliferative activities [35]. Comparing these results with those obtained from [$Cp_2W$(maltolato)]Cl and $Cp_2W$(malonate), a higher activity is observed for tungstenocene derivatives on HT-29 cells and a different behavior on MCF-7. Therefore, the metal plays an important role in the behavior and activity of the metallocenes, becoming sometimes difficult to predict.

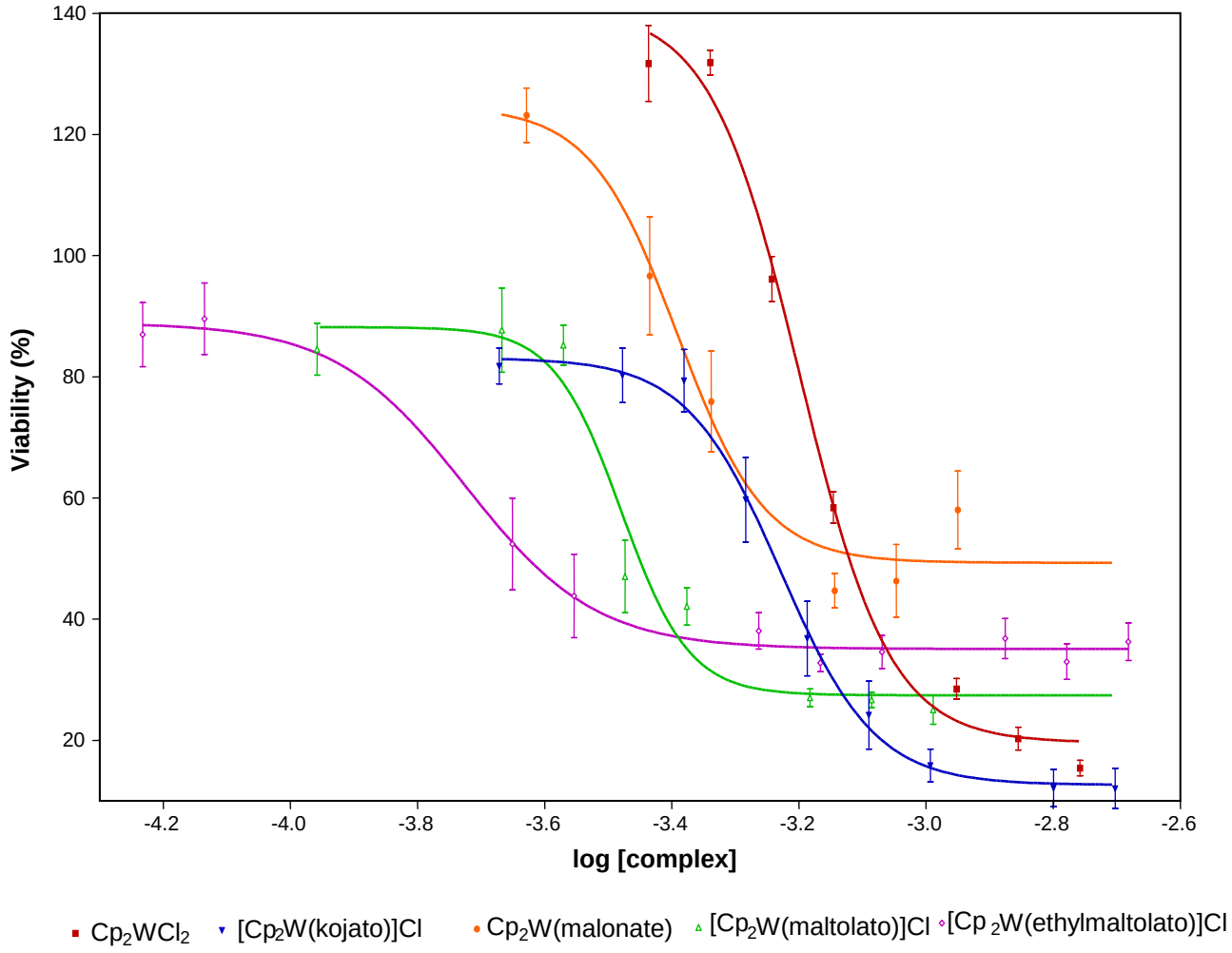


**Figure 3.3** Dose response curve of tungstenocene and its derivatives against breast cancer cell MCF-7

| Complex | $IC_{50}$ (mM) | SD (± mM) |
|---|---|---|
| $Cp_2WCl_2$ | 0.63 | 0.01 |
| [$Cp_2W$(kojato)]Cl | 0.59 | 0.03 |
| $Cp_2W$(malonate) | 0.41 | 0.03 |
| [$Cp_2W$(maltolato)]Cl | 0.33 | 0.01 |
| [$Cp_2W$(ethylmaltolato)]Cl | 0.19 | 0.04 |

**Table 3.2** Cytotoxic activity of tungstenocene and its derivatives against breast cancer cell MCF7.

# 4. Biological interaction of tungstenocene dichloride and its derivatives with human serum albumin (HSA) and human apo-transferrin (apo-hTf)

## 4.1 Materials and methodology

### 4.1.1 Tris buffer solution

A Tris buffer solution was used for the protein interaction studies to perform experiments under physiological conditions. This buffer solution was used to dissolve both protein and complexes. One liter of a Tris buffer solution was prepared by weighting 0.566 g of sodium chloride, and 12.114 g of tris(hydroxymethyl) aminomethane, which were dissolved in deionized water to obtain a concentration of 100 mM and 10 mM respectively. After dissolution, the pH was adjusted to approximately 7.4 using HCl 1.0 M.

### 4.1.2 Proteins solutions

The proteins, human apo-transferrin 97% (cell culture tested) and human serum albumin 99% (agarose gel electrophoresis, lyophilized powder) were used and obtained from Sigma-Aldrich. HSA and apo-hTf solutions at predetermined concentrations for each technique were prepared in buffer solution (see 4.1.1. section). Their concentrations were determined by UV-Vis using the absorbance at 280 nm in the Beer-Lambert equation, taking the absorptivity coefficient (ε) value as 35495$M^{-1}cm^{-1}$ for HSA and 93000 $M^{-1}cm^{-1}$ for apo-hTf and a cell width (b) of 1 cm. The absorbance measurements were performed on a Jasco V-560 UV-Vis spectrophotometer.

### 4.1.3 Complex solutions

Proper amounts of tungstenocene dichloride (Sigma Aldrich) and its derivatives were weighted and dissolved in buffer solution (see 4.1.1. section) in order to obtain predetermined

concentrations for each technique. The tungstenocene dichloride solution was sonicated during one hour approximately to obtain total dissolution.

### 4.1.4 Interaction studies by fluorescence spectroscopy

1.0 mL of HSA protein solution ($2.7x10^{-6}$ M) was titrated with 14 μL aliquots of complex solutions ($6.0\ x10^{-4}$ M), to reach molar equivalent of metal:protein to 1:3. 1.0 mL of apo-hTf protein solution ($7.5x10^{-7}$ M) was titrated with 15 μL aliquots of complex solutions ($6.0\ x10^{-4}$ M), to reach molar equivalent of metal:protein to 1:12. The fluorescence quenching spectra were obtained at two different temperatures, the excitation wavelength of $\lambda_{ex}$=280 nm and $\lambda_{em}$= 300–400 nm for emission in a RF-5301 PC spectrofluorophotometer Shimadzu equipped with a temperature controller and the data was recorded using RF-530XPC Software. All measurements were performed in duplicate.

### 4.1.5 Interaction studies by cyclic voltammetry

The interactions between protein (HSA and apo-hTf) and the complexes were evaluated through of change in the oxidation/reduction behavior by cyclic voltammetry. Ten mL of compound solutions ($5.0x10^{-4}$ M) were prepared in buffer and were titrated with 250 μL aliquots of HSA and apo-hTf solutions ($2.5\ x10^{-5}$ M). After each addition, a voltammogram was recorded between 1.0 and 0.0 V using glassy carbon as working electrode, Ag/AgCl as reference electrode and platinum wire as counter electrode.

The glassy carbon electrode was polished with 0.05 μm alumina slurry, sonicated by 2 minutes in deionized water and dried with gaseous nitrogen. This process was performed before each

electrochemical measurement. The measurements were performed in triplicates, using a scan rate of 100 mV/s in the Epsilon Voltammetric analyzer with BASi Cell Stand C3, with Epsilon EC-2000XP software.

## 4.2 Results and Discussion

### 4.2.1 Interaction by fluorescence spectroscopy

Titration studies between the proteins (HSA and apo-hTf) and the complexes by fluorescence spectroscopy were achieved with the objective to obtain information regarding metal-protein interaction. The fluorescence of HSA and apo-hTf is caused by three fluorophores; tryptophan, tyrosine, and phenylalanine residues. Actually, the fluorescence of both proteins comes almost completely from tryptophan, since phenylalanine has a very low quantum yield and tyrosine is quenched almost totally when an amino group, a carboxyl group, or a tryptophan is close. Tryptophan and tyrosine residues are excited at 280 nm, while at 295 nm only tryptophan is excited [46, 47, 48].

Figure 4.1 shows the fluorescence quenching spectra of HSA at different concentrations of tungstenocene dichloride and the new complexes. The plots show that the emission fluorescence intensity at 345 nm decreases with the addition of the tungstenocene complexes due to an intermolecular interaction with the protein. The decrease of maximum emission intensity for the titration with $[Cp_2W(ethylmaltolato)]Cl$, $[Cp_2W(maltolato)]Cl$, and $[Cp_2W(kojato)]Cl$ complexes is higher than with $Cp_2WCl_2$ and $Cp_2W(malonate)$ complexes, suggesting a higher interaction for them. Additionally, they promote the emission maximum wavelength of HSA to shift to a larger wavelength. This is due to a change in the micro-environment around the tryptophan residues,

particularly Trp-214, placing it in a less hydrophobic environment after addition of these complexes, suggesting that the interaction is occurring mainly in the hydrophobic cavity of HSA, producing a change in the structure and polarity of the protein [47, 49].

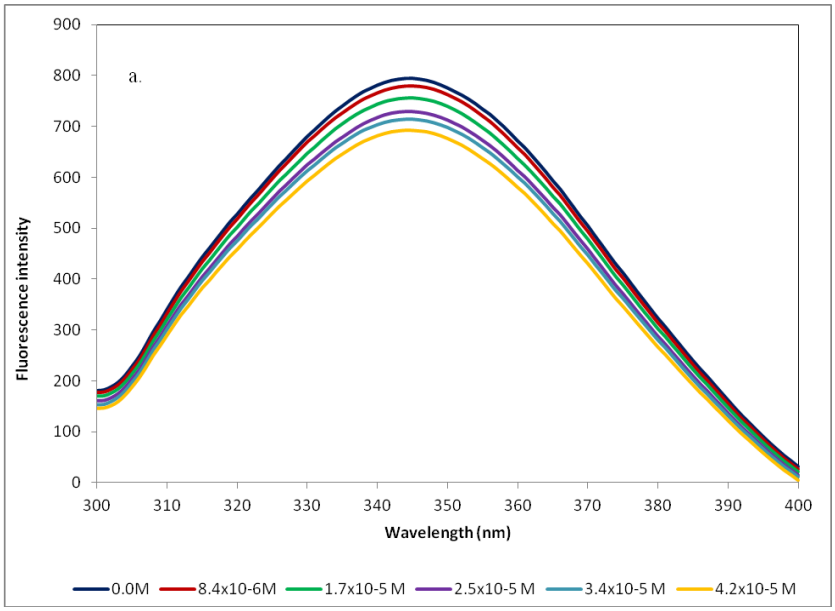


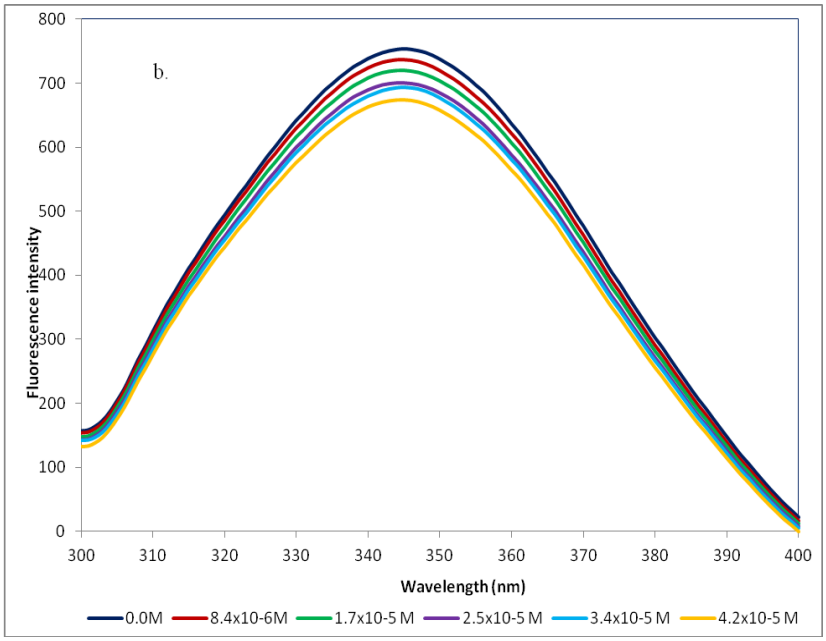

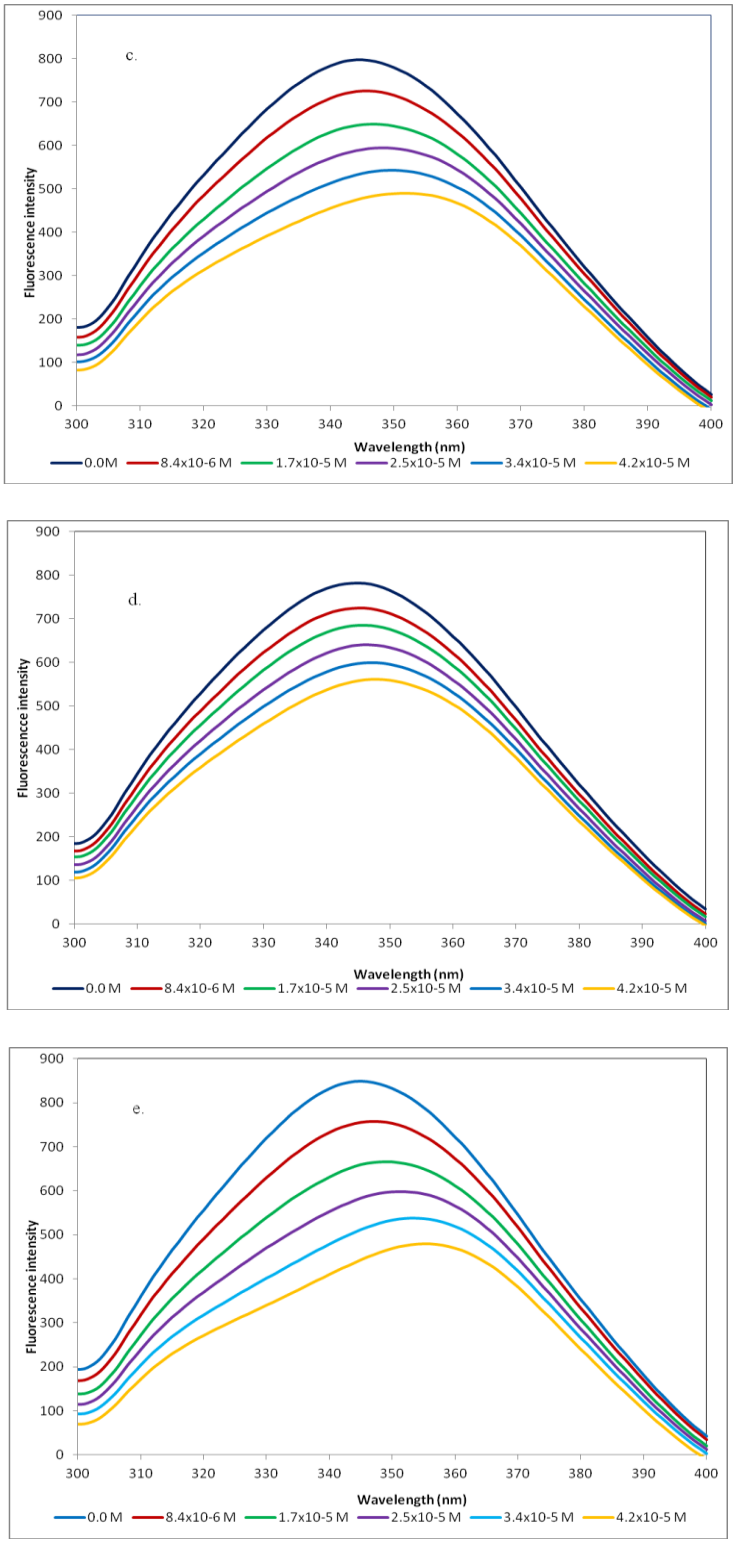


**Figure 4.1** Fluorescence quenching spectra of HSA with different complexes. a. $Cp_2WCl_2$, b. $Cp_2W$(malonate), c. [$Cp_2W$(ethylmaltolato)]Cl, d. [$Cp_2W$(kojato)]Cl, e. [$Cp_2W$(maltolato)]Cl.

Figure 4.2 shows the fluorescence quenching spectra of apo-hTf at different concentrations of tungstenocene dichloride and the new complexes. The plots show the emission maximum fluorescence intensity at 336 nm approximately, which decreases with the addition of solutions of the complexes due to an intermolecular interaction. Likewise as HSA titration spectra, the intensity of the emission decreases in a greater extent for [$Cp_2W$(ethylmaltolato)]Cl, [$Cp_2W$(maltolato)]Cl, and [$Cp_2W$(kojato)]Cl complexes than for $Cp_2WCl_2$ and $Cp_2W$(malonate). Most likely, the complexes that contain a 3-hydroxy-4-pyrone group are more hydrophobic, promoting stronger hydrophobic interactions with both proteins.

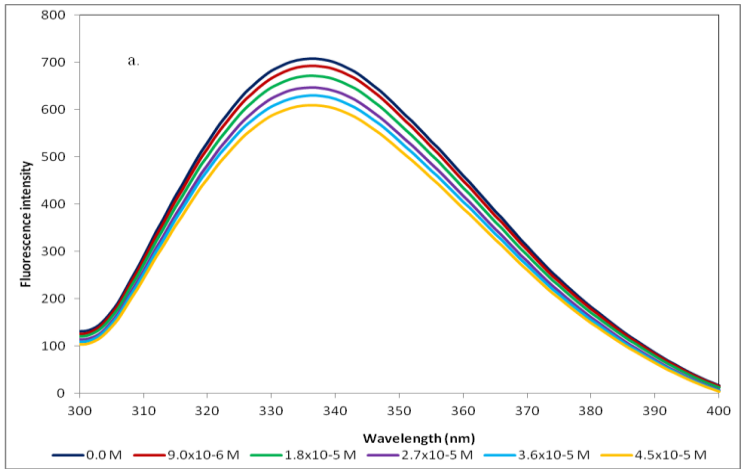


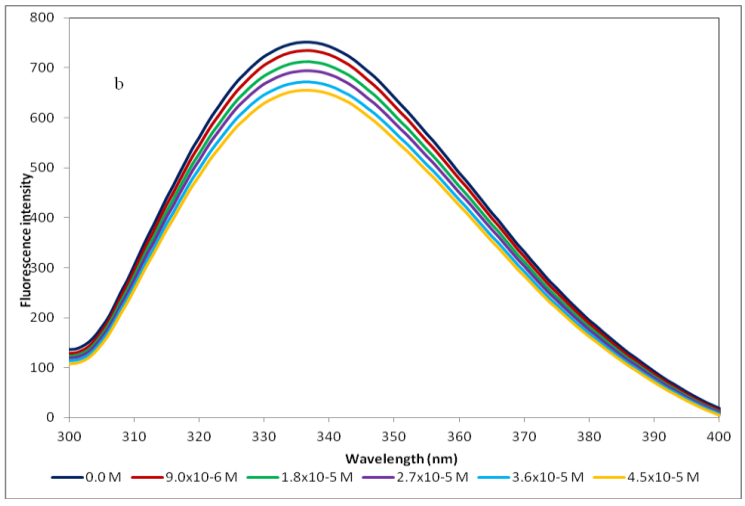

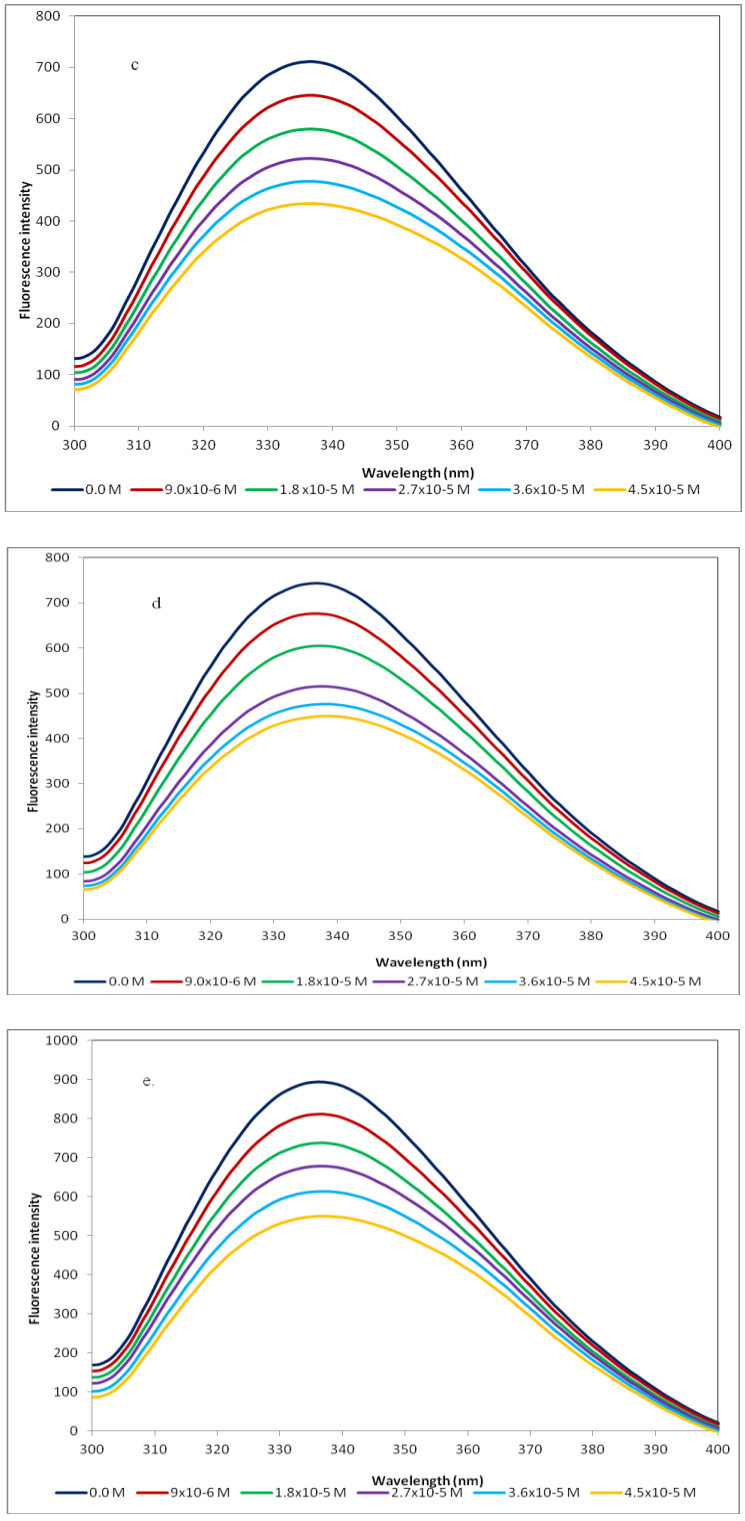


**Figure 4.2** Fluorescence quenching spectra of apo-hTf with different complexes. a. $Cp_2WCl_2$, b. $Cp_2W$(malonate), c. [$Cp_2W$(ethylmaltolato)]Cl, d. [$Cp_2W$(kojato)]Cl, e. [$Cp_2W$(maltolato)]Cl.

There are two types of quenching: dynamic and static. The first one depends of the diffusion of quencher toward fluorophore, therefore they are in contact only during the lifetime of the excited state. Whereas, static quenching is related with the complex formation between fluorophore and quencher [50]. One way to determine the quenching mechanism is to examine the fluorophore behavior in presence of quencher at different temperatures; hence the fluorescence quenching data was obtained at two different temperatures, and was analyzed using Stern-Volmer equation (equation 4.1), which exhibits a linear relationship between the fluorescence intensity and the quencher concentration, where $F_0$ and F are the fluorescence intensities in the absence and presence of quencher, respectively. $k_q$ is the biomolecular quenching constant, $\tau_0$ is the lifetime of the fluorescence in absence of quencher (for a biomolecule is $10^{-8}$ $s^{-1}$), [Q] is the concentration of quencher, and $K_{sv}$ is the Stern–Volmer quenching constant.

$$\frac{F_0}{F} = 1 + k_q \tau_0 [Q] = 1 + K_{sv}[Q] \qquad \textbf{Equation 4.1}$$

Dynamic quenching depends upon diffusion, hence that the quenching constants increase with rising temperature. Whereas, the static quenching is characterized by a decrease in the static quenching constants when the temperature increases, due to decrease in the stability of complexes. Also, a static quenching is observed when the values of $k_q$ are larger than the limiting diffusion constant $K_q$ of a biomolecule with various quenchers ($2.0 \times 10^{10}$ $M^{-1}$ $s^{-1}$) [47]. Figure 4.3 presents Stern-Volmer plots of HSA protein at 15°C and 37°C for tungstenocene dichloride and for the new complexes. They show a good linear relationship within the concentration range evaluated. The table 4.1 shows the Stern Volmer constants ($K_{sv}$) and biomolecular quenching constant, $k_{q,}$ for each complex.

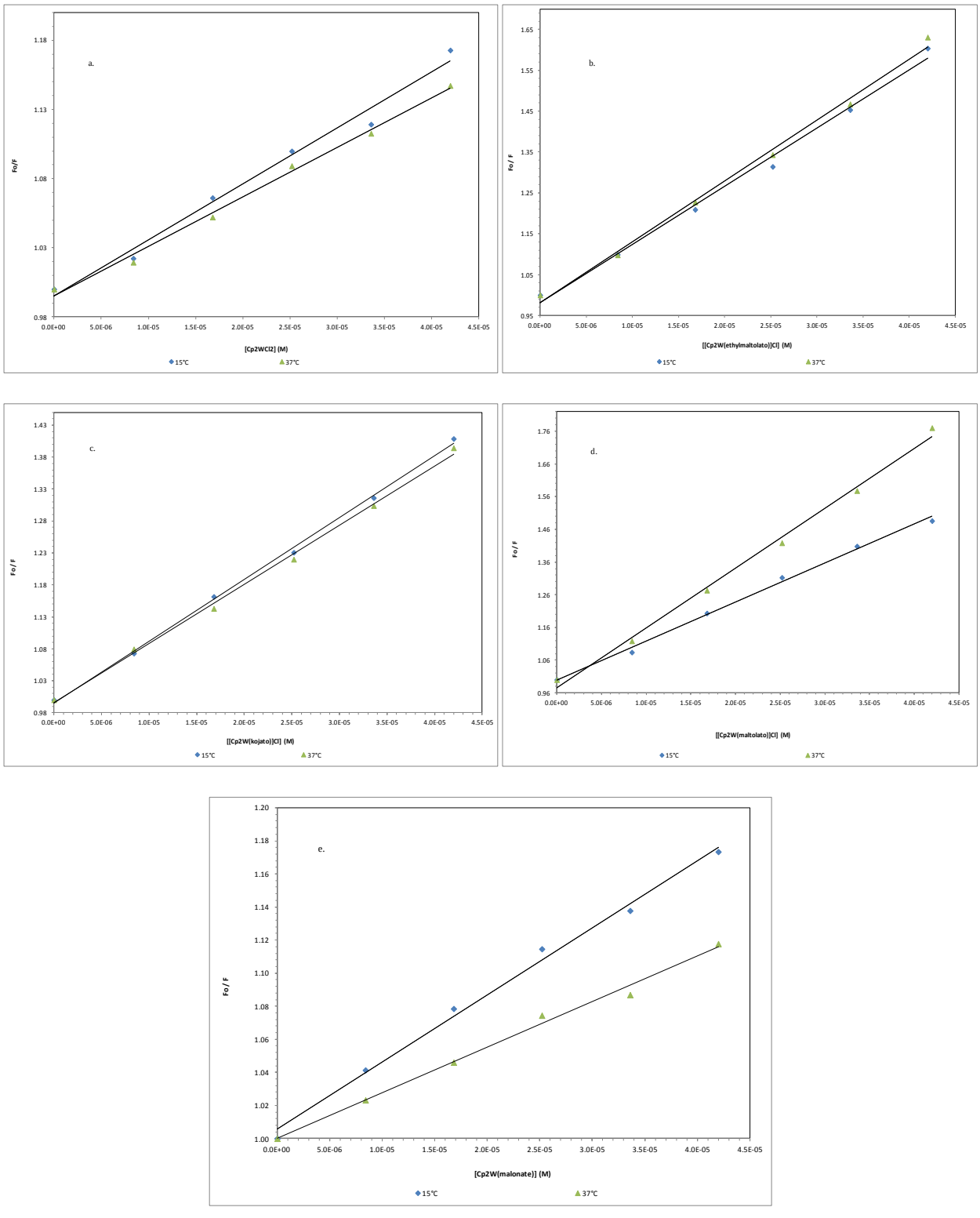


**Figure 4.3** Stern-Volmer plots of HSA at 15°C and 37°C with different complexes. a. $Cp_2WCl_2$, b. $[Cp_2W(ethylmaltolato)]Cl$, c. $[Cp_2W(kojato)]Cl$ , d.$[Cp_2W(maltolato)]Cl$, e. $Cp_2W(malonate)$.

| Complex | T(K) | $K_{sv}$ (L/mol) | $k_q$ (L/mol s) | $R^2$ |
|---|---|---|---|---|
| $Cp_2WCl_2$ | 288 | 4.04E+03 | 4.04E+11 | 0.9859 |
| | 310 | 3.58E+03 | 3.58E+11 | 0.9942 |
| [$Cp_2$W(ethylmaltolato)]Cl | 288 | 1.42E+04 | 1.42E+12 | 0.9929 |
| | 310 | 1.49E+04 | 1.49E+12 | 0.9949 |
| [$Cp_2$W(kojato)]Cl | 288 | 9.67E+03 | 9.67E+11 | 0.9984 |
| | 310 | 9.26E+03 | 9.26E+11 | 0.9971 |
| [$Cp_2$W(maltolato)]Cl | 288 | 1.19E+04 | 1.19E+12 | 0.9961 |
| | 310 | 1.83E+04 | 1.83E+12 | 0.9952 |
| $Cp_2$W(malonate) | 288 | 4.06E+03 | 4.06E+11 | 0.9938 |
| | 310 | 2.75E+03 | 2.75E+11 | 0.9935 |

**Table 4.1** Quenching constant of the interaction between HSA and complexes.

The slopes of Stern-Volmer plots for $Cp_2WCl_2$, $Cp_2$W(malonate) and [$Cp_2$W(kojato)]Cl complexes decrease with increasing the temperature, and the $k_q$ values obtained are higher than the diffusion biomolecular constant ($K_q$). Therefore, the fluorescence quenching is due to a complex formation.

On other hand, the slopes of Stern-Volmer plots for [$Cp_2$W(ethylmaltolato)]Cl, [$Cp_2$W(maltolato)]Cl complexes increase with increase the temperature suggesting a dynamic mechanism, however the $k_q$ values obtained are higher than the $K_q$ constant. Therefore, the fluorescence quenching suggests that both dynamic and static mechanisms can be present, and the fluorophore is quenched by both collision and complex formation with the same quencher. In this condition, ($F/F_0$) is given by the product of the fraction not complexed (*f*) and the fraction not quenched by collisional. Therefore;

$$\frac{F}{F_0} = f\left(\frac{\gamma}{\gamma + k_q[Q]}\right) = \left(\frac{1}{1 + K_D[Q]}\right) \quad \textbf{Equation 4.2}$$

where γ is the ratio of decay rate in absence of quencher, and (γ + $k_q$[Q]) is the total decay rate in the presence of quencher, and $K_D$ is the constant of Stern-Volmer from dynamic quenching, due to collisional quenching. Taking (1/*f*) = 1 + $K_s$ [Q], where $K_S$ represent the association constant for complex formation from a static quenching, and replacing in the equation 4.2, a modification of Stern-Volmer equation is obtained:

$$\frac{F_0}{F} = (1 + K_D[Q])(1 + K_S[Q]) = 1 + (K_D + K_S)[Q] + K_D K_S[Q]^2 \quad \textbf{Equation 4.3}$$

Taking $K_{app}$ = ($K_D$ + $K_S$)[Q] + $K_D K_S$[Q]$^2$ , it is obtained that:

$$\frac{F}{F_0} = 1 + K_{app}[Q] \qquad \textbf{Equation 4.4}$$

$$\text{Therefore;} \quad K_{app} = \frac{(F_0 / F) - 1}{[Q]} = (K_D + K_S) + K_D K_S[Q] \qquad \textbf{Equation 4.5}$$

Hence, in principle a plot of [($F_0$/F)-1]/[Q] versus 1/[Q] should produce a straight line with a slope of $K_D K_S$ [53]. We applied equation 4.5 to our fluorescence data and neither [$Cp_2$W(ethylmaltolato)]Cl nor [$Cp_2$W(maltolato)]Cl presented a linear behavior. Consequently, we cannot suggest a specific mechanism of interaction for [$Cp_2$W(ethylmaltolato)]Cl and [$Cp_2$W(maltolato)]Cl complexes, however the plot suggests that the mechanism is static due to the change in emission as well as $k_q$ values.

Figure 4.4 presents Stern-Volmer plots of apo-hTf protein at 25°C and 37°C for tungstenocene dichloride and for the new complexes, which show a good linear relationship within the concentration range evaluated, and Table 4.2 shows the Stern Volmer constants ($K_{sv}$) and biomolecular quenching constant for each complex.

The slopes of Stern-Volmer plots in apo-hTf for [$Cp_2W$(ethylmaltolato)]Cl, [$Cp_2W$(maltolato)]Cl and $Cp_2W$(malonate) complexes decrease with increase of the temperature, and the $k_q$ values obtained are higher than diffusion biomolecular constant ($K_q$), suggesting formation of a complex. On other hand, the slopes of $Cp_2WCl_2$ and [$Cp_2W$(kojato)]Cl complexes increase with increase of the temperature suggesting a dynamic mechanism; however the $k_q$ values obtained are higher than $K_q$, suggesting that both dynamic and static mechanisms may be present. Thus, a plot of $[(F_0/F)-1]/[Q]$ versus $1/[Q]$ was carried out for the complexes, and none presented linear behavior. Therefore, we cannot suggest a specific mechanism of interaction for the $Cp_2WCl_2$ and [$Cp_2W$(kojato)]Cl complexes.

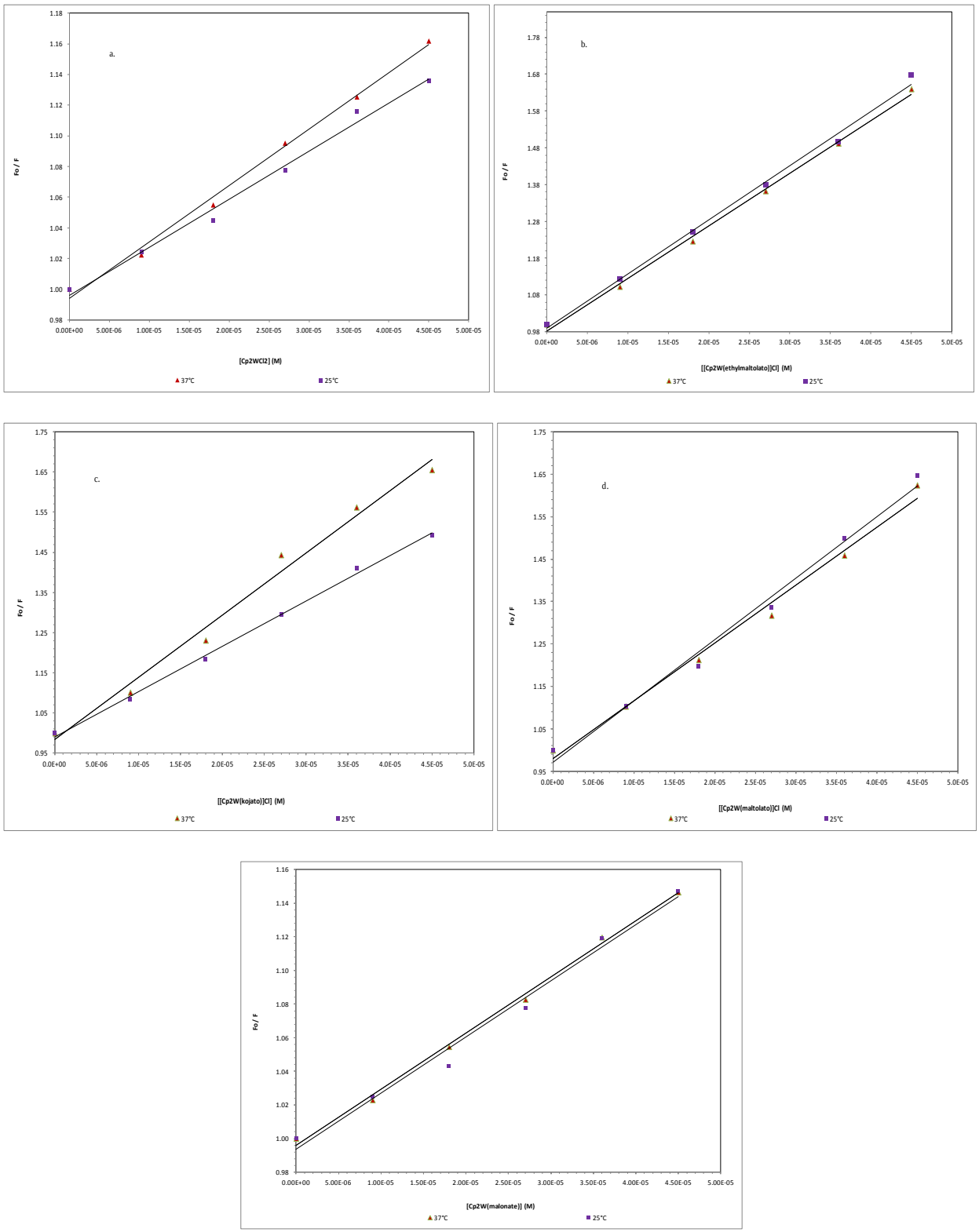


**Figure 4.4** Stern-Volmer plots of apo-hTf at 25°C and 37°C. a. $Cp_2WCl_2$, b. [$Cp_2W$(ethylmaltolato)]Cl, c. [$Cp_2W$(kojato)]Cl , d.[$Cp_2W$(maltolato)]Cl, e. $Cp_2W$(malonate).

| Complex | T(K) | $K_{sv}$ (L/mol) | $k_q$ (L/mol s) | $R^2$ |
|---|---|---|---|---|
| $Cp_2WCl_2$ | 298 | 3.14E+03 | 3.14E+11 | 0.9907 |
| | 310 | 3.68E+03 | 3.68E+11 | 0.9950 |
| [$Cp_2$W(ethylmaltolato)]Cl | 298 | 1.47E+04 | 1.47E+12 | 0.9952 |
| | 310 | 1.43E+04 | 1.43E+12 | 0.9971 |
| [$Cp_2$W(kojato)]Cl | 298 | 1.13E+04 | 1.13E+12 | 0.9973 |
| | 310 | 1.55E+04 | 1.55E+12 | 0.9867 |
| [$Cp_2$W(maltolato)]Cl | 298 | 1.45E+04 | 1.45E+12 | 0.9894 |
| | 310 | 1.36E+04 | 1.36E+12 | 0.9903 |
| $Cp_2$W(malonate) | 298 | 3.35E+03 | 3.35E+11 | 0.9854 |
| | 310 | 3.34E+03 | 3.34E+11 | 0.9967 |

**Table 4.2** Quenching constant of the interaction between apo-hTf and complexes.

Additionally, some thermodynamic parameters were calculated to determine the strength of interaction using the Van`t Hoff equation (equation 4.6). In this way the enthalpy change (ΔH) and entropy change (ΔS) can be calculated, if the enthalpy change does not vary significantly with the temperature.

$$\ln K_a = -\frac{\Delta H}{RT} + \frac{\Delta S}{R} \quad \textbf{Equation 4.6}$$

where $K_a$ is analogous to $K_{sv}$ and R is the gas constant (8.314 J/molK). Thus, a plot ln $K_{sv}$ versus 1/T was carried out in the figure 4.5 to obtain the ΔH and ΔS. In addition, the change in free energy (ΔG) also can be estimated by the equation 4.7 [50].

$$\Delta G = \Delta H - T\Delta S \quad \textbf{Equation 4.7}$$

The intermolecular interactions present between small molecules and macromolecules during small changes in temperature are: H-bonding, van der Waals, electrostatic and hydrophobic interactions. Table 4.3 shows the ΔG, ΔH and ΔS values of the interaction between HSA with the complexes. All the complexes present negative ΔG values, which means that the binding is spontaneous. The Van`t Hoff plots for the complexes are presented in figure 4.6, and the table 4.3 presents the thermodynamic parameters. The ΔG values of [$Cp_2$W(ethylmaltolato)]Cl, [$Cp_2$W(maltolato)]Cl, and [$Cp_2$W(kojato)]Cl complexes are similar and more negative than $Cp_2WCl_2$ and $Cp_2$W(malonate) complexes suggesting that the interaction is more favored for the first ones.

Positive ΔH and ΔS values imply a hydrophobic interaction, negative ΔH and ΔS values involve van der Waals force or hydrogen bonding; and $\Delta H \approx 0$ with $\Delta S > 0$ values reflect an electrostatic force [54]. Therefore, the binding between HSA and [$Cp_2$W(ethylmaltolato)]Cl and [$Cp_2$W(maltolato)]Cl complexes is endothermic and the interaction is hydrophobic mainly. The interaction with [$Cp_2$W(kojato)]Cl, $Cp_2WCl_2$ and $Cp_2$W(malonate) is exothermic, based on hydrophobic and electrostatic interactions; since positive ΔS value involves hydrophobic interactions, and negative ΔH value imply an electrostatic interaction [47, 49, 52].

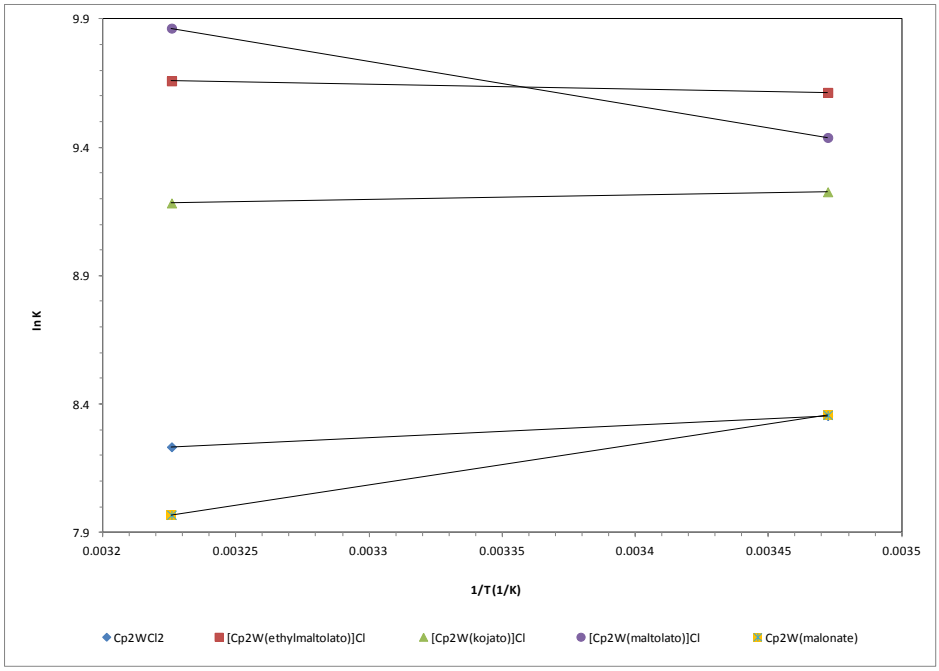


**Figure 4.5** Van`t Hoff plots of interaction between HSA with the complexes.

| Complexes | T(K) | ΔG(KJ/mol) | ΔH (KJ/mol) | ΔS (J/molK) |
|---|---|---|---|---|
| $Cp_2WCl_2$ | 288 | -19.88 | -4.10 | 54.82 |
| | 310 | -21.09 | | |
| [$Cp_2$W(ethylmaltolato)]Cl | 288 | -22.90 | 1.51 | 84.76 |
| | 310 | -24.77 | | |
| [$Cp_2$W(kojato)]Cl | 288 | -21.97 | -1.47 | 71.19 |
| | 310 | -23.54 | | |
| [$Cp_2$W(maltolato)]Cl | 288 | -22.48 | 14.36 | 127.92 |
| | 310 | -25.29 | | |
| $Cp_2$W(malonate) | 288 | -19.96 | -13.22 | 23.40 |
| | 310 | -20.47 | | |

**Table 4.3** Thermodynamic parameters of the interaction between HSA with the complexes

The figure 4.6 shows the a Van`t Hoff plot from the interaction between apo-hTf with the complexes and table 4.4 shows the ΔG, ΔH and ΔS values for the interaction, where all the complexes present a spontaneous interaction (ΔG < 0). Likewise as HSA interaction, ΔG values of [$Cp_2$W(ethylmaltolato)]Cl, [$Cp_2$W(maltolato)]Cl, and [$Cp_2$W(kojato)]Cl complexes are similar and more negative than $Cp_2WCl_2$ and $Cp_2$W(malonate) complexes suggesting an interaction more spontaneous for the first ones.

The binding between apo-hTf with $Cp_2WCl_2$ and [$Cp_2$W(kojato)]Cl complexes is endothermic and its interaction is mainly hydrophobic. The interaction with $Cp_2$W(malonate) is exothermic and the negative enthalpy value close to cero involve an electrostatic interaction. The interaction with [$Cp_2$W(ethylmaltolato)]Cl and [$Cp_2$W(maltolato)]Cl is exothermic, based on hydrophobic and electrostatic interactions, since positive value of ΔS involves hydrophobic interactions and negative ΔH value implies an electrostatic interaction [47, 49, 52].

The fluorescence results of protein-complex interaction using HSA and apo-hTf as proteins, showed the presence of interaction due to quenching process, where [$Cp_2$W(ethylmaltolato)]Cl, [$Cp_2$W(maltolato)]Cl, and [$Cp_2$W(kojato)]Cl complexes show a higher degree of interaction than $Cp_2WCl_2$ and $Cp_2$W(malonate). This suggests that probably the 3-hydroxy-4-pyrone group from these compounds allow a better interaction for a possible delivery to the cancer cell.

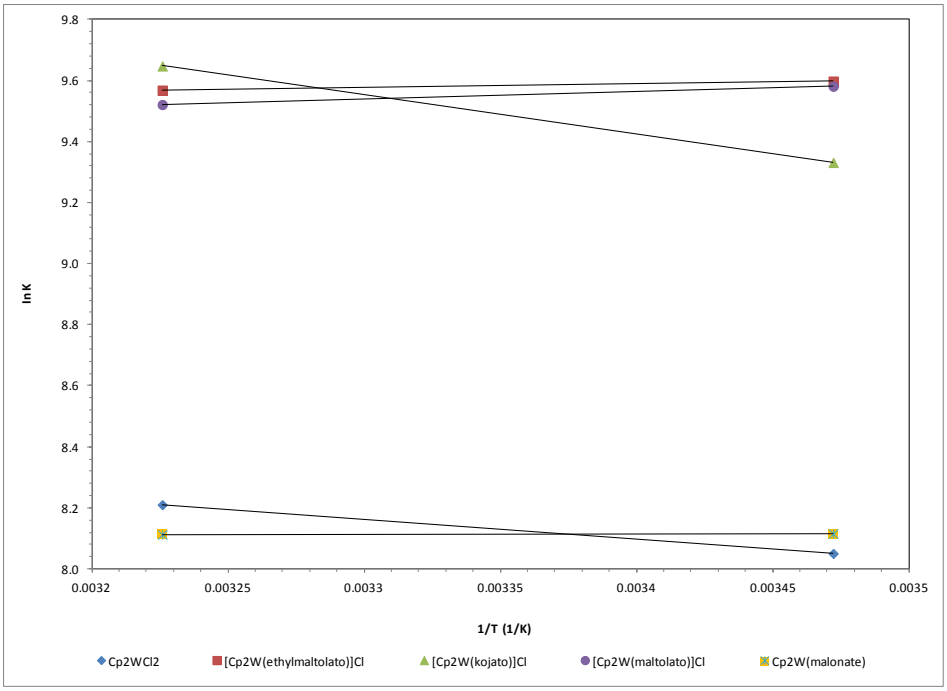


**Figure 4.6** Van`t Hoff plots of interaction between apo-hTf with the complexes.

| Complex | T(K) | ΔG(KJ/mol) | ΔH (KJ/mol) | ΔS (J/molK) |
|---|---|---|---|---|
| $Cp_2WCl_2$ | 298 | -19.95 | 10.22 | 101.22 |
| | 310 | -21.16 | | |
| [$Cp_2W$(ethylmaltolato)]Cl | 298 | -23.78 | -1.89 | 73.44 |
| | 310 | -24.66 | | |
| [$Cp_2W$(kojato)]Cl | 298 | -23.12 | 20.23 | 145.46 |
| | 310 | -24.86 | | |
| [$Cp_2W$(maltolato)]Cl | 288 | -23.74 | -3.85 | 66.75 |
| | 310 | -24.54 | | |
| $Cp_2W$(malonate) | 288 | -20.11 | -0.20 | 66.82 |
| | 310 | -20.91 | | |

**Table 4.4** Thermodynamic parameters of the interaction between apo-hTf with the complexes.

### 4.2.2 Interaction by cyclic voltammetry

Protein-complex binding studies were monitored by cyclic voltammetry to observe the changes in redox behavior of W(IV) complexes when a protein binds the metal center. Initially, the complex solutions were titrated with four aliquots of 250 uL of buffer solution to observe the dilution effect (as a blank), then the titration was carried out with the protein, and after each addition a voltammogram was recorded.

Figure 4.7 shows the tungstenocene dichloride titration voltammograms with Tris buffer, HSA and apo-hTf. The voltammograms are characterized by an irreversible redox behavior, which exhibit two oxidation peaks attributed to the formation of W(V) and a stable metal-oxo species. During the buffer and apo-hTf titrations (figure 4.7, a and c) there is not a significant change after each addition, therefore the coordination environment does not change neither exist interaction between them. However, upon addition of HSA (figure 4.7 b), the oxidation peak moves and eventually disappear exhibiting a decrease in current and $E_{pa}$ moves toward positive values (anodic shift). The titrations of $[Cp_2W(maltolato)]Cl$, $[Cp_2W(ethylmaltolato)]Cl$ and $[Cp_2W(kojato)]Cl$ complexes (figure 4.8, 4.9 and 4.10 respectively) present a similar behavior, where the buffer does not exhibit a significant change. While that the titrations with both HSA and apo-hTf proteins, the oxidation peak decreases in current and $E_{pa}$ moves toward positive values (anodic shift). On other hand, the $Cp_2W(malonate)$ titration voltammogram with buffer (figure 4.11 a) exhibits a significant change, decreasing the current. This complex shows that the addition of proteins to the complex solution also exhibit significant changes, where oxidation peak decrease in current and $E_{pa}$ moves toward positive values.

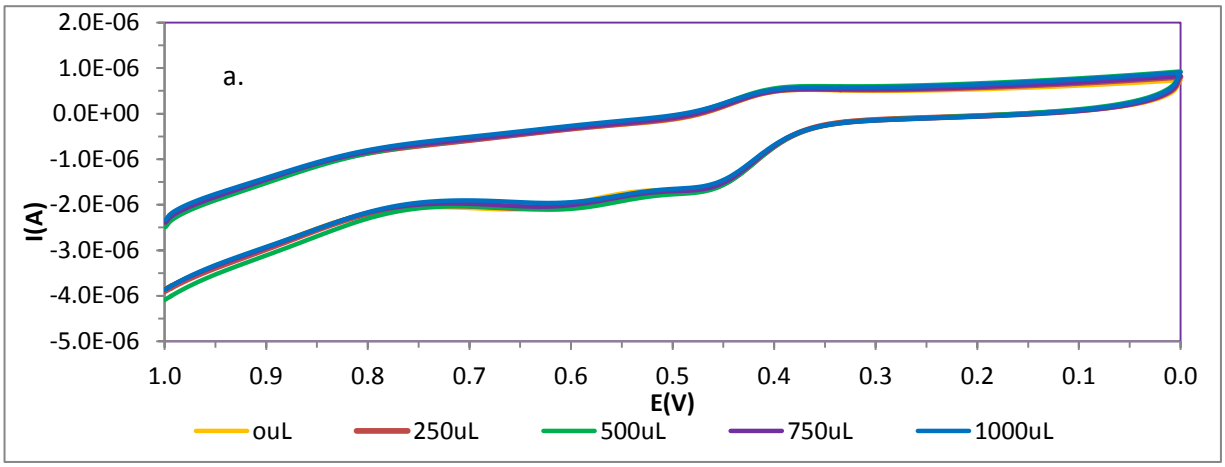


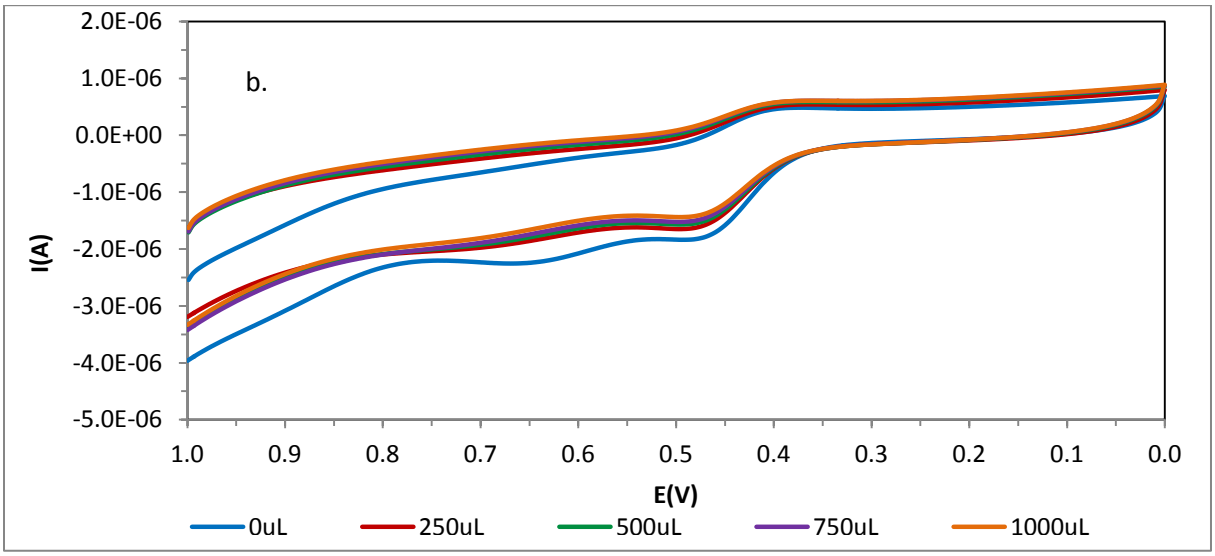


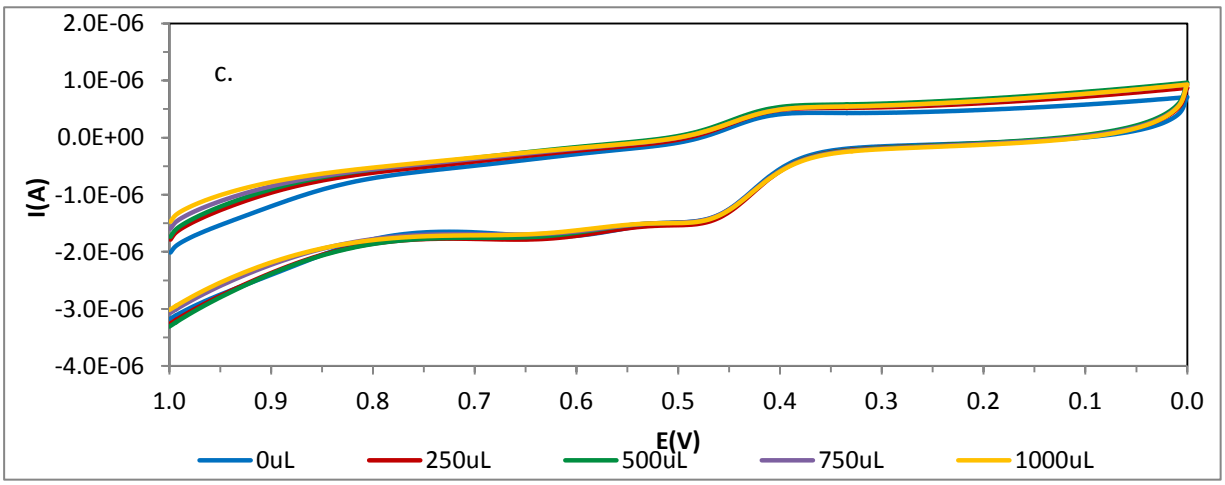


**Figure 4.7** $Cp_2WCl_2$ Titration voltammograms. a) buffer, b) HSA, and c) apo-hTf

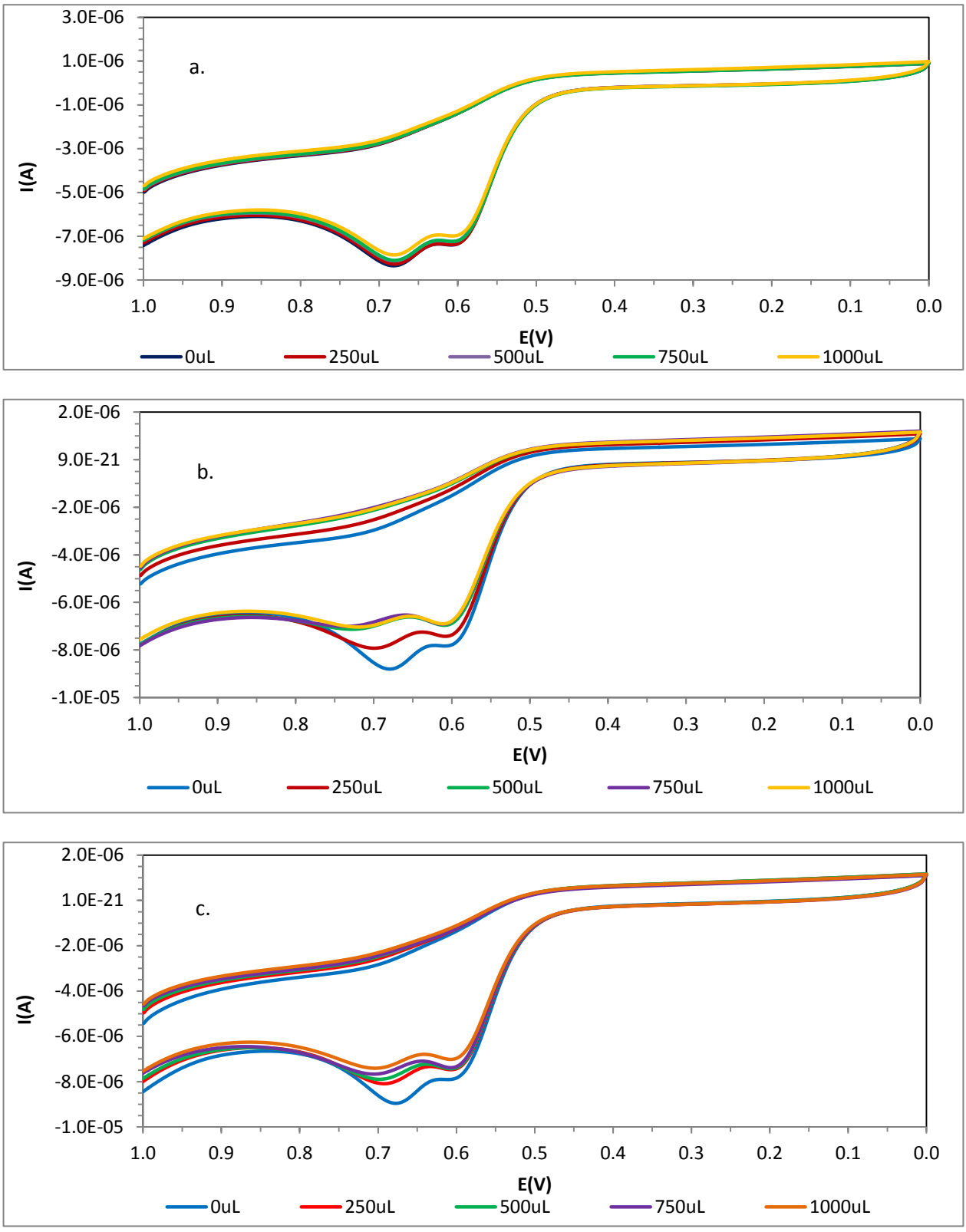


**Figure 4.8** [$Cp_2W$(maltolato)]Cl titration voltammograms. a) buffer, b) HSA, and c) apo-hTf

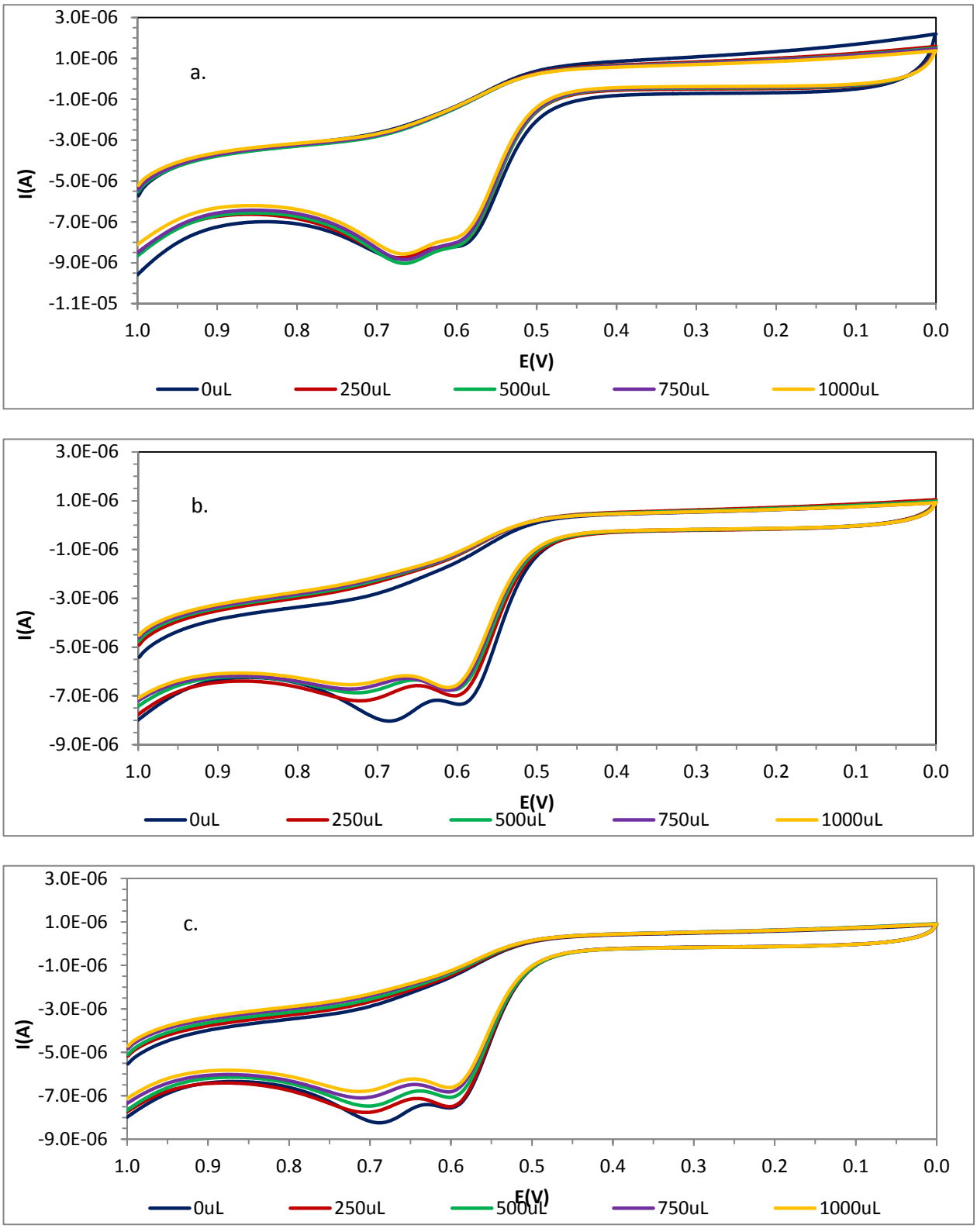


**Figure 4.9** [$Cp_2W$(ethylmaltolato)]Cl titration voltammograms. a) buffer, b)HSA, c) apo-hTf

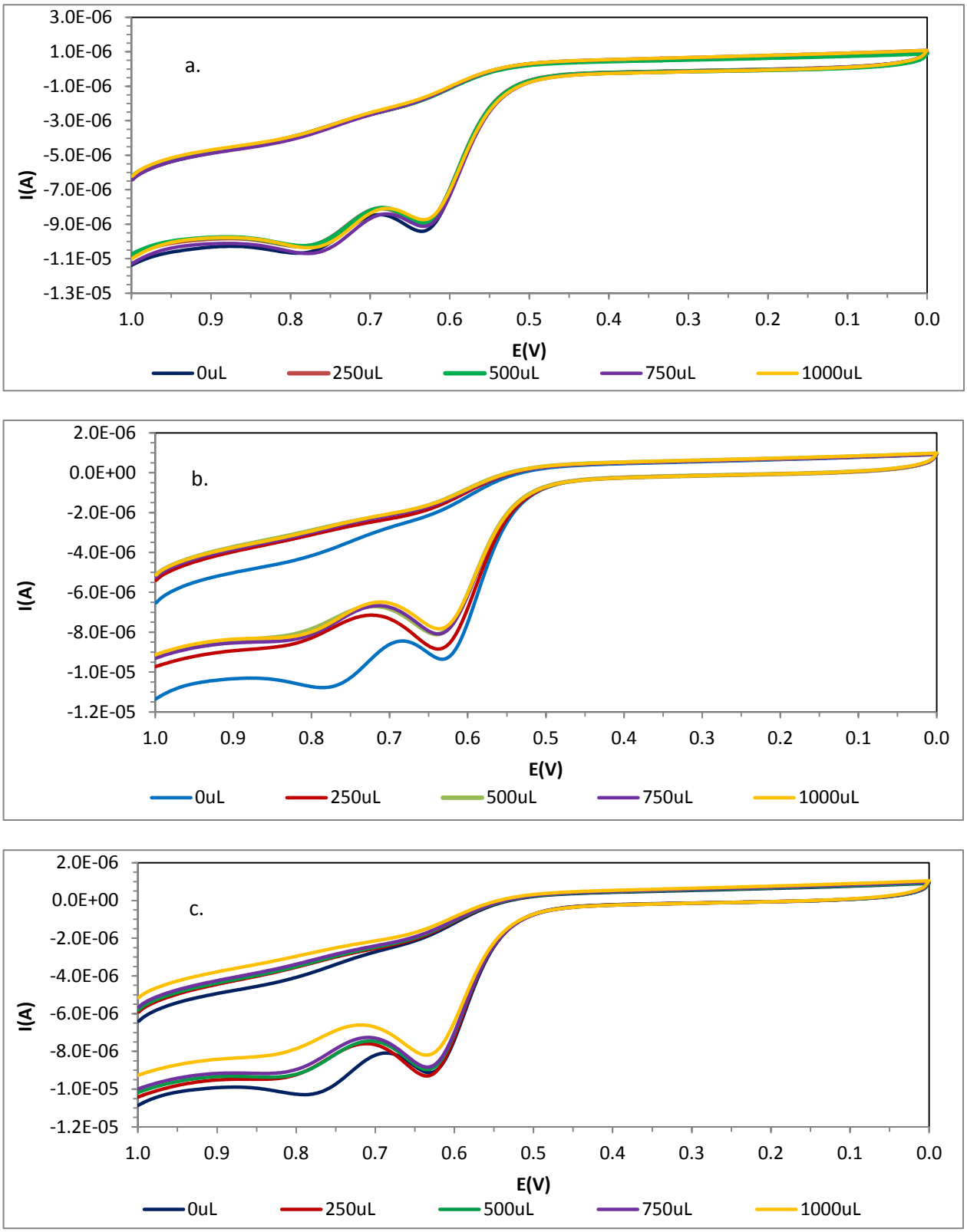


**Figure 4.10** [$Cp_2W$(kojato)]Cl titration voltammograms. a) buffer, b) HSA, and c) apo-hTf

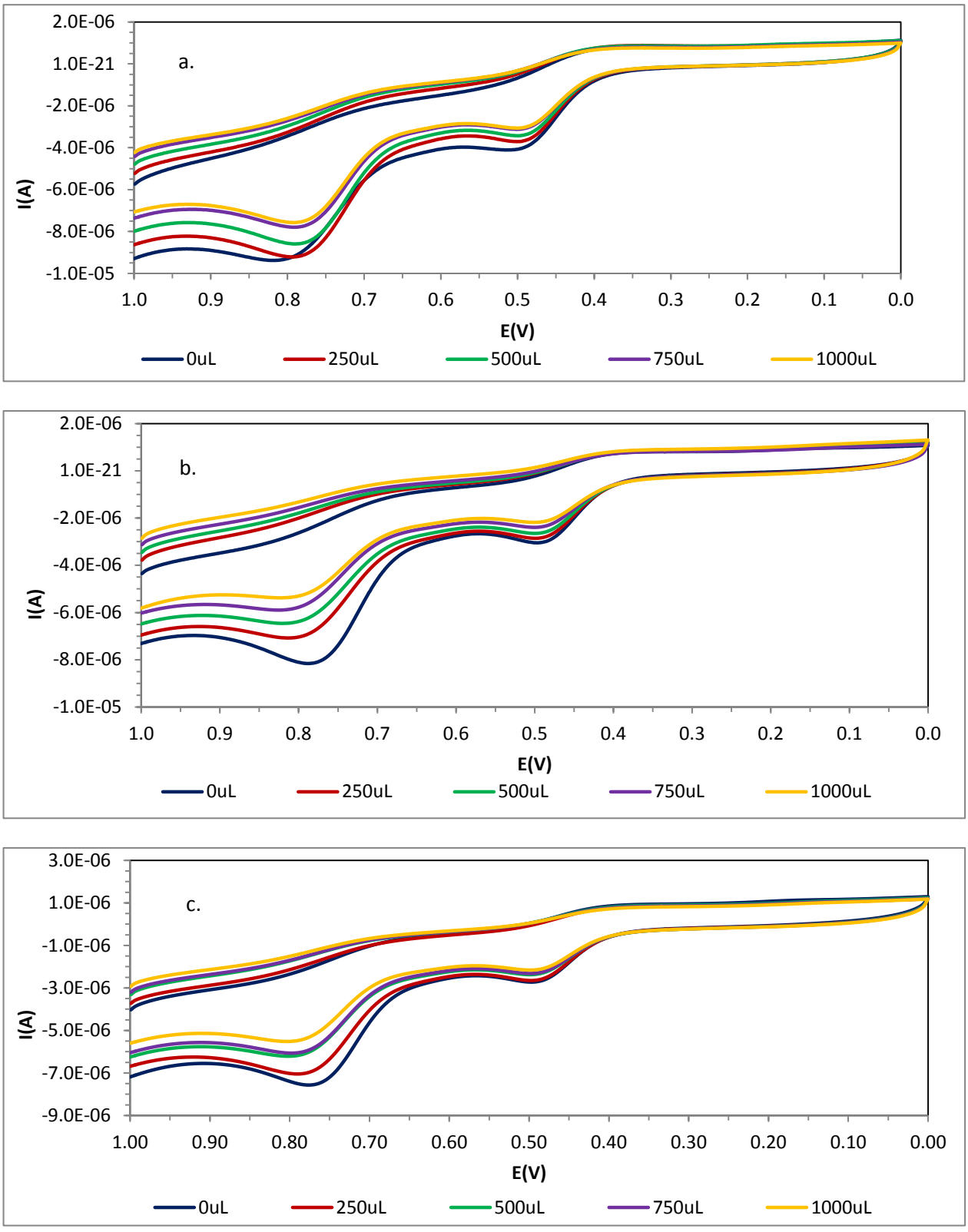


**Figure 4.11** $Cp_2W$(malonate) titration voltammograms. a) buffer, b) HSA, and c) apo-hTf

The percent of interaction between the complexes and the proteins (HSA and apo-hTf) was calculated comparing both buffer and proteins titration voltammograms through using the changes in current ($I_{pa}$), by the equation 4.7.

$$Interaction\ (\%) = \left( \frac{I_{pa}(complex) - I_{pa}(complex + protein)}{I_{pa}(complex)} \right) \times 100 \qquad \textbf{Equation 4.7}$$

Table 4.5 shows the binding percentages of HSA for the two oxidation peaks. Since the change in $I_{pa}$ is more significant for the second peak (peak at more positive potentials) than for the first peak according the figures 4.9 to 4.12, hence the second peak is considered more reliable. The changes in potentials are more sensitive to the coordination environment than the changes in current [55], whereas the current changes are related to a change in the diffusion, which could be due to the complex is being loaded in a hydrophobic pocket of the protein [35]. A change in coordination environment is not expect, since it is very unlikely that the complexes undergoes a ligand stripping process, losing stability to be coordinated as W(IV). Therefore the current was used as an indicator of metal-protein interactions.

In this regard, using the change in current, $Cp_2W$(malonate) showed a higher interaction with 29.1 %, showing that the interaction order is: $Cp_2W$(malonate) > [$Cp_2W$(ethylmaltolato)]Cl > [$Cp_2W$(kojato)]Cl > [$Cp_2W$(maltolato)]Cl > $Cp_2WCl_2$. In general the new complexes exhibited higher interaction as compared to tungstenocene dichloride, probably the tungstenocene derivatives interact with the HSA residing in one of the hydrophobic pockets typically occupied by fatty acids.

| | First peak | | Second peak | |
|---|---|---|---|---|
| **Complex** | **Int $I_{pa}$ (%)** | **SD (±)** | **Int $I_{pa}$ (%)** | **SD (±)** |
| $Cp_2WCl_2$ | 12.2 | 0.2 | 3.51 | 0.06 |
| [$Cp_2$W(maltolato)]Cl | 1.25 | 0.02 | 10.4 | 0.2 |
| [$Cp_2$W(ethylmaltolato)]Cl | 15.8 | 0.4 | 23.7 | 0.8 |
| [$Cp_2$W(kojato)]Cl | 8.2 | 0.2 | 15.1 | 0.4 |
| $Cp_2$W(malonate) | 29.0 | 0.1 | 29.1 | 0.1 |

**Table 4.5** Interaction percentage between HSA and complexes by cyclic voltammetry

Table 4.6 shows the binding interactions for apo-hTf. Similar to HSA interaction, the second peak is considered for the calculations due to its higher sensitivity. During the titration, a change in coordination environment is not expected. Therefore, the results in current showed that $Cp_2$W(malonate) exhibits highest interaction with 27%, $Cp_2$W(malonate) > [$Cp_2$W(ethylmaltolato)]Cl > [$Cp_2$W(kojato)]Cl > $Cp_2WCl_2$ > [$Cp_2$W(maltolato)]Cl. Thus, with exception of [$Cp_2$W(maltolato)]Cl, the new complexes present a higher interaction than tungstenocene dichloride.

| | First peak | | Second peak | |
|---|---|---|---|---|
| **Complex** | **Int $I_{pa}$ (%)** | **SD (±)** | **Int $I_{pa}$ (%)** | **SD (±)** |
| $Cp_2WCl_2$ | 8.8 | 0.3 | 13.0 | 0.6 |
| [$Cp_2$W(maltolato)]Cl | 0.4 | 0.01 | 5.7 | 0.2 |
| [$Cp_2$W(ethylmaltolato)]Cl | 16.2 | 0.3 | 20.5 | 0.6 |
| [$Cp_2$W(kojato)]Cl | 3.8 | 0.1 | 14.7 | 0.5 |
| $Cp_2$W(malonate) | 30 | 1 | 27 | 1 |

**Table 4.6** Interaction percentage between apo-hTf and complexes by cyclic voltammetry

In both cases HSA and apo-hTf interaction, $Cp_2W$(malonate) shows a higher degree of interaction. This suggests that probably this compound diffuses easier inside the proteins. However, examining all interaction results of cyclic voltammetry, it is difficult to measure the interaction between the proteins and the complexes due to the experiments should be taken with caution and could lead to wrong conclusions since that species formed by potential application are unknown. Nevertheless, a weak interaction is notable by cyclic voltammetry and probably it is due to a hydrophobic interaction.

## 5. Conclusions and future works

This study is the starting point for the development of new and promising tungstenocene (IV) derivatives as complexes with anticancer properties. Thus, four tungstenocene derivatives complexes that contain bidentade ligands, (O,O')-donors, were synthesized in aqueous solution; $[Cp_2W(maltolato)]Cl$, $[Cp_2W(ethylmaltolato)]Cl$, $[Cp_2W(kojato)]Cl$ and $Cp_2W(malonate)$. Their structures were characterized by different techniques, indicating that ligands bound to W(IV), forming 5- and 6-membered chelating ring.

The chloride replacement by the bidentade ligands in tungstenocene dichloride improves significantly the cytotoxic activity against HT-29 colon cancer cells, decreasing between one to two orders of magnitude approximately the concentration range. Complexes with 3-hydroxy-4-pyrone group (maltolato, ethylmaltolato and kojato) as ligand have higher cytotoxic activity than $Cp_2W(malonate)$; probably this functional group enhances the activity in this type of cancer cell. On other hand, all complexes exhibited $IC_{50}$ values with same order of magnitude in MCF-7 cells with concentrations slightly lower for the new complexes, demonstrating that substitution of the chloride ligands does not improve significantly the cytotoxic activity on this type of cancer cells.

Comparing cytotoxic results from $[Cp_2W(maltolato)]Cl$ and $Cp_2W(malonate)$ with $[Cp_2Mo(maltolato)]Cl$ and $Cp_2Mo(malonate)$ from literature [35] a higher activity is observed for similar tungstenocene derivatives in HT-29 cells. Contrary to proliferative behavior presented by the molybdenocene derivatives in MCF-7 cells, a cytotoxic activity is exhibited by the tungstenocene derivatives. Hence, the metal center plays an important role in the cytotoxic

activity of the isostructural metallocenes becoming difficult to predict their behavior on different cancer cells.

The fluorescence results of protein-complex interaction using HSA and apo-hTf as proteins, suggest binding affinity for all complexes, based mainly in hydrophobic and electrostatic interactions. According to change in free energy, [$Cp_2W$(ethylmaltolato)]Cl, [$Cp_2W$(maltolato)]Cl, and [$Cp_2W$(kojato)]Cl complexes show a higher degree of interaction than $Cp_2WCl_2$ and $Cp_2W$(malonate). This suggests that probably the 3-hydroxy-4-pyrone group from these compounds allow a better interaction with these proteins. Upon examination of both the $IC_{50}$ values of HT-29 cancer cell and interaction studies by fluorescence, it is possible to speculate that there is a relation between the cytotoxic activity and HSA or apo-hTf binding. Since both demonstrated higher cytotoxic activity and interaction for [$Cp_2W$(ethylmaltolato)]Cl, [$Cp_2W$(maltolato)]Cl, and [$Cp_2W$(kojato)]Cl, suggesting that 3-hydroxy-4-pyrone group from these compounds allow a better interaction for a possible delivery to HT-29 cancer cell.

The cyclic voltammetry results of protein-complex interaction suggested a weak interaction with both HSA and apo-hTf proteins. The interaction order showed for HSA was: $Cp_2W$(malonate) > [$Cp_2W$(ethylmaltolato)]Cl > [$Cp_2W$(kojato)]Cl > [$Cp_2W$(maltolato)]Cl > $Cp_2WCl_2$, and for apo-hTf was: $Cp_2W$(malonate) > [$Cp_2W$(ethylmaltolato)]Cl > [$Cp_2W$(kojato)]Cl > $Cp_2WCl_2$ > [$Cp_2W$(maltolato)]Cl. Therefore, the interaction between $Cp_2W$(malonate) and both proteins was higher with a 29.1 % and 27 % for HSA and apo-hTf respectively. Probably this compound diffuses easier inside the proteins. However, these results could lead to wrong conclusions since that species formed by potential application are unknown. Nevertheless, a weak interaction is notable and probably it is due to a hydrophobic interaction with the proteins.

Finally, as recommendations for future works should be described in more detail the nature of the interaction between the tungstenocene derivative complexes with both HSA and apo-hTf proteins, using techniques such as circular dichroism and theoretical calculations. Also, in order to complete the characterization of cytotoxic activity, should be evaluated the effect of the complexes on others cancer cells lines. Additionally, it is possible to carry out the synthesis of tungstenocene derivatives with (O,N) or (O,S)-donor ligands, in order to compare, understand and enhance the cytotoxic properties of tungstenocene derivatives and in their interaction with proteins in order to develop new alternatives in the cancer treatment.

# Appendix

## A.1. $^{1}$H- NMR Spectrums

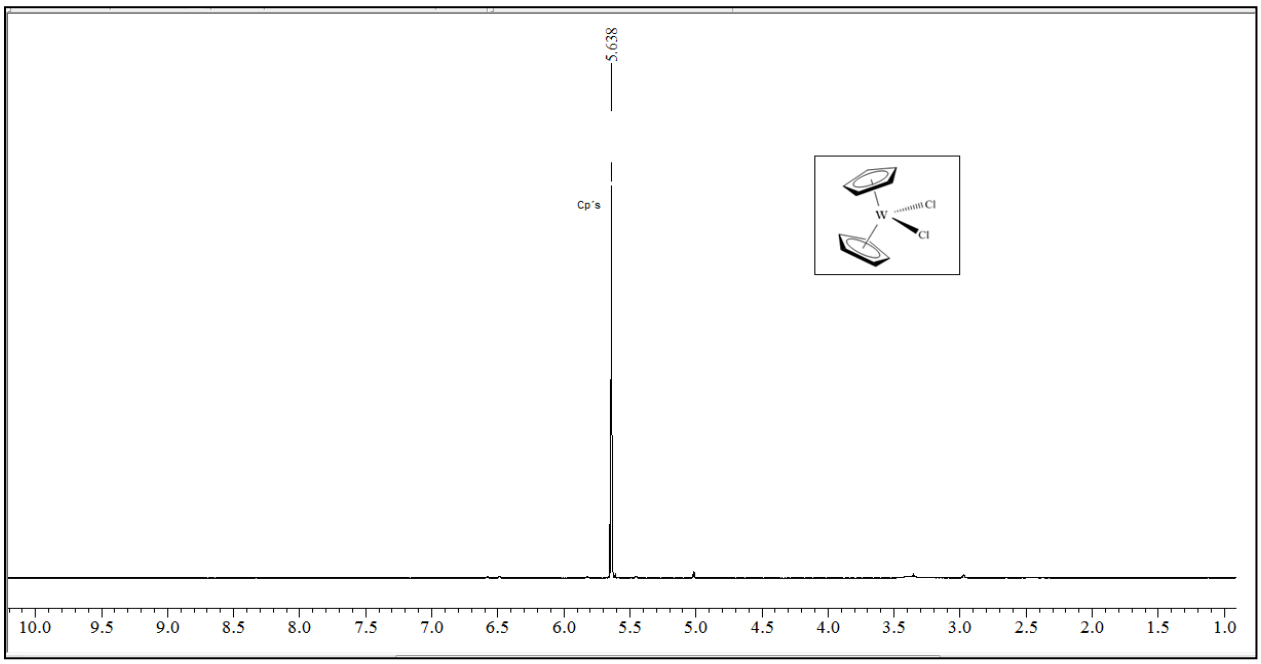


**A.1.1.** $^{1}$H-NMR spectrum of tungstenocene dichloride in DMSO-$d_6$

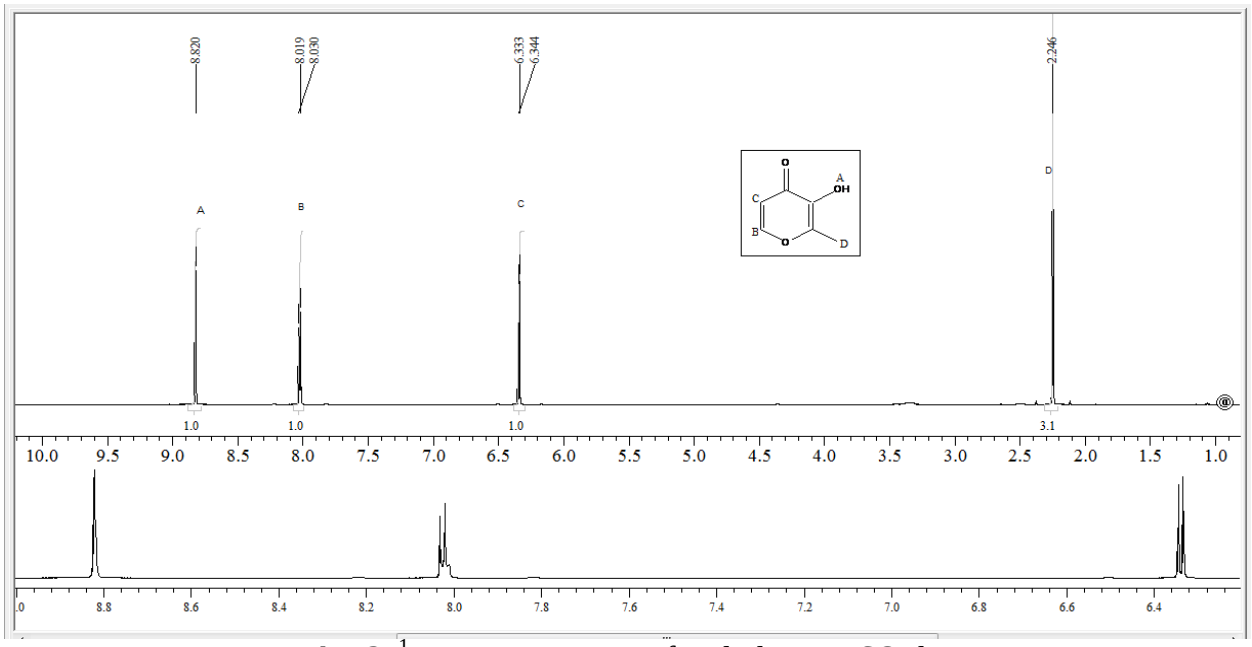


**A.1.2.** $^{1}$H-NMR spectrum of maltol in DMSO-$d_6$

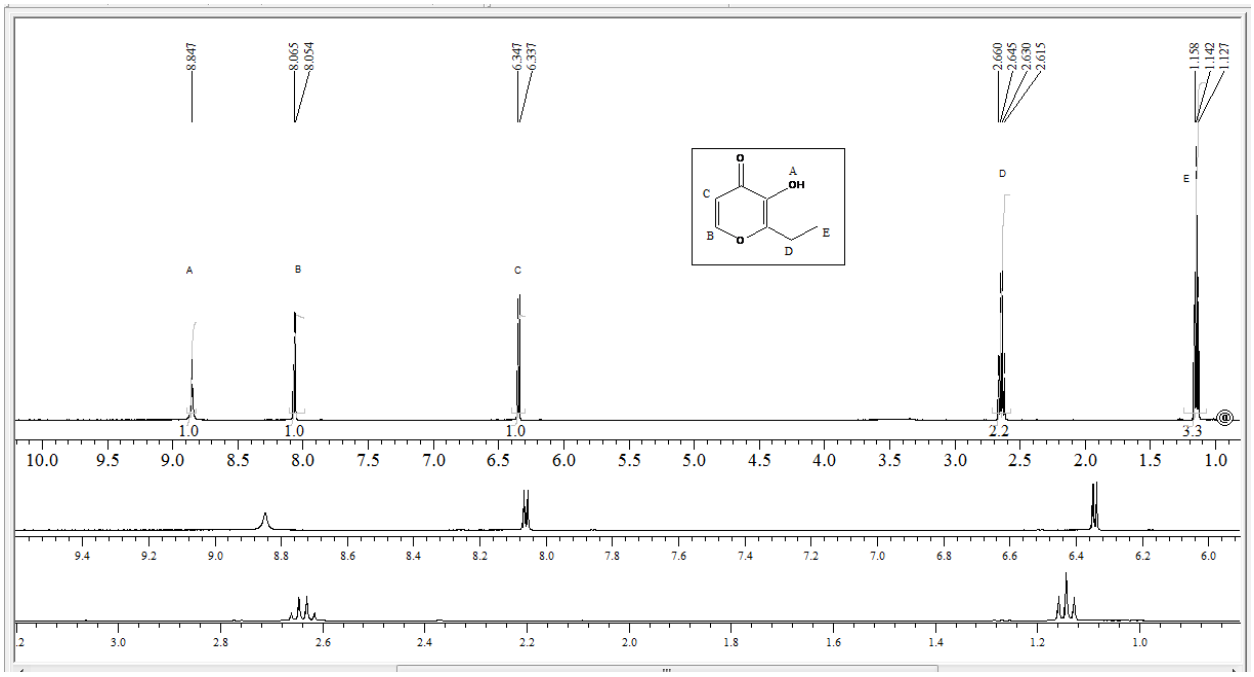


**A.1.3.** $^{1}$H-NMR spectrum of ethylmaltol in DMSO-$d_6$

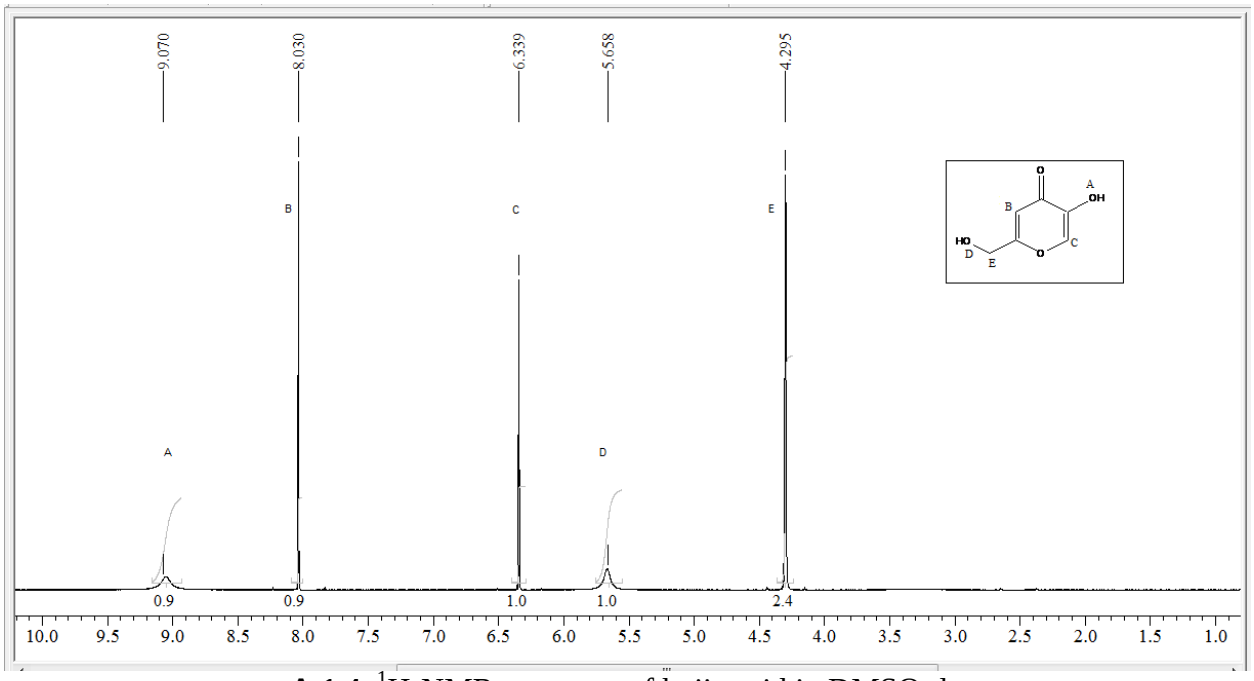


**A.1.4.** $^{1}$H-NMR spectrum of kojic acid in DMSO-$d_6$

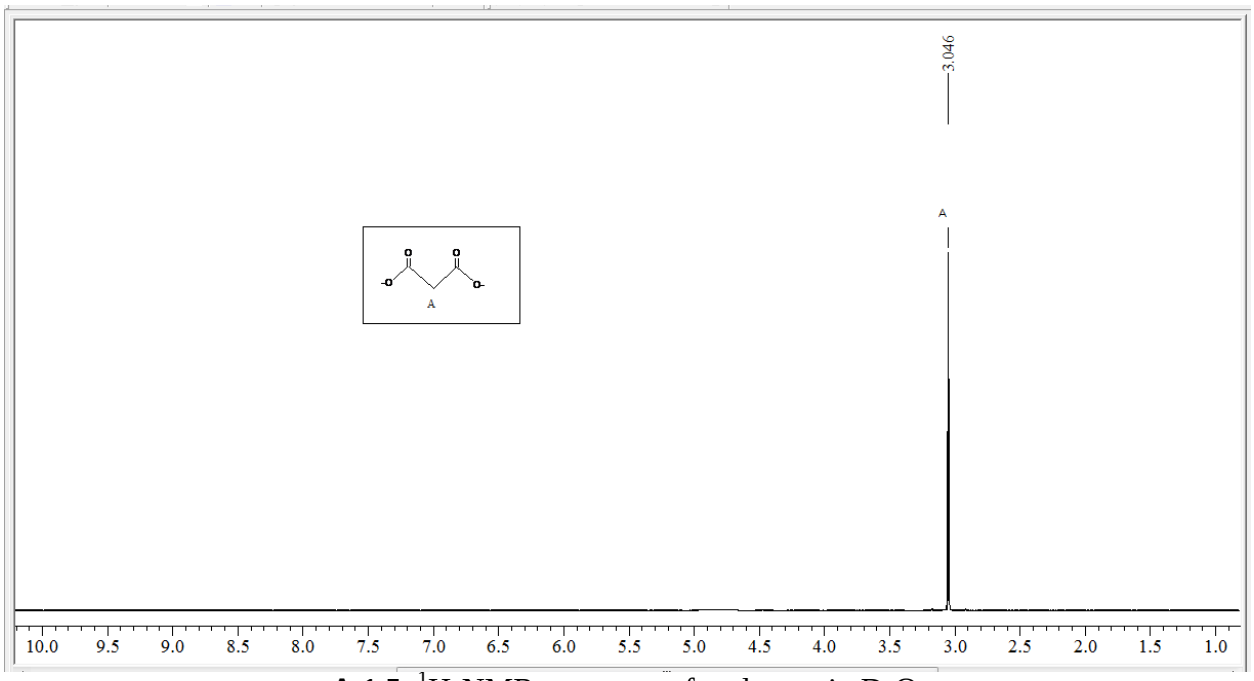


**A.1.5.** $^{1}$H-NMR spectrum of malonate in $D_2O$

## Bibliography


1. American Cancer Society. Cancer Facts & Figures 2010. Atlanta: American Cancer Society; 2010. www.cancer.org

2. World health organization. www.who.int/

3. Rheingold S., Neugut A., Meadows A. Secondary Cancers: Incidence, Risk Factors, and Management. in Frei E., Kufe D. W., Holland J. F. Cancer medicine**,** 6. *Hamilton, Ont: BC Decker*. **2003**, 2399.

4. Ferlay J., Shin H., Bray F., Forman D., Mathers C., and Parkin D. M. Estimates of worldwide burden of cancer in 2008: GLOBOCAN 2008. *Int. J. Cancer*. **2010**, 127, 2893–2917.

5. National center institute. www.cancer.gov/

6. Rosenberg, B. Platinum complexes for the treatment of cancer: why the search go on. In *Cisplatin chemistry and biochemistry of a leading anticancer drug*; Lippert, B. ed; Wiley-VCH: Weinhheim, **1999**, 3-27.

7. Kostova I. Platinum Complexes as Anticancer Agents. *Recent Patents on Anti-Cancer Drug Discovery.* **2006,** 1, 1, 1-22.

8. Sadler P.J., Guo Z. Metal complexes in medicine: Design and mechanism of action. *Pure & Appl. Chem.* **1998**, 70, 4, 863-871.

9. Harding M.M., Mokdsi, G. Antitumor metallocenes: Structure activity studies and interactions with biomolecules. *Current Medicinal Chemistry.* **2000**, 7, 1289-1303.

10. Melendez, E. Titanium complexes in cancer treatment: *Crit. Rev. Oncol. Hematol.* **2002**, 42, 309.

11. Kopf Maier. Tumor inhibition by metallocenes: Antitumor activity of niobocene and tungstocene dichlorides. *Journal of Inorganic and nuclear chemistry*.**1980**, 42, 12, 1789-1791.

12. Melendez E. Bioorganometallic Chemistry of Molybdenocene Dichloride and Its Derivatives, *Journal of Organometallic Chemistry.* **2012**, doi: 10.1016/j.jorganchem.2012.02.006

13. Alama A., Tasso B., Novelli., Sparatore F. Organometallic compounds in oncology: implications of novel organotins as antitumor agents. *Drug Discovery Today.* **2009**, 14, 9, 500-508.

14. Jung Y., Lippard S. Direct Cellular Responses to Platinum-Induced DNA Damage. *Chemical Reviews.* **2007**, 107, 5, 1387-1407.

15. Fuertes M., Alonso C., Perez J. Biochemical modulation of cisplatin mechanisms of action: enhancement of antitumor activity and circumvention of drug resistance. *Chemical Reviews.* **2003**, 103, 3, 646-662.

16. Bakhtiar R., Ochiai E. Pharmacological applications of inorganic complexes. *General Pharmacology.* **1999**, 32, 525–540.

17. Clarke M., Zhu M., and Frasca D. Non-Platinum Chemotherapeutic Metallopharmaceuticals. *Chem. Rev.* **1999**, 99, 2511-2533.

18. Harvey J., McFadden M., Smith F., Joubert L., Schein P. Phase I study of oral spirogermanium. *Investigational new drugs.* **1990**, 8, 53-56.

19. Canfield V., Lyss A. A phase II trial of gallium nitrate in advanced previously untreated colorectal cancer. *Investigational new drugs.* **1993**, 11, 335.

20. Chitambar C., Purpi D., Woodliff J., Yang M., and Wereley J. Development of Gallium compounds for treatment of lymphoma: Gallium Maltolato, a novel hydroxypyrone Gallium compound, induces apoptosis and circumvents lymphoma cell resistance to Gallium nitrate. *JPET.* **2007**, 322, 1228–1236.

21. Murray, J.H., Harding, M.M. Organometallic anticancer agents: The effects of the central metal and halide ligands on the interaction of metallocenes dihalides $Cp_2MX_2$ with nucleic acid constituents. *J. Med. Chem.* **1994**, 97, 1936-1941.

22. Gao L., Matta J., Rheingold A., and Melendez E. Synthesis, structure and biological activity of amidefunctionalized titanocenyls: improving their cytotoxic properties. *Journal of Organometallic Chemistry.* **2009**, 694, 26, 4134–4139.

23. Gao L.M. and Melendez E. Cytotoxic properties of titanocenyl amides on breast cancer cell Line MCF-7. *Metal-Based Drugs.* **2010**, 1-6.

24. Gao L.M., Vera J.L., Matta J. Melendez E. Synthesis and cytotoxicity studies of steroid-functionalized titanocenes as potential anticancer drugs: sex steroids as potential vectors for titanocenes. *J Biol Inorg Chem.* **2010,** 15, 6, 851-859.

25. Hernandez R., Mendez J., Lamboy J., Torres M., Roman F., Melendez E. Titanium (IV) complexes: cytotoxicity and cellular uptake of titanium (IV) complexes on caco-2 cell line. *Toxicology in Vitro.* **2010**, 24, 178–183.

26. Thompson K., Barta C.A., and Orvig C. Metal complexes of maltol and close analogues in medicinal inorganic chemistry. *Chem. Soc. Rev.* **2006**, 35, 545–556.

27. Carland M., Tan K.J., White J.M., Stephenson J., Murray V., Denny W.A., McFadyen D. Synthesis, crystal structure and cytotoxicity of diamine platinum(II) complexes containing maltol. *Journal of Inorganic Biochemistry***. 2005**, 99, 1738–1743.

28. Chua M., Bernstein L.R., Li R., and So S. Gallium Maltolato is a Promising Chemotherapeutic Agent for the Treatment of Hepatocellular Carcinoma. *Anticancer research.* **2006**, 26, 1739-1744.

29. Kandioller W., Hartinger C., Nazarov A.A, Kasser J., John R., Jakupec M.A., Arion V.B., Dyson P.J., Keppler B.K. Tuning the anticancer activity of maltol-derived ruthenium complexes by derivatization of the 3-hydroxy-4-pyrone moiety. *Journal of Organometallic Chemistry.* **2009**, 694, 922–929.

30. Reddy V.D., Dayal D., Szalda D.J., Cosenza S.C., Ramana M.V. Syntheses, structures, and anticancer activity of novel organometallic rutheniumemaltol complexes. *Journal of Organometallic Chemistry.* **2012,**700, 180-187.

31. Kandioller W., Kurzwernhart A., Hanif M., Meier S.M., Henke H., Keppler B.K., Hartinger C. Pyrone derivatives and metals: From natural products to metal-based drugs. *Journal of Organometallic Chemistry.* **2011,** 696, 999-1010.

32. Emami S., Hosseinimehr S., Taghdisi S.M., and Akhlaghpoor S. Kojic acid and its manganese and zinc complexes as potential radioprotective agents. *Bioorganic & Medicinal Chemistry Letters.* **2007,** 17, 45–48.

33. Wei Y., Zhang C., Zhao P., Yang X., Wang K. A new salicylic acid-derivatized kojic acid vanadyl complex: Synthesis, characterization and anti-diabetic therapeutic potential. *Journal of Inorganic Biochemistry*. **2011**, 105, 1081–1085.

34. Xing Y., Lou L., Chen X, Ye Q., Xu Y., Xie C., Jiang J., Liu W. Synthesis and cytotoxicity of diam(m)ineplatinum(II) complexes with 2,2-bis(hydroxymethyl)malonate as the leaving group. *Bioorganic & Medicinal Chemistry Letters.* **2012,** 22, 2239–2241.

35. Feliciano I., Matta J., Melendez E. Water-soluble molybdenocene complexes with both proliferative and antiproliferative effects on cancer cell lines and their binding interactions with human serum albumin. *J Biol Inorg Chem*. **2009**, 14, 1109–1117.

36. Ghuman J., Zunszain P.A., Petitpas I., Bhattacharya A.A., Otagiri M., and Curry S. Structural Basis of the Drug-binding Specificity of Human Serum Albumin. *J. Mol. Biol*. **2005**, 353, 38–52.

37. Sugio S., Kashima A., Mochizuki S., Noda M., Kobayashi K. Crystal structure of human serum albumin at 2.5 A resolution. *Protein Eng*. **1999**, 12, 439-446.

38. Tinoco A.D., Eames E.V., and Valentine A.M. Reconsideration of Serum Ti(IV) Transport: Albumin and Transferrin Trafficking of Ti(IV) and Its Complexes**.** *J. AM. CHEM. SOC***. 2008**, 130, 2262-2270.

39. Ravera M., Gabano E., Baracco S., Osella D. Electrochemical evaluation of the interaction between antitumoral titanocene dichloride and biomolecules. *Inorganica Chimica Acta.* **2009,** 362, 1303–1306.

40. Wu S., YuanW., Wang H., Zhang Q., Liu M., Yu K. Synthesis, crystal structure and interaction with DNA and HSA of (N,N-dibenzylethane-1,2-diamine) transition metal complexes. *Journal of Inorganic Biochemistry.* **2008**, 102, 2026–2034.

41. Sun H., Li H., Sadler P. J. Transferrin as a metal ion mediator. *Chem Rev.* **1999**, 2817-2842.

42. Transferrin Structure. www.cs.stedwards.edu/chem/Chemistry/CHEM43/CHEM43/Projects04/Transferrin/structure.htm

43. Guo M., Sun H., McArdle H. J., Gambling L., Sadler P.J. Ti (IV) uptake and release by human serum transferrin and recognition of Ti IV-Transferrin by Cancer Cells: understanding the mechanism of action of the anticancer drug titanocene dichloride. *Biochemistry.* **2000**, 39, 10023-10033.

44. Bochmann, M. *Organometallics 2. Complexes with Transition Metal-Carbon p- Bonds*; Oxford: New York, **1994**; Vol. 13.

45. Kotz J., Vining W., Coco W., and Rosen R. Oxidative Electrochemistry of Compounds of the Type $(\eta^5\text{-}C_5H_5)_2MX_2$, Where M = Ti(IV), Mo(IV), and W(1V) and X = Halide, Thiolate, or Ferrocenyl. *Organometallics.* **1983**, 2, 68-79.

46. Sarzehi S., Chamani J. Investigation on the interaction between tamoxifen and human holo-transferrin:Determination of the binding mechanism by fluorescence quenching, resonancelight scattering and circular dichroism methods. *International Journal of Biological Macromolecules.* **2010,** 47, 558–569.

47. Lu Y., Feng Q., Cui F., Xing W., Zhang G., Yao X. Interaction of 30-azido-30-deamino daunorubicin with human serum albumin: Investigation by fluorescence spectroscopy and molecular modelingmethods. *Bioorganic & Medicinal Chemistry Letters.* **2010,** 20, 6899–6904.

48. Sułkowska A., Bojko B., Rownicka J., Sułkowski W.W. Paracetamol and cytarabine binding competition in high affinity binding sites of transporting protein. *Journal of Molecular Structure.* **2006,** 792–793, 249–256.

49. Tian J., Liu J., Xie J., Yao X., Hu Z., Chen X.. Binding of wogonin to human serum albumin: a common binding site of wogonin in subdomain IIA. *Journal of Photochemistry and photobiology B: Biology.* **2004,** 74, 39–45.

50. Guo X., Sun X., Xu S. Spectroscopic investigation of the interaction between riboflavin and bovine serum albumin. *Journal of Molecular Structure.* **2009,** 931, 1-3, 55-59.

51. Chamani J., Vahedian-Movahed H., Reza Saberi M. Lomefloxacin promotes the interaction between human serum albumin and transferrin: A mechanistic insight into the emergence of antibiotic's side effects. *Journal of Pharmaceutical and Biomedical Analysis.* **2011,** 55, 114–124.

52. Cui F., Fan J., Lib J., and Hu Z. Interactions between 1-benzoyl-4-p-chlorophenyl thiosemicarbazide and serum albumin: investigation by fluorescence spectroscopy. *Bioorganic & Medicinal Chemistry.* **2004,** 12, 151–157.

53. Lakowicz J. Principles of fluorescence spectroscopy. 3ed, *Springer*, Baltimore-USA, **2006**.

54. Ross P., Subramanian S. Thermodynamics of Protein Association Reactions: Forces contributing to Stability. *Biochem.* **1981**, 20, 3096–3102.

55. Rodriguez M.I., Chavez-Gil T., Colon Y., Díaz N., Melendez E. Molybdenocene-DNA interactions studies using electrochemical analysis. *J. Electroanal. Chem*. **2005**, 576, 315-322.